

**DEVELOPMENT OF A NEAR-
TRANSPARENT
AND LOW-COST LIQUID ANTENNA**

TAN WEI YANG

UNIVERSITI TUNKU ABDUL RAHMAN

**DEVELOPMENT OF A NEAR-TRANSPARENT
AND LOW-COST LIQUID ANTENNA**

TAN WEI YANG

**A project report submitted in partial fulfilment of the
requirements for the award of Bachelor of Mechatronics
Engineering with Honours**

**Lee Kong Chian Faculty of Engineering and Science
Universiti Tunku Abdul Rahman**

April 2024

DECLARATION

I hereby declare that this project report is based on my original work except for citations and quotations which have been duly acknowledged. I also declare that it has not been previously and concurrently submitted for any other degree or award at UTAR or other institutions.

Signature :  _____

Name : TAN WEI YANG _____


ID No. : 1902808 _____

Date : 29th April 2024 _____

APPROVAL FOR SUBMISSION

I certify that this project report entitled “**DEVELOPMENT OF A NEAR-TRANSPARENT AND LOW-COST LIQUID ANTENNA**” prepared by **TAN WEI YANG**, has met the required standard for submission in partial fulfillment of the requirements for the award of Bachelor of Mechatronics Engineering with Honours at Universiti Tunku Abdul Rahman.

Approved by,

Signature : 

Supervisor : Dr. Low Jen Hahn
Date : 29 April 2024

The copyright of this report belongs to the author under the terms of the copyright Act 1987 as qualified by Intellectual Property Policy of Universiti Tunku Abdul Rahman. Due acknowledgement shall always be made of the use of any material contained in, or derived from, this report.

© 2024, TAN WEI YANG. All right reserved.

ACKNOWLEDGEMENTS

I want to thank everyone who contributed to the successful completion of this project. I want to express my gratitude to my research supervisor, Dr. Low Jen Hahn, for his invaluable advice, guidance, and enormous patience throughout the research development.

In addition, I would also like to express my gratitude to my loving parents and friends who helped and encouraged me to complete my final year project when I faced many obstacles.

ABSTRACT

This study presents an innovative approach to antenna design, exploring the potential of low-cost and near-transparent liquid antennas for modern wireless communication. It provides a comprehensive historical background on antenna technology, tracing its evolution from its early stages to its current role in 5G networks. The research then delves into developing near-transparent liquid antennas, significantly departing from traditional designs. The study introduces two distinct antenna models using novel methodologies and materials such as ethyl acetate and water. CST software simulations evaluated these models based on their dielectric properties, cost-efficiency, and performance. The ethyl acetate DRA (Dielectric Resonator Antenna) has a ground measuring 61.99 mm in width and 61.99 mm in length, with a cylinder height of 40.06 mm. Similarly, the distilled water DRA has a ground measuring 40.01 mm in width and 40.01 mm in length, with a cylinder height of 17.66 mm. The ethyl acetate DRA and distilled water DRA exhibit resonant frequencies of 2.408 GHz and 2.4 GHz, respectively, with simulated maximum gains of 5.13 dBi and 4.13 dBi. Moreover, the study highlights the transparency of these liquid antennas, noting a minor reduction in light intensity compared to conventional DRAs. The ethyl acetate DRA and distilled water DRA reduce only 20% in light illumination, as opposed to the 70% reduction seen with conventional DRAs. Furthermore, the practical application of these antennas is demonstrated through integration into a Web-Connected Smart Lighting system. This application enables wireless lighting control via a web server, showcasing the proposed antenna design's functionality, cost-effectiveness, and aesthetic appeal.

TABLE OF CONTENTS

DECLARATION		i
APPROVAL FOR SUBMISSION		ii
ACKNOWLEDGEMENTS		iv
ABSTRACT		v
TABLE OF CONTENTS		vi
LIST OF TABLES		ix
LIST OF FIGURES		x
LIST OF SYMBOLS / ABBREVIATIONS		xv
LIST OF APPENDICES		xvi
CHAPTER		
1	INTRODUCTION	1
1.1	Background of Antenna	1
1.2	Importance of the Study	2
1.3	Antenna Configuration	3
1.3.1	Antenna Working Principle	3
1.3.2	Antenna Components	4
1.3.3	Antenna Parameters	5
1.4	Problem Statement	7
1.5	Aim and Objectives	8
1.6	Scope of the Study	8
1.7	Limitations of the Study	8
1.8	Contribution of the Study	9
1.9	Outline of the Report	10
2	LITERATURE REVIEW	11
2.1	Introduction	11
2.2	Recent Advancements in the Field of Transparent Antenna	11
2.3	Transparent Geometry	12

2.4	Transparent Material of Antenna	13
	2.4.1 Transparent Conducting Oxide	13
	2.4.2 Silver Nanowire	14
	2.4.3 Water	15
2.5	Types of Liquid Use in Liquid Antenna	16
	2.5.1 Metallic Liquid	17
	2.5.2 Non-metallic Liquids	19
2.6	Factors Affecting the Performance of Liquid DRA	24
	2.6.1 Type of Dielectric Liquid Effect	25
	2.6.2 Ground Size	25
	2.6.3 Feeding Effect	26
	2.6.4 Liquid Holder's Diameter Effect	27
2.7	Summary	28
3	METHODOLOGY AND WORK PLAN	29
3.1	Introduction	29
3.2	Design Flow	29
3.3	Simulation Software and Setup	31
3.4	The Material Selection	31
3.5	Designing Stage	32
	3.5.1 Designing of the Antenna	32
	3.5.2 Conceptual and Actual Design of the Antenna	35
3.6	Fabrication and Assembly of Antenna	38
	3.6.1 Molding, Curing and Demolding Process	38
	3.6.2 Mesh Ground Plane Fabrication	40
	3.6.3 SMA Connector Fabrication	43
	3.6.4 Assembly of Antenna Parts	45
3.7	Characterization	46
	3.7.1 Reflection coefficient, S_{11}	46
	3.7.2 Far-field Measurement	49
	3.7.3 Transparency Evaluation	52
	3.7.4 Antenna Signal Strength Assessment using ESP-32 Cam	54

	3.7.5 Web-connected Smart Lighting (IoT Application)	57
	3.8 Gantt Chart	61
4	RESULTS AND DISCUSSION	62
	4.1 Introduction	62
	4.4 Parametric Sweep Analysis	66
	4.4.1 Liquid Diameter	67
	4.4.2 Liquid Height	67
	4.4.3 Mesh Ground Width	68
	4.4.4 Mesh Ground Length	69
	4.4.5 Ground Plane Size	70
	4.4.6 SMA Probe Length	71
	4.5 Analysis of Result	72
	4.5.1 S-parameter, S_{11}	72
	4.5.2 Input Impedance, Z_{11}	73
	4.5.3 Far-field Radiation Gain	75
	4.5.4 E-field and H-field	79
	4.6 Antenna's Signal Strength Assessment using ESP-32 Cam	81
	4.7 Antenna's Transparency Evaluation	83
	4.8 Web-Connected Smart Lighting (IoT Application)	85
	4.9 Summary	88
5	CONCLUSIONS AND RECOMMENDATIONS	90
	5.1 Conclusions	90
	5.2 Recommendations for Future Work	91
	REFERENCE	92
	APPENDICES	98

LIST OF TABLES

Table 3.1:	Gantt Chart for FYP 1.	61
Table 3.2:	Gantt Chart for FYP 2.	61
Table 4.1:	Parts Label of Ethyl Acetate Antenna Model.	64
Table 4.2:	Dimensions of Antenna for Ethyl Acetate Model.	65
Table 4.3:	Parts Label of Distilled Water Antenna Model.	65
Table 4.4:	Dimensions of Antenna for Distilled Water Model.	66

LIST OF FIGURES

Figure 1.1:	Working Principle of Antenna (Y, n.d.).	3
Figure 1.2:	Radiation Pattern of Antenna (everythingRF, 2018).	7
Figure 2.1:	Semi-Transparent Antenna Using Mesh Method (Jang et al., 2016).	13
Figure 2.2:	Transparent Antenna Using ITO Film (Colombel et al., 2009).	14
Figure 2.3:	Classification of Liquid Antennas (Huang et al., 2021).	16
Figure 2.4:	An Adjustable-length Liquid-metal Monopole Antenna Positioned Above a Ground Plane (Morishita et al., 2014).	18
Figure 2.5:	Liquid-metal Microfluidic Antenna (Dey et al., 2016).	19
Figure 2.6:	Water Patch Antenna (Sun and Luk, 2017).	20
Figure 2.7:	Sea Water Antenna (Xing, 2015).	21
Figure 2.8:	Liquid Antenna Using Transformer Oil (Konca and Warr, 2015).	24
Figure 2.9:	Ground Plane Width, Resonant Frequency, and Fractional Bandwidth (Xing et al., 2015).	26
Figure 2.10:	Cross-sectional View of Antenna.	27
Figure 2.11:	Effect of Liquid Holder's Diameter on Antenna's Resonant Frequency (Xing et al., 2015).	28
Figure 2.12:	Effect of Liquid Holder's Height on Antenna's Resonant Frequency (Xing et al., 2015).	28
Figure 3.1:	Flow Chart of The Overall Process of The Study.	30
Figure 3.2:	CST Studio Software.	31
Figure 3.3:	Ecoflex 0030.	32
Figure 3.4:	Price of Ethyl Acetate (KSFE, 2021).	32
Figure 3.5:	Price of Ecoflex (Ubuy.com, n.d.).	32

Figure 3.6:	Dimensions Setting.	34
Figure 3.7:	Preliminary Design of Liquid DRA.	36
Figure 3.8:	Secondary Antenna Design (a) Ethyl Acetate Model and (b) Water Model.	37
Figure 3.9:	Ground Plane Modification (a) Conceptual Design without Mesh and (b) Using Mesh Technique.	37
Figure 3.10:	Final Antenna Design (a) Ethyl Acetate Model and (b) Water.	38
Figure 3.11:	DRA Mould Design of (a) Ethyl Acetate Model and (b) Water Model.	38
Figure 3.12:	Cap Mould Design of (a) Ethyl Acetate Model and (b) Water Model.	39
Figure 3.13:	Preparation of Ecoflex.	39
Figure 3.14:	3D Printing Mould (a) Before Ecoflex Filling and (b) After Ecoflex Filling.	39
Figure 3.15:	Vacuum Pump with Chamber.	40
Figure 3.16:	The DRA and Cap are Extracted from The Mold.	40
Figure 3.17:	Silhouette Portrait Cutter.	41
Figure 3.18:	Slot Design of Ground in (a) Ethyl Acetate Model and (b) Water Model.	41
Figure 3.19:	Trial Cutting Process.	42
Figure 3.20:	Copper Sheet (a) Before and (b) After Cut.	42
Figure 3.21:	Final Product.	42
Figure 3.22:	Copper Sheet with Transparent Plastic (a) Top View and (b) Bottom View.	43
Figure 3.23:	SMA with Copper.	43
Figure 3.24:	Measurement of Copper.	44
Figure 3.25:	Soldering Station.	44
Figure 3.26:	SMA with External Copper.	44

Figure 3.27: Distilled Water DRA Ground Plane with SMA (a) Top View and (b) Bottom View.	45
Figure 3.28: Assembly of Prototypes (a) Before Assembly and (b) After Assembly.	45
Figure 3.29: Vector Network Analyser (VNA).	46
Figure 3.30: Calibration Setup.	46
Figure 3.31: Connector Cable with Device Under Test (DUT).	47
Figure 3.32: Setup of S_{11} Measurement.	47
Figure 3.33: Setup of Liquid Dielectric Properties Measurement.	48
Figure 3.34: Equipment (a) Signal Generator and (b) Spectrum Analyser.	49
Figure 3.35: Setup of Far-field Measurement.	50
Figure 3.36: Setup of Cable Loss Measurement.	51
Figure 3.37: Setup of Space Loss and Antenna Gain Measurement.	51
Figure 3.38: 360° Marking.	52
Figure 3.39: Orientation of Antenna at $\Phi = 90$.	52
Figure 3.40: Phyphox Application Logo.	52
Figure 3.41: Three Different Designs of Antennas.	54
Figure 3.42: Setup of Illumination Measurement for (a) Ethyl Acetate DRA and (b) Distilled Water DRA.	54
Figure 3.43: Selections of External or On-board Antenna.	55
Figure 3.44: Desoldering Product indicates that the External Antenna has been Selected.	55
Figure 3.45: Soldering Station.	56
Figure 3.46: Setup of Signal Strength Measurement.	57
Figure 3.47: Result Presentation of Signal Strength Measurement.	57
Figure 3.48: Electrical Circuit Diagram of ESP32-Cam with Laptop.	57
Figure 3.49: RSSI Measurement Program Code.	59

Figure 3.50: Electrical Circuit Diagram of the Smart Lighting Application.	60
Figure 3.51: Setup of IoT Application Experiment.	60
Figure 4.1: Antenna Components.	62
Figure 4.2: Results of Simulated Parametric Sweep of Liquid Diameter in Container.	67
Figure 4.3: Results of Simulated Parametric Sweep of Liquid Height in Container.	68
Figure 4.4: Results of Simulated Parametric Sweep Results of Mesh Ground Cutting Slot Width.	69
Figure 4.5: Results of Simulated Parametric Sweep Results of Mesh Ground Cutting Slot Length.	70
Figure 4.6: Results of Simulated Parametric Sweep Results of Ground Plane Size.	71
Figure 4.7: Results of Simulated Parametric Sweep Results of SMA Pin Length.	72
Figure 4.8: Measured and Simulated Reflection Coefficient of Ethyl Acetate Model.	73
Figure 4.9: Measured and Simulated Reflection Coefficient of Distilled Water Model.	73
Figure 4.10: Simulated Z-parameter of the Ethyl Acetate Model.	75
Figure 4.11: Simulated Z-parameter of the Distilled Water Model.	75
Figure 4.12: Spherical Coordinate System.	76
Figure 4.13: Far-field Gain at $\Phi = 90$ of Ethyl Acetate Model.	77
Figure 4.14: Far-field Gain at $\Phi = 0$ of Ethyl Acetate Model.	77
Figure 4.15: Far-field Gain at $\Phi = 90$ of Distilled Water Model.	78
Figure 4.16: Far-field Gain at $\Phi = 0$ of Distilled Water Model.	78
Figure 4.17: Simulated E-field of Ethyl Acetate Model.	79
Figure 4.18: Simulated E-field of Distilled Water Model.	80
Figure 4.19: Simulated H-field of Ethyl Acetate Model.	80

Figure 4.20:	Simulated H-field of Distilled Water Model.	81
Figure 4.21:	RSSI of Ethyl Acetate DRA.	82
Figure 4.22:	RSSI of Distilled Water DRA.	82
Figure 4.23:	Removal of DRAs.	82
Figure 4.24:	RSSI Result When Antenna is Removed (Ethyl Acetate DRA).	83
Figure 4.25:	RSSI Result When Antenna is Removed (Distilled Water DRA).	83
Figure 4.26:	Light Illuminance (a) Without Antenna and (b) With Distilled Water DRA.	84
Figure 4.27:	Light Illuminance with (a) Ethyl Acetate DRA and (b) Conventional DRA.	84
Figure 4.28:	Illuminance Test with Three Different DRAs.	85
Figure 4.29:	Light is (a) OFF and (b) Turned On with Ethyl Acetate DRA.	85
Figure 4.30:	Light is Turn Off Again with Ethyl Acetate DRA.	86
Figure 4.31:	Removal of DRA.	86
Figure 4.32:	Light is Turn Off Without DRA.	86
Figure 4.33:	Light is Unable to Turn On Without DRA.	87
Figure 4.34:	Web Server Not Responding With Ethyl Acetate DRA.	87
Figure 4.35:	Reconnect Ethyl Acetate DRA with ESP32 Microcontroller.	87
Figure 4.36:	Web Server Reactivated with Ethyl Acetate DRA.	88
Figure 4.37:	Light is Turned On Again With Ethyl Acetate DRA.	88

LIST OF SYMBOLS / ABBREVIATIONS

AZO	Aluminum-zinc oxide
CP	Circularly polarised
Cu	Copper
DRA	Dielectric Resonant Antennas
DDPA	Dense dielectric patch antenna
DUT	Device Under Test
EGaIn	Eutectic gallium indium
FTO	Fluorine-doped tin oxide (FTO)
GZO	Gallium-doped zinc oxide
IoT	Internet of Things
ITO	Indium-tin-oxide
IZTO	Indium-zinc-tin oxide
LM	Liquid metal
LDRA	Liquid Dielectric Resonator Antenna
ϵ_r	Permittivity
PG	Propylene glycol
PDMS	Polydimethylsiloxane
PET	Polyethylene terephthalate
PCBs	Printed circuit boards
RF	Radio-frequency
RCS	Radar cross-section
S_{11}	Reflection Coefficient
Ag	Silver
AgNWs	Silver nanowires
AgNFs	Silver nanofilms
S_{12}	Transmission Coefficient
TCO	Transparent conductive oxides
VNA	Vector Network Analyzer
VSWR	Voltage Standing Wave Ratio

LIST OF APPENDICES

Appendix A: Supporting Attachment for Antenna Signal Strength Assessment	98
Appendix B: Supporting Attachment for Web-connected Smart Lighting Application	101
Appendix C: Supporting Attachment of Being Shortlisted for The FYP Poster Competition	104
Appendix D: Supporting Documentation of Silver Award in FYP Competition	105

CHAPTER 1

INTRODUCTION

1.1 Background of Antenna

In modern technology, antennas facilitate seamless wireless communication across various devices. These devices are integral to daily lives, enabling connectivity in homes and offices (seimw.com, 2020). Antennas are critical for receiving and transmitting signals, making their design and functionality significant. A well-designed antenna effectively captures desired signals, ensuring clear communication via phones and radios. Conversely, poorly constructed antennas can hinder signal reception and disrupt communication. Beyond their fundamental functions, antennas also serve as transducers, impedance-matching tools, radiators, and sensors.

When James Clerk Maxwell created Maxwell's Equations in 1873, the history of antennas began, laying the foundation for understanding electromagnetic waves. Maxwell was the first to transmit and receive radio waves. Then, in 1886, Heinrich Rudolph Hertz's tests showed that wireless transmission was possible. In his laboratory, he created a spark at a wavelength of 4 meters that was detected as a spark in the gap of a neighbouring loop. Then, in 1901, Guglielmo Marconi achieved a breakthrough. He successfully sent signals across long distances, connecting Cornwall, England, and Newfoundland. Marconi's achievement marked a pivotal moment in wireless communication. These pioneers, including Maxwell, Hertz, and Marconi, established the foundation for antenna development, driving the rapid advancement of communication technology (Balanis, 1992). As wireless communication becomes integral to modern life, the forthcoming 5G revolution promises faster transmission and extensive device connectivity, aligned with the Internet of Things (IoT) concept (Helena et al., 2020).

The evolution of antennas can be traced back to their wire-based predecessors, such as dipoles, helices, and rhombuses, which were used individually or in arrays before World War II. Post-World War II, new radiator designs emerged, including common types like dipole, horn, Yagi-Uda, and rectangular patch antennas (Balanis, 1992). A significant development in

antenna technology occurred with the introduction of Dielectric Resonant Antennas (DRAs) in the 1980s. Conceived initially to address the high loss associated with metal antennas at high frequencies, DRAs are adaptable, cost-effective, and ideal for low to high-frequency applications. As a result, DRAs find several practical uses (Leung et al., 2012).

The liquid antenna has recently garnered significant research interest due to its distinct qualities such as transparency, liquidity, low-cost, and widespread availability. Researchers have dedicated considerable efforts to leverage these unique attributes to create practical and functional liquid antennas, enhancing their performance and capabilities. In such scenarios, transparency can be combined with essential coverage and bandwidth needs, making them suitable for integration into building windows, vehicle windshields, towers, trees, and smart windows. Employing various materials and techniques, such as thin-film, transparent liquid, and mesh-grid approaches, transparent antenna design transforms conventional antenna components into transparent elements. This progressive approach ensures efficiency and contributes to an improved and visually appealing wireless communication landscape.

In summary, antennas have transformed from essential tools to intricate communication devices. Currently, the main challenge lies in effectively integrating antennas while managing costs. Notably, transparent antennas offer an ingenious solution by seamlessly blending into their surroundings. By striving for both affordability and transparency, the stage is set for reshaping technology and optimising antenna deployment.

1.2 Importance of the Study

Developing nearly transparent, low-cost liquid antennas is essential to advancing wireless communication technologies. By offering almost transparent characteristics and significantly reducing production costs, these antennas present an innovative approach that allows seamless integration into various surroundings without sacrificing aesthetics. Their accessibility makes them more widely adopted, especially when conventional antennas are too expensive. Furthermore, because of their nearly transparent nature, which guarantees minimum visible effect, they are suitable for situations where

aesthetics are crucial, such as wearable technologies or architectural designs. By concentrating on these traits, this field's study not only fosters innovation but also holds the potential to democratise access to wireless communication technologies, which will eventually help consumers and businesses worldwide.

1.3 Antenna Configuration

1.3.1 Antenna Working Principle

An antenna serves as a component designed to transmit or receive electromagnetic waves, requiring a receiver and a transmitter. It transforms RF signals into electromagnetic energy and ensures efficient signal transfer through impedance matching, as shown in Figure 1.1. Impedance matching minimises reflections and maximises power transfer. Antennas function as radiators and sensors, emitting electromagnetic waves during transmission and collecting them during reception. In transmission, guided waves are converted to free-space waves or transmission line signals, and free-space waves are transformed into guided waves during reception (Balanis, 1992). The receiver captures radio waves and transforms them into electrical signals for radios or televisions. In contrast, a transmitter, a distinct type of antenna, converts electrical signals into radio waves, facilitating their transmission over great distances (MobileSystems, 2017b). The critical principle involves electrons vibrating within antennas to generate and detect radio waves, maintaining the same characteristics during transmission or reception (MobileSystems, 2017a).

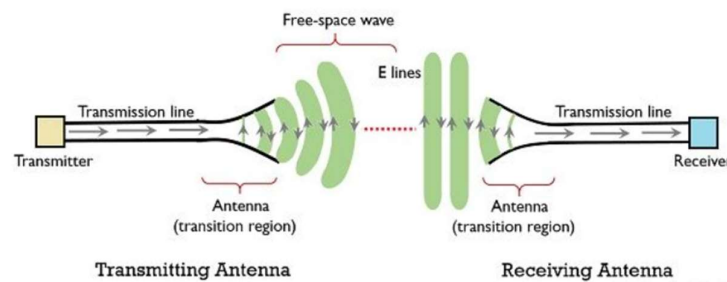


Figure 1.1: Working Principle of Antenna (Y, n.d.).

Antennas exhibit reciprocity, preserving their characteristics regardless of transmitting or receiving (vlab.amrita.edu, 2011). A high-performance antenna, for instance, can increase TV broadcast reception because well-

designed antennas boost system performance (Balanis, 1992). The antenna functions as an electromagnetic transducer, converting energy forms while ensuring impedance matching for efficient signal transfer without reflections. Transmitting antennas emit electromagnetic waves, while receiving antennas detect and capture these waves, exemplifying their dual function as radiators and sensors of electromagnetic energy.

1.3.2 Antenna Components

Antenna components are the physical elements that make up an antenna system. These components work together to enable the antenna to transmit and receive electromagnetic signals. The basic antenna components include conducting wire elements, connectors, and transmission lines. Antennas used for radio frequency communication primarily consist of conducting wire elements, categorised as driven or parasitic, which are pivotal for generating an electromagnetic field during transmission or connecting to receiving circuitry during reception.

Antenna connectors ensure smooth RF signal transmission between antennas and radio equipment. Different connector types, such as SMA, RP-SMA, N-Type, MMCX, U.FL, and FME, exist to suit various applications. Ensuring matching polarity between connectors is vital for secure connections and effective signal transmission. Male connectors possess a centre pin and threads, while female connectors have a socket and threads. Male connectors cover their female counterparts when mated, ensuring secure connections and efficient signal transmission. Moreover, SMA Connector is the ideal connector for high-performance wireless applications such as WiFi and Bluetooth. It is suitable for high frequencies up to 18 GHz and a small size for portable devices (Redmond, 2023).

Transmission lines are essential for signal propagation and can be parallel wires, waveguides, or coaxial cables. Coaxial cables featuring a central wire within an insulating layer are commonly used. Some antennas have baluns, short for “balanced/unbalanced”, to bridge the gap between balanced antennas and unbalanced transmission lines, optimising energy transfer and minimising reflections (Frenzel, 2021).

The radiating element is a vital component of an antenna, responsible for emitting or capturing electromagnetic waves by converting electrical

currents. This process defines the antenna's core function, affecting properties like radiation pattern, gain, and polarisation. Diverse antenna types, such as dipoles, monopoles, patches, and helices, utilise different radiating elements, each optimised for specific applications and frequency ranges. These elements collectively contribute to the antenna's overall performance and efficacy within its designated context (Perez, 1998).

1.3.3 Antenna Parameters

Antenna parameters offer insights into antenna performance. Common parameters include S-parameters, gain, bandwidth, and radiation pattern.

S-parameters describe power exchange between ports in an electrical system, which is crucial for antenna analysis. S_{11} indicates the reflection coefficient, with lower values signifying better energy delivery. For instance, S_{12} denotes the power transfer from Port 2 to Port 1, and S_{21} denotes electricity transmission from Port 1 to Port 2. These parameters are frequency-dependent and crucial in antenna analysis. The reflection coefficient or return loss is measured by the S_{11} value, which is frequently used for antennas. S_{11} measures the reflection coefficient or return loss. S-parameters, often measured with Vector Network Analysers, calculated from reflected and input power, indicate antenna performance. More negative return loss suggests better performance (Antenna_Theory, 2015). When S_{11} is 0 dB, it indicates that the antenna reflects all the power, and no radiation occurs. Conversely, when it is -10 dB, the antenna accepts some of the power.

For example, the reflected power is -7 dB when $S_{11} = -10$ dB and 3 dB of power is applied to the antenna. Consider a situation where some of the power sent into the antenna is reflected due to a mismatch at the antenna port. To illustrate, inputting 10 watts of power and 1 watt is reflected results in a return loss of -10 dB. It also signifies that the device receives 90% of the input power and less than 10% of the reflected power. This can be proved by this equation:

$$\text{Return Loss} = 10 \log \frac{\text{reflected power}}{\text{input power}} \quad (1)$$

In contrast, the return loss increases to -3.01 dB when the reflected power reaches 5 watts. Furthermore, the return loss changes to -13.01 dB if the

reflected power is 0.5 watts. These findings show that the antenna operates efficiently when the return loss is more negative, which denotes little reflected power.

Antenna gain enhances signal strength by focusing RF energy in a particular direction, measured in decibels relative to an ideal isotropic radiator. It does not generate new RF signals but amplifies energy in chosen directions, influencing coverage. Higher-gain antennas target distant points, while lower-gain ones distribute signals widely based on coverage needs. Bandwidth signifies the frequency range an antenna supports, with broader bandwidth enabling more applications. Notably, bandwidth differs from antenna efficiency, where efficiency is a ratio of input power to radiated power, usually given as a percentage or in decibels (inhand, 2022).

The radiation pattern visually illustrates how an antenna emits electromagnetic energy across different directions, showing field strength versus direction. Electromagnetic waves travel when a transmitter activates an antenna, forming near-field and far-field areas. As shown in Figure 1.2, the near-field comprises reactive (where electric and magnetic fields are out of phase) and radiative zones (where fields shift from reactive to radiating while the far-field is dominated by radiating fields). The Radiative Near-field lies between these two and exhibits changing radiation patterns (A.H.Systems, 2023). The near-field region's dimensions are defined by equations related to antenna size and wavelength. Where the far-field region starts beyond a certain distance from the antenna. The reactive near-field region, radiative far-field region, and far-field region can be expressed as (everythingRF, 2018):

$$\text{Reactive Near-field Region} < 0.62\sqrt{D^2/\lambda} \quad (2)$$

$$0.62\sqrt{D^2/\lambda} < \text{Radiative Near-field Region} < \frac{2D^2}{\lambda} \quad (3)$$

$$\text{Far-field Radiation} > \frac{2D^2}{\lambda} \quad (4)$$

where

D = Largest dimension of the antenna aperture.

λ = Wavelength of the electromagnetic wave.

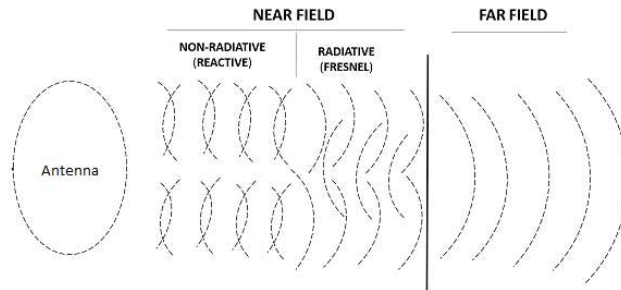


Figure 1.2: Radiation Pattern of Antenna (everythingRF, 2018).

1.4 Problem Statement

The demand for transparent liquid antennas has surged due to the necessity of integrating wireless communication devices into modern architectural designs, wearables, and smart windows. Due to their numerous uses in industries like healthcare, security, sports, smart cities, and the Internet of Things (IoTs), transparent antennas, a subset of transparent electronic devices, hold enormous appeal. These antennas provide a breakthrough solution by harmoniously blending into environments while upholding operational functionality (Redmond, 2023).

Other than that, the financial aspect of antenna materials and manufacturing processes is also essential. Identifying cost-effective materials becomes paramount, as reduced costs foster innovative antenna designs without financial constraints. Moreover, ensuring accessibility and inclusivity is pivotal, making advanced wireless technology affordable across industries and individuals. This cost-effective approach also holds the potential for downsizing antenna dimensions, catering to confined spaces (Leung et al., 2012).

Nevertheless, the existing approach to antenna design, relying on materials such as metals and specific dielectrics, yields non-transparent antennas that hinder seamless integration.

1.5 Aim and Objectives

This project aims to design and fabricate a low-cost and near-transparent liquid antenna. To achieve this aim, these objectives have been established:

1. To design a near-transparent and low-cost liquid antenna that can operate at the resonant frequency of 2.4 GHz.
2. To fabricate the near-transparent and low-cost antenna using transparent dielectrics and meshed ground plane.
3. To apply the near-transparent and low-cost antenna in the Internet of Things (IoT) application.

1.6 Scope of the Study

This research explores the potential of near-transparent antennas to operate at 2.4 GHz while emphasising cost-effectiveness and transparency. The investigation will focus on utilising low-cost materials to design and analyse Dielectric Resonator Antennas (DRAs) known for their low-loss properties.

Two distinct antenna models will be created, each employing different transparent liquids: ethyl acetate and water. These liquids possess varying dielectric properties and loss tangents, facilitating a comprehensive comparative analysis. Although ethyl acetate has a higher cost than water, its performance outperforms the water antenna model.

Moreover, Ecoflex, an economically viable and optically semi-transparent material, will be utilised for a dual function, acting as an insulator to separate the liquid from the metallic base and as the material for carving the cylindrical container enclosing the DRA. Additionally, the rigid metallic base will be engraved using a mesh technique to enhance the transparency of the antenna. The performance of the antenna will be simulated and evaluated using CST software.

1.7 Limitations of the Study

Several material limitations need to be addressed, as the search for a material that is both low-cost and transparent presents particular challenges. Water, for instance, stands out as an inexpensive and widely available option, but its suitability needs to improve when dealing with higher frequencies, particularly those exceeding 2 GHz. Water's high loss tangent at these frequencies can

considerably diminish antenna efficiency, necessitating a delicate balance between cost and performance (Wang and Chu, 2019). Moreover, the use of water comes with a notable drawback, its electromagnetic properties are significantly influenced by temperature changes. Sub-zero temperatures cause water to freeze into solid ice, resulting in a considerable shift in its electromagnetic properties and physical characteristics (Huang et al., 2021). Ethyl acetate, although it is more expensive than water, has an outstanding performance when utilised in liquid DRA.

Furthermore, achieving full transparency in the liquid antenna structure poses challenges due to the cost-effective requirement. While materials like K9 glass, plexiglass, acrylic, and pyrex have the potential to render the liquid antenna structure fully transparent, their fabrication processes are complex and costly. Additionally, incorporating a metal ground plane to support the dielectric resonator antenna (DRA) trades off the overall optical transparency of the antenna structure. Similarly, a small feeding probe prevents the antenna from achieving complete transparency. The pursuit of transparency in antenna design thus involves navigating intricate trade-offs between material properties, availability, and cost.

1.8 Contribution of the Study

Several valuable contributions emerged from this study. The feasibility of utilising a low-cost and near-transparent antenna composed of water and ethyl acetate has been successfully demonstrated. The study has highlighted the adaptability and versatility of this near-transparent liquid antenna, showcasing its ability to be fine-tuned for optimal performance by adjusting the amount of water and the antenna size. Furthermore, the research has underscored the antenna's capacity to achieve high gain when the liquid is ethyl acetate, indicating its proficiency in efficiently transmitting signals with minimal loss. The adoption of water and Ecoflex materials in the antenna's construction is commendable from an environmental perspective, considering their eco-friendliness compared to alternatives like plastics or heavy metals. Notably, incorporating water, ethyl acetate, and Ecoflex has contributed to cost-effectiveness in antenna fabrication. Furthermore, the rigid metallic base will be carved using a mesh technique, enhancing transparency. Beyond its technical

aspects, the antenna's aesthetic enhancement and compatibility with modern designs are notable. Its integration potential with other products and seamless placement in IoT applications due to its near-transparency are also highlighted. This study advances antenna design with functionality, eco-friendliness, cost-effectiveness, and visual appeal.

1.9 Outline of the Report

The report is organised into five chapters, each focusing on specific aspects of the study. Chapter 1 serves as an introduction, providing background information on the antenna, its working principle, basic components, and parameters. It also outlines the research's problem statement, objectives, importance, and limitations.

Chapter 2 delves into a comprehensive literature review covering recent advancements in transparent antennas, transparent geometries, materials used in transparent antennas, types of liquids used in liquid antennas, and factors affecting the performance of liquid DRA.

In Chapter 3, the overall process of the study is depicted through a flowchart. The chapter also lists and explains the simulation software, materials, and equipment required for the study. Furthermore, it discusses the design, fabrication, and characterisation stages in detail.

Chapter 4 focuses on the parametric sweep analysis to determine the optimum performance of the antenna. It includes discussions on antenna geometry, dimensions, simulation results, and measurements. Additionally, this chapter evaluates the performance of the antenna.

Finally, Chapter 5 presents the conclusions drawn from the study and provides recommendations for future research directions.

CHAPTER 2

LITERATURE REVIEW

2.1 Introduction

Future wireless communication systems may benefit significantly from transparent and low-cost antennas. The advancement of transparent electronics, essential for discreetly embedding electronic devices on surfaces while maintaining optical transparency, has opened up a multitude of novel industrial possibilities across various sectors. These applications span from displays, eyewear, and solar panels to land-based communication systems, integrated circuits, and sensor technologies (Moharram and Kishk, 2016). The earliest transparent antennas were studied for windows, car windshields, and mobile wireless communications (Ito and Wu, 1991), (Yasin et al., 2011), and (Simons and Lee, 1997). This section will discuss the transparent material of the antenna, the transparent geometry, and the type of liquid antenna. Besides, the fabrication methods for producing the antenna will also be included in the discussion.

2.2 Recent Advancements in the Field of Transparent Antenna

Emerging materials and fabrication technologies have driven recent advancements in transparent wireless electronics. The choice of materials is critical for transparent antenna design, focusing on high optical transparency to avoid interference with other components. Numerous materials have been investigated, including indium-tin-oxide (ITO), indium-zinc-tin oxide (IZTO), transparent polymer film AgHT-4, and fluorine-doped tin oxide (FTO). However, these materials are often scarce, complex to fabricate, and costly. Glass has been used for specific applications like dielectric resonator antennas (DRAs) but lacks the flexibility required for curved surfaces, limiting its use in wearables and similar systems. Moreover, most transparent antennas still rely on metallic grounds, hindering full optical transparency.

An exciting development in antenna design involves leveraging nanotechnology to create intricate nanostructured transparent conductors (Sa'ad, Rahim et al., 2014). These nanostructures enhance electrical and optical characteristics, improving antenna performance. Additionally, researchers have

been working on designing transparent antennas capable of adjusting their operating frequencies, offering versatility for different communication standards. Notably, novel transparent and conductive materials like graphene and carbon nanotubes have emerged, enhancing electrical conductivity and optical transparency, thus paving the way for more efficient transparent antennas.

2.3 Transparent Geometry

Meshed conductors are traditional metal-based conductors that incorporate pre-fashioned grids, pores, or gaps on their surfaces to allow for light transmission (Clasen and Langley, 2004). These conductors are distinct from transparent thin films and offer lower optical transparency because they are made from unconventional, inherently transparent metals. While retaining high levels of electrical conductivity, they use the open areas inside their structures to facilitate light transmission. The primary metals used in manufacturing metal mesh films are copper (Cu) and silver (Ag), with copper being more commonly used due to its lower cost and greater availability. However, there is a trade-off, as optimising optical properties may lead to higher sheet resistance, necessitating a balance. Narrow grid widths and larger gaps are required to enhance transparency, but this can also increase sheet resistance and fail to maintain stability.

A semi-transparent antenna was developed using copper micromesh. This research introduces a novel method for creating semi-transparent and flexible RF small antennas utilising stretchable micromesh structures, as shown in Figure 2.1 (Jang et al., 2016). This highlights the potential of metal mesh films as suitable options for crafting flexible transparent antennas, emphasising the importance of manufacturing techniques for their durability. Additionally, it underscores that achieving good electrical conductivity may require some trade-offs in transparency levels. It shows that the antenna at the same resonant frequency with the difference at the mesh plane has a different bandwidth, gain, and radiation efficiency. The antenna without grid mesh obtained a 10 dB bandwidth of 2.93%, a gain of -3.04 dB, and a radiation efficiency of 85.4%. The antenna with grid mesh obtained a higher bandwidth of 3.53% but a lower radiation efficiency of 79.1% and a gain of -3.04 dB due to low conductivity.

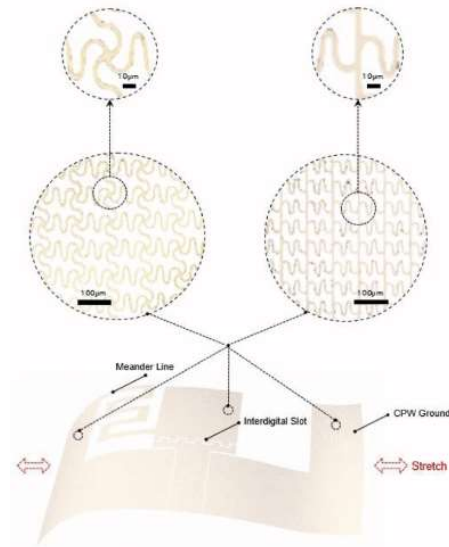


Figure 2.1: Semi-Transparent Antenna Using Mesh Method (Jang et al., 2016).

2.4 Transparent Material of Antenna

Due to the emergence of new materials and manufacturing techniques over the past several years, substantial improvements have been made to creating transparent wireless electronics. Further developments in the study of materials and production have become essential. The features of certain transparent conducting materials, including transparent conducting oxide, silver nanowires, and water, are highlighted in this section.

2.4.1 Transparent Conducting Oxide

Transparent conductive oxides (TCOs) are commonly used materials for transparent conductors due to their ability to facilitate Ohmic conduction. TCOs boast high carrier concentrations and excellent optical transparency, making them popular for transparent antenna fabrication. While their electrical conductivity is promising (typically around 10^5 S/m), it falls short of copper (5.8×10^7 S/m), resulting in higher antenna losses. Achieving both low sheet resistance and high optical transparency in TCOs is challenging. Common transparent conducting oxides (TCOs) include indium-tin oxide (ITO), fluorine-doped tin oxide (FTO), aluminium-zinc oxide (AZO), and gallium-doped zinc oxide (GZO). These materials are known for their ability to combine

transparency and electrical conductivity, making them valuable in various applications.

Transparent conducting oxides, however, have several uses, such as touch screens, front contacts for displays, and solar cells. An ITO film was used to build a transparent antenna (Colombel et al., 2009). As shown in Figure 2.2, the ITO film has an optical transparency of 80% and a sheet resistance of 8.6 Ω/Sq . This antenna achieved a gain of -4.1 dBi. Similarly, the development of a transparent antenna using an FTO film, where the FTO film had a sheet resistance of 7 Ω/Sq and an optical transparency of 74.29%, was explored (iZamudio et al., 2016). The resulting antenna had a gain of 0.43 dBi.

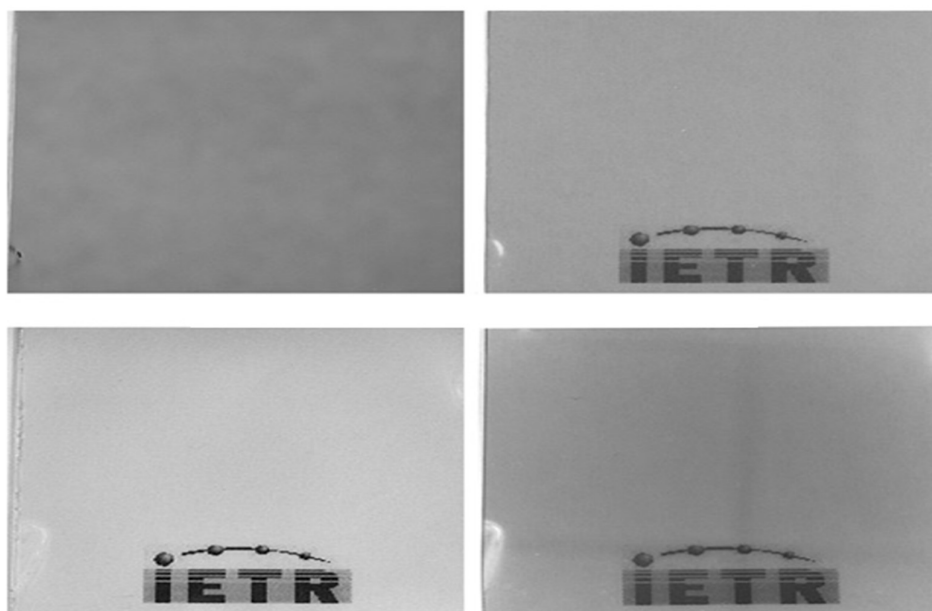


Figure 2.2: Transparent Antenna Using ITO Film (Colombel et al., 2009).

2.4.2 Silver Nanowire

Silver nanowires (AgNWs) and silver nanofilms (AgNFs) hold significant promise for flexible and transparent electronic applications due to their outstanding characteristics, including exceptional optical transparency, effective electrical conductivity, and mechanical durability suitable for flexible usage. For instance, a flexible and transparent fractal antenna is designed to operate in Wi-Fi, Bluetooth, and low-band 5G applications. This antenna was constructed using AgNW deposited on a polyethylene terephthalate (PET)

substrate. The AgNW patterns exhibited consistently low sheet resistance values ranging from 1.1 Ω/Sq to 9.2 Ω/Sq and high optical transparency levels ranging from 75.2% to 92.6% (Li et al., 2020). In another study, a transparent and flexible bowtie antenna was created by employing AgNWs patterned using a screen-printing method on a PET substrate. The resulting AgNW film displayed a commendably low sheet resistance of 8.5 Ω/Sq and an impressive transparency of nearly 85%, achieving a radiation efficiency of 52% (Goliya et al., 2019).

2.4.3 Water

Due to its beneficial properties, water is a possible material for creating flexible and transparent electrical devices. These include being readily available, affordable, transparent, outstanding liquid, easy to handle, having a high dielectric constant, and having decent electrical conductivity. Specifically, pure water is a dielectric substance characterised by substantial permittivity and notable dielectric loss while delivering nearly complete optical transparency within the visible light spectrum. Salt considerably improves the conductivity of clean water because it has limited conductivity without salt. Researchers have explored water-based antennas, utilising pure and saltwater to enhance performance and investigate water-based reconfigurable antennas.

A new water-based antenna was introduced, the dense dielectric patch antenna (DDPA) (Li and Luk, 2015). The patch and ground of a water-based patch antenna were created and contained in transparent plexiglass. The antenna functioned at a frequency of 2.4 GHz, producing conical radiation patterns in all directions, maintaining an 8% impedance bandwidth, achieving a peak gain of 7.3 dBi, and demonstrating an operational efficiency of 70% throughout its designated frequency range. While having high RF performance and transparency, these water-based antennas had bigger dimensions and lacked flexibility because of inflexible transparent materials in water holders. According to a different study, water was contained within transparent, bendable chambers constructed of PDMS polymer, creating very flexible, robust, small, and transparent antennas. With a tunable working frequency range of 2.38 GHz to 2.67 GHz, peak gain variations range from 2.28 dBi to 3.27 dBi, and efficiency variations range from 44.1% to 50.4%, it reaches a peak gain of

3.2 dBi and an efficiency of 51%. These findings demonstrate the great potential of water for developing durable, transparent, and flexible antennas (Sayem et al., 2021). Water's unique properties make it a promising candidate for creating transparent and flexible antennas, as demonstrated by the research ranging from water-filled antennas to highly flexible water-based designs with improved RF performance and transparency.

2.5 Types of Liquid Use in Liquid Antenna

An extensive overview of liquid antennas is provided in this section, where the primary conductor is a dielectric liquid. Figure 2.3 illustrates the categorisation of materials into metallic and non-metallic types, further divided into water-based and non-water-based variants. It is crucial to note that non-metallic liquid materials may exhibit conductive and non-conductive properties, whereas metallic liquid materials consistently possess conductivity.

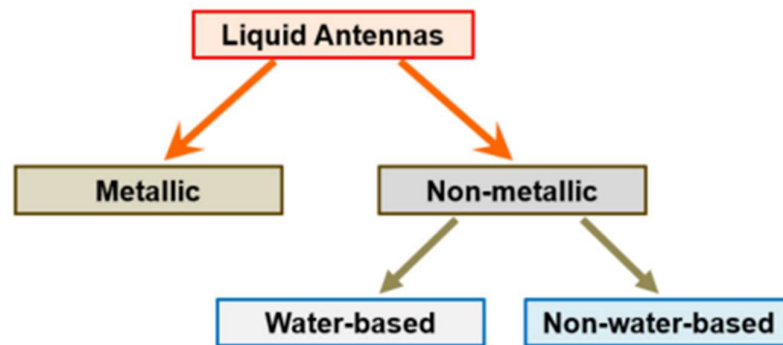


Figure 2.3: Classification of Liquid Antennas (Huang et al., 2021).

Liquid antennas, made from metals or non-metals, possess unique properties such as reconfigurability, flexibility, and reversibility. They can withstand mechanical changes and return to their original shapes. Using liquid to create antennas emerged in 1999 as a solution to challenges in constructing dielectric resonator antennas (DRAs) with solid materials (Kingsley and O'Keefe, 1999).

2.5.1 Metallic Liquid

In the 1990s, researchers began experimenting with liquid metals to create flexible and shape-changing antennas. They did this by putting liquid metal into a flexible material like PDMS. Mercury, although toxic, was initially used because of its liquid state at room temperature and good electrical conductivity. With a melting point of -39°C , mercury is a metal that remains liquid at ambient temperature and has an excellent electrical conductivity of $1 \times 10^6 \text{ S/m}$ (Zou et al., 2016). However, the toxicity limits its application. The challenge was to find alternative safe liquid metals that remained in a liquid state without being too costly.

Some metals, such as gallium, francium, caesium, and rubidium, can maintain a liquid state under certain circumstances. Within the realm of gallium-based liquid metal alloys, options like Eutectic gallium indium (EGaIn) and eutectic gallium indium tin (EGaInSn or Galinstan) have gained prominence, especially in the context of flexible antenna applications. For instance, EGaIn has excellent electrical conductivity and a melting point of 16°C . These liquid metals create a thin oxide layer when they come into contact with air, improving their mechanical stability and preventing evaporation (Paracha et al., 2019).

With a lower melting point of -19°C than EGaIn, the liquid metal alloy galinstan, made of gallium, indium, and tin, has comparable performance characteristics (Vorobyov et al., 2016). Limited options exist for alternative liquid metal materials suitable for antenna construction. GaIn ink, for instance, is a conductive fluid composed of 10% indium, 90% gallium, and around 0.026 % oxygen, providing the required viscosity for its ink-like application. Silver nano-ink is used to print antennas. These materials offer unique antenna design and fabrication possibilities, contributing to the diversity of available solutions in the field (Boley et al., 2014). However, the high melting point of silver nano-ink and its tendency to dry at room temperature present limitations (Baytöre et al., 2018). These metallic liquid materials typically have electrical conductivities in the range of 10^6 S/m , they significantly contribute to achieving high radiation efficiency when utilised as antenna materials. Galinstan is a leading choice in this category due to its favourable properties.

Liquid metal antennas offer flexibility and reconfigurability compared to conventional rigid antennas. EGaIn, a stable liquid metal alloy at room

temperature, has been utilised in various designs (Bo et al., 2018). Examples include foldable, stretchable patch antennas and flexible microstrip patch antennas. These antennas excel in mechanical adaptability and electromagnetic performance (Hayes et al., 2012; Low et al., 2019).

Recent innovations involve microfluidic technology and liquid pumps integrated with liquid metal, resulting in reconfigurable liquid antennas. Fluidic metal can move freely within the liquid channel, allowing significant modifications to the antenna's shape. Due to their flexible nature, liquid metal antennas offer a more comprehensive tuning range in frequency and emission pattern (Dey et al., 2016). In Figure 2.4, a two-octave tunable liquid-metal monopole antenna achieves frequency tuning from 2.0 GHz to 9.5 GHz. Figure 2.5 showcases a monopole antenna using liquid metal (specifically Hg) pumping technology and microfluidic channels. This setup achieved an impressive frequency tuning range from 1.29 GHz to 5.17 GHz across the frequency band (Dey et al., 2016).

Reconfigurable liquid metal antennas offer higher overall efficiency than electrically tunable antennas, which suffer from loss generation by active switches and diodes. Moreover, liquid metal antennas exhibit a significantly broader tuning range in frequency and emission pattern alteration due to their more adaptable antenna structure modifications.

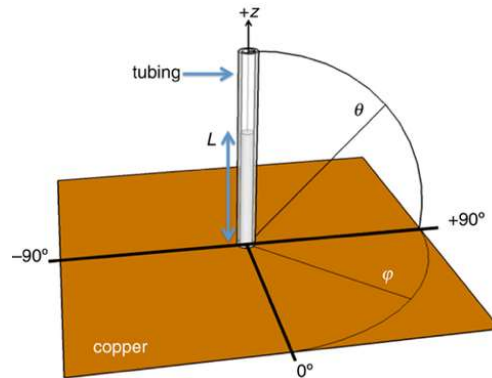


Figure 2.4: An Adjustable-length Liquid-metal Monopole Antenna Positioned Above a Ground Plane (Morishita et al., 2014).

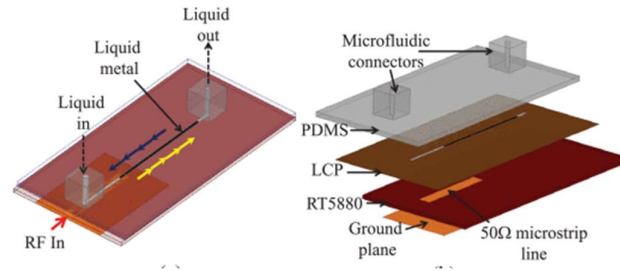


Figure 2.5: Liquid-metal Microfluidic Antenna (Dey et al., 2016).

However, they have limitations, including complex fabrication and slower tuning response. Integrating liquid pumps and microfluidic channels can increase antenna size and complexity. These antennas can be applied to rigid and flexible substrates, enabling versatile designs, including 3D printing of conductive fluids (Singh et al., 2019). In addition to flexible materials like PDMS, silicone rubber, and 3D-printable NinjaFlex, rigid substrates like Rogers RT Duroid 5880 have also been employed. Even the direct writing and printing of conductive fluids onto substrates with different architectures is now possible due to innovative approaches (Park et al., 2019).

Liquid metal antennas are useful in wearable and implantable applications, as they can conform to the body's skin and withstand movement-induced deformations. They have been employed in wireless sensor tags, wireless power transfer coils, and flexible electronic systems, showcasing their practical applications in wearable technology (Jobs et al., 2013).

2.5.2 Non-metallic Liquids

2.5.2.1 Water Based Liquid

Water-based liquid antennas have emerged as a favoured option owing to their cost-effectiveness, accessibility, eco-friendliness, and compact sizing relative to permittivity (ϵ_r), reduced radar cross-section (RCS) when drained, and transparency for discreet applications, rendering them suitable for discrete applications. Within this domain, two primary categories of water-based liquid antennas are being explored: saline and pure water antennas.

Water-based antennas are temperature-sensitive. Water freezes below 0°C , while saline water remains liquid to around -32°C with high salt content. Researchers have mixed water with substances like propylene glycol (PG) to

overcome this limitation to lower its freezing point. The addition of PG affects antenna efficiency, with a blend of water and 5% - 10% PG appearing to be the optimal choice for these antennas. However, adding PG also impacts the antenna's efficiency by decreasing performance (Martínez et al., 2022).

Research has explored various water-based antenna designs, including distilled water antennas with adjustable radiation patterns, broadband antennas optimised for saline water, broadband monopole antennas with dielectric layers, antennas for maritime wireless communication using seawater, and frequency-reconfigurable antennas enhanced with water properties (Fayad and Record, 2006, Kingsley and O'Keefe, 1999), (Subashini et al., 2022, Xing, et al., 2015), and (Chen et al., 2022).

Pure water antennas have been developed, including tunable and polarization-switchable designs (Zhong et al., 2018). Some employ auto-control systems for efficient tuning (Wang and Chu, 2019, Xing et al., 2019). Also, a water patch antenna was successfully engineered with impressive characteristics. This innovative antenna design boasted a wide bandwidth, reaching a remarkable 35% at $S_{11} < -10\text{dB}$, signifying its versatility across various frequencies (Sun & Luk, 2017). The antenna exhibited a substantial far-field gain of up to 4 dBi, showcasing its efficiency in emitting electromagnetic waves in a specific direction. Notably, the antenna achieved a remarkable radiation efficiency of 70%, indicating its exceptional ability to convert input power into radiated electromagnetic energy. The designed antenna is shown in Figure 2.6.

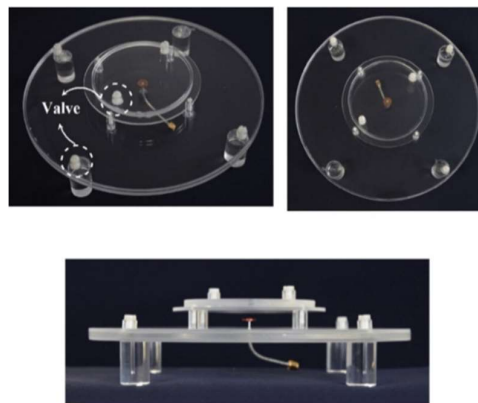


Figure 2.6: Water Patch Antenna (Sun and Luk, 2017).

The U.S. Navy developed a seawater antenna that demonstrates long-range performance across a wide frequency range (2 MHz to 400 MHz), as shown in Figure 2.7. This antenna offers customisation, compactness, and the ability to blend into the surroundings when unused. Research in water-based antennas inspired improved bandwidth, reconfigurability, and radiation efficiency, such as the fractional bandwidth $> 70\%$ for $S_{11} < -10$ dB. Meanwhile, the bandwidth of an identical metal antenna only achieves a bandwidth of less than 20% (Xing, 2015).



Figure 2.7: Sea Water Antenna (Xing, 2015).

Saline water antennas face challenges related to efficiency, influenced by the liquid's loss tangent or conductivity. Research has shown that radiation efficiency is highest (80%) when the conductivity is either very low (0.001 S/m (acting as an excellent dielectric resonator antenna) or very high 1000 S/m (functioning as a good conducting antenna) (Xing et al., 2012). Techniques like adding metallic elements to the antenna design have been employed to improve radiation efficiency. Saline water antennas offer continuous frequency tuning and adjustable bandwidth (Hua et al., 2014).

Hybrid antennas combine pure water dielectric resonator antennas with metal antennas to address challenges like low efficiency or narrow bandwidth. These hybrids increase radiation efficiency and broaden bandwidth. Pure water's transparency makes it ideal for wearable and IoT applications. For instance, it has been proposed to use conductive mesh and an optically transparent wearable antenna to convert the antenna's bidirectional radiation pattern into a unidirectional broadside pattern, with excellent radiation

efficiency (51% at 2.45 GHz), and low specific absorption rates have been achieved (Sayem et al., 2020).

Water-based liquid antennas offer many properties, including size reduction and cost-effectiveness advantages, strong radiation efficiency at lower frequencies, and broad bandwidth. They enable the reconfiguration of radiation patterns, polarisation, and discrete or continuous frequency adjustment. They should be designed with practical considerations like loss, frequency, and temperature fluctuations.

2.5.2.2 Non-water Based Liquid

In response to the limitations posed by the sensitivity of water-based materials to temperature and frequency fluctuations in liquid antennas, researchers have developed non-water-based liquid materials. These alternatives typically fall into two main categories: solvents, oils, and ionic liquids. By exploring these alternative materials, researchers aim to mitigate the drawbacks associated with water-based solutions, thereby enhancing the stability and performance of liquid antennas.

Research has explored the utilisation of non-aqueous liquids in antenna design, including ionic liquids, low-loss organic solvents such as acetone and ethyl acetate, and oils like mineral and transformer oil. These fluids are advantageous for antenna applications because they maintain stability due to temperature and frequency variations (Bennett et al., 2019). Most of these liquids exhibit relative permittivity values ranging from 2 to 30 over frequencies and electrical conductivities less than 0.001 S/m. Unlike water-based materials, they offer more stable properties against changes in temperature and frequency, such as more minor loss tangents, stable dielectric relaxation, and lower freezing points. For instance, ethyl acetate's liquid organic solvent has a loss tangent of 0.04 and a relative permittivity of around 6. It remains stable until 50°C and freezes below -20°C. Oils are another option for making antennas, but their relative permittivity is typically low (around 2.5), and their high loss tangent (around 0.1) might not make them suitable for many antennas (Konca and Warr, 2015). However, solvents and oils often pose safety concerns due to flammability and volatility, making them less safe and non-environmentally friendly, particularly for high-power applications.

Ionic liquids, which are salts that remain liquid at average temperature, hold great potential for RF and microwave applications because of their excellent qualities, such as thermal stability, low vapour pressures, changeable electric conductivity, nonflammability, and a broad electrochemical range (Song et al., 2019). Ionic liquids at room temperature are mixtures of inorganic anions and organic cations, and several tests have been made to learn more about their electromagnetic properties (Song et al., 2019).

Solvents and oils like ethyl acetate have created liquid Dielectric Resonator Antennas (DRAs) within glass housing, offering reconfigurability in pattern and polarization (Chen and Wong, 2017; Ren et al., 2020). These antennas have achieved over 80% radiation efficiency within the 3.5 GHz to 4.5 GHz frequency range. Also, it achieves a positive gain > 6 dB. However, some oils and solvents might not be able to bond chemically with particular types of plastic, which might lead to problems with disintegration over time. When ethyl acetate is present, the 3D-printed container and liquid pipelines may disintegrate over time.

Liquid-assisted or hybrid reconfigurable antennas have utilised transformer and castor oil, recognised for their chemical stability. Despite their relatively low permittivity, they effectively broaden the tunable impedance bandwidth, achieving up to 32%. Oil injected into a chamber beneath standard metal antenna radiators, such as patch antennas, allows adjustments to the antenna's frequency by carefully controlling the oil volume. For instance, in a patch antenna configuration, the bandwidth extended from 1.42 GHz to 1.96 GHz, surpassing conventional microstrip patch antennas, as shown in Figure 2.8. Radiation efficiency remained consistently high, exceeding 85% across the entire frequency spectrum, demonstrating the efficacy of these dielectric oil-based materials (Konca and Warr, 2015).

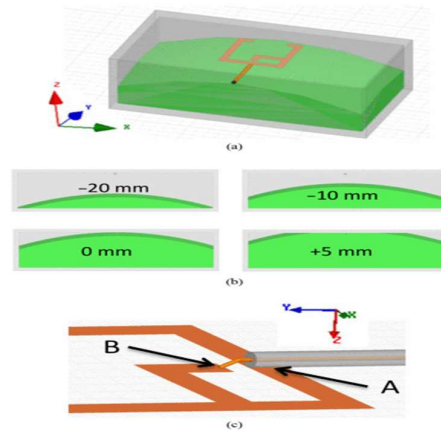


Figure 2.8: Liquid Antenna Using Transformer Oil (Konca and Warr, 2015).

Another intriguing avenue explores Ionic Liquid Antennas, where innovative materials are employed effectively. Choline L-alanine, for instance, has been used to craft a wideband circularly polarised (CP) liquid DRA featuring a unique spiral-shaped feeding structure (Song et al., 2019). It leads to impressive antenna performance with a CP bandwidth of 34% and over 80% total efficiency. T-chloride, another low-loss ionic liquid, has been employed as a dielectric antenna loading material, enabling a 40% reduction in antenna size while maintaining high efficiency across a wide frequency band. Additionally, combining a DRA and a magnetoelectric dipole (ME dipole) submerged in an ionic liquid has produced a performance with an efficient overall bandwidth of 73.5%. These non-water-based liquid materials reduce the sensitivity of liquid antennas to temperature and frequency changes, enhancing reliability and performance across various applications.

2.6 Factors Affecting the Performance of Liquid DRA

There are two types of frequency-reconfigurable antennas with liquid mechanisms. One of the categories is to physically or by dielectric loading alter the electrical length of the radiators. Another is to dynamically change the antenna's resonant mode, which resonates at various frequencies. To the best of available knowledge, the antenna's resonant modes are intrinsic and challenging to change to fulfil demands such as maintaining the stability of radiation performance at various resonant modes.

2.6.1 Type of Dielectric Liquid Effect

The critical material properties of interest include permittivity, conductivity, and permeability. Liquid dielectric materials offer advantages because of their fluidity and ability to conform to various shapes. This flexibility is valuable in designing antennas that can be reconfigured. In liquid-based antennas, where a dielectric liquid is the main radiating element, the antenna's shape can be easily adjusted by changing the liquid's height, volume, or shape. High permittivity dielectric liquids like water (with a permittivity of approximately 80) can help reduce the antenna's size. Still, they become less efficient at higher frequencies (> 1 GHz) due to increased loss tangent. Adding salts like NaCl or KCl to water enhances conductivity and widens the antenna's bandwidth. Water's permittivity varies with temperature, offering a tuning mechanism, but this can also limit its operation to a specific temperature range. Some organic liquids with broader temperature ranges have been proposed. Oils, for instance, have lower losses, potentially improving radiation efficiency, but their permittivity is much lower than that of water, affecting their tuning range. Some ionic liquids, such as ethyl acetate, are proposed. However, it has a low permittivity, resulting in a bigger size. Generally, a higher permittivity in the dielectric liquid allows for a broader frequency tuning range (Motovilova and Huang, 2020).

2.6.2 Ground Size

The impact of varying the ground plane length on a reference antenna was investigated, with other parameters constant. Figure 2.9 shows significant changes in the resonant frequency and fractional bandwidth. Initially, increasing ground length led to a significant decrease in the resonant frequency and a notable increase in fractional bandwidth. However, when ground length exceeded approximately 150 mm, equivalent to one wavelength of the 2 GHz resonant frequency, further changes in ground length had decreasing impacts on the fractional bandwidth and the resonant frequency. This finding is consistent with the rule that a ground plane for monopole devices should be at least one wavelength large to minimise edge diffraction and radiative power loss (Xing et al., 2015).

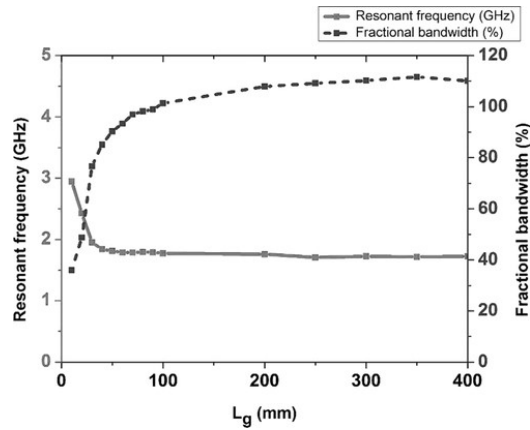


Figure 2.9: Ground Plane Width, Resonant Frequency, and Fractional Bandwidth (Xing et al., 2015).

2.6.3 Feeding Effect

The feeding configuration of a symmetric antenna structure was studied by adjusting the feeding offset, which shows where the SMA connection is located to the water's centre and the probe length within the water, as shown in Figure 2.10. These alterations were explored while keeping all other parameters constant, similar to the reference antenna. The results showed a clear relationship between feeding effects and water conductivity. Modifications in the feeding offset and probe length within the water don't impact the resonant frequency and fractional bandwidth as long as the water conductivity exceeds approximately 4 S/m, equivalent to seawater conductivity. The water antenna functions more like a conducting antenna under these circumstances than a dielectric resonant antenna, which makes it more resistant to changes in the feeding pin and probe. Conversely, when the water conductivity is substantially lower than 4 S/m, the water antenna behaves like a Dielectric Resonant Antenna (DRA). The antenna's performance may be changed by varying the feeding pin's position while tweaking the conductive probe's length to achieve impedance matching. This problem often occurs with most DRAs but not this monopole water antenna (Xing et al., 2015).

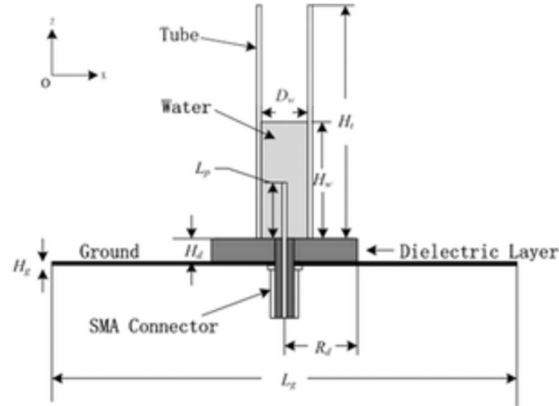


Figure 2.10: Cross-sectional View of Antenna.

2.6.4 Liquid Holder's Diameter Effect

When varying the diameter of the liquid holder between 4 mm and 40 mm, the antenna exhibited two resonant frequencies below 4 GHz, resembling a conventional conductive monopole antenna. As the water tube diameter was increased, the second resonant frequency (referred to as “resonant frequency 2”) shifted downward, approaching the first resonant frequency (“resonant frequency 1”). Changes in current distributions further illustrated this. The current distribution drastically altered with increased water tube diameter, notably for the second resonant frequency. The current pattern for the second resonant frequency resembled the first one when the water tube diameter increased, expanding the antenna’s bandwidth. Like a conducting monopole, a thicker antenna resulted in a wider bandwidth.

As for variations in water height, ranging from 34 mm to 74 mm, the simulation results shown in Figure 2.11 and Figure 2.12 indicated that the fractional bandwidth remained relatively unaffected by these changes. However, the resonant frequency experienced a reduction from 1.88 GHz to 1.40 GHz (a significant deviation from the expected 0.94 GHz for a conductive antenna). Additionally, the radiation efficiency at the central frequency decreased slightly, dropping from 58% to 47%. Doubling the water height did not yield a halving of the resonant frequency, primarily due to material losses as electromagnetic waves traveled through the water.

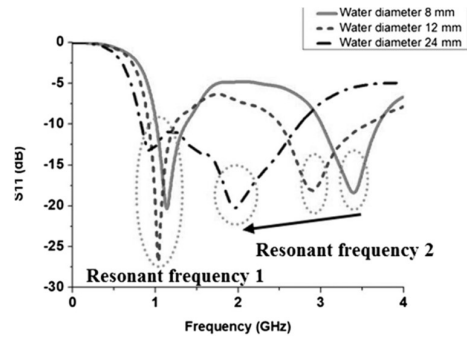


Figure 2.11: Effect of Liquid Holder's Diameter on Antenna's Resonant Frequency (Xing et al., 2015).

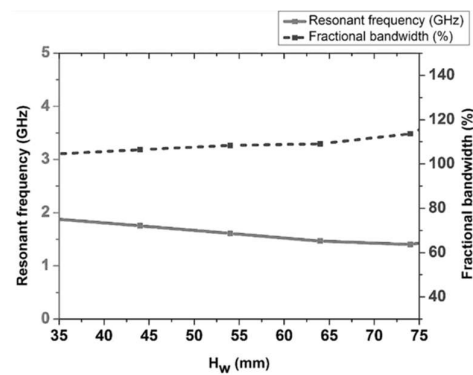


Figure 2.12: Effect of Liquid Holder's Height on Antenna's Resonant Frequency (Xing et al., 2015).

2.7 Summary

This section discusses the advancements in transparent antennas, the introduction of liquid antennas, the materials used to make them transparent, and the various types of antennas. It also explores the factors that affect antenna performance.

In comparing different liquids, it was found that ethyl acetate, due to its low loss tangent and affordable cost, can achieve the best radiation efficiency for dielectric resonator antennas. Conversely, water has a high dielectric constant and high loss tangent, providing an interesting comparison to ethyl acetate.

Additionally, flexible materials like silicone rubbers such as PDMS and Ecoflex can be utilised in antenna fabrication. These materials are easy to work with and can conform to soft and irregular surfaces. Their flexibility allows for bending and shaping, enhancing their antenna application capabilities.

CHAPTER 3

METHODOLOGY AND WORK PLAN

3.1 Introduction

This chapter will explore the simulation software, materials, and equipment for creating a cost-effective, nearly transparent antenna. The primary focus is designing a dielectric resonator antenna (DRA) using Ecoflex and ethyl acetate. An antenna design utilising Ecoflex and water as the liquid was also modelled for comparison. Furthermore, this chapter comprehensively describes the antenna fabrication process and a detailed flowchart illustrating the study's workflow and progress. With a better understanding of the prototype behaviour, several evaluation methods are introduced, including transparency and signal strength. An IoT Smart Lighting application is also introduced to demonstrate the prototype's potential use.

3.2 Design Flow

The project adheres to a structured workflow comprising several vital stages, antenna design using CST simulation software, material preparation, mould creation through 3D printing, antenna fabrication, and characterisation of the fabricated antenna. Should the antenna fail to meet specifications, iterative refinements are made to the fabrication process until the desired measurements are achieved. The prototype evaluation process is initiated once the design meets specifications, such as resonating at 2.4 GHz and having an S_{11} lower than -10 dB. This workflow is illustrated in Figure 3.1.

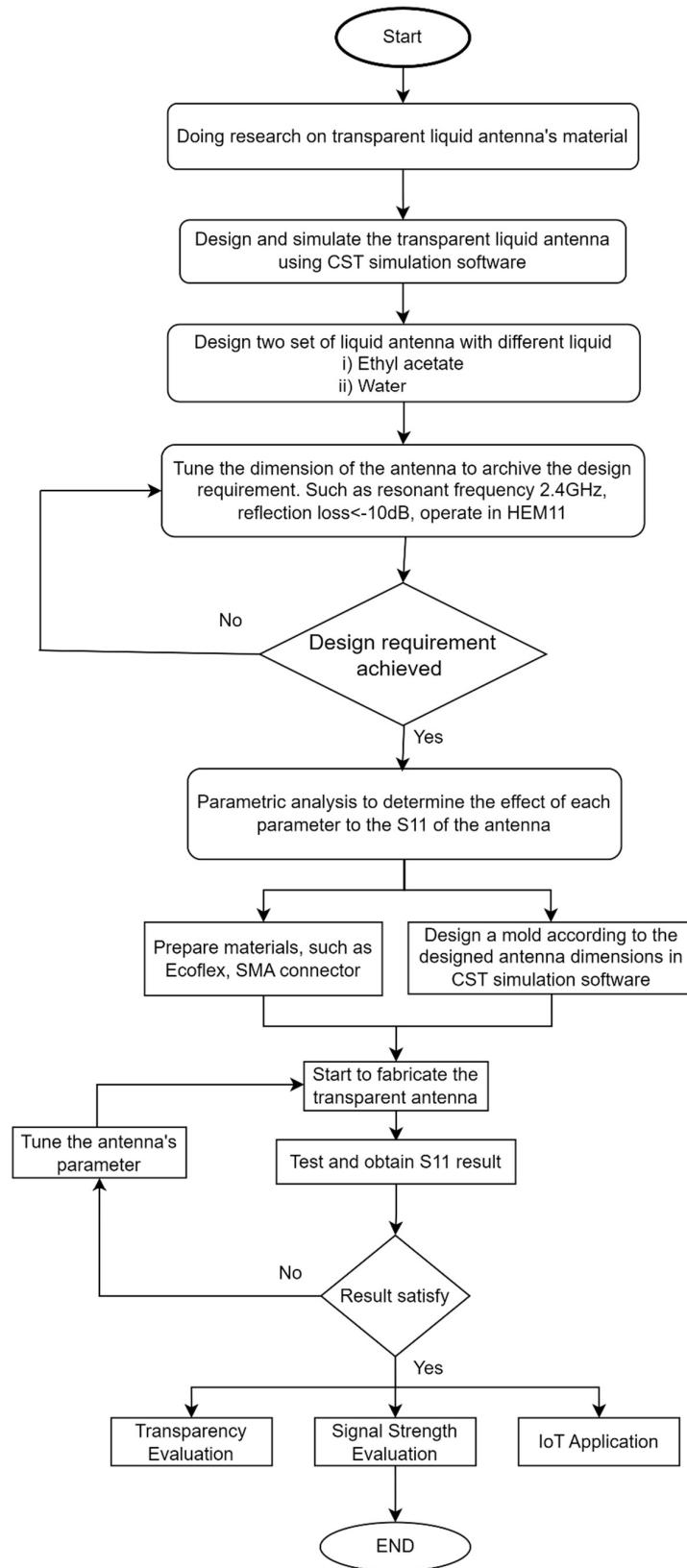


Figure 3.1: Flow Chart of The Overall Process of The Study.

3.3 Simulation Software and Setup

In this project, the software CST (Computer Simulation Technology) Studio Suite is depicted in Figure 3.2. It is an electromagnetic simulation software and is user-friendly. Following each simulation, it furnishes users with essential results, such as S-parameters indicating the resonant frequency, far-field gain at specific frequencies, and other pertinent data. This capability enhances the analysis of electromagnetic waves (EM waves) and facilitates the validation of antenna designs with heightened accuracy and efficiency.

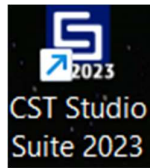


Figure 3.2: CST Studio Software.

3.4 The Material Selection

The antenna comprises a metallic ground plane, a liquid holder, and a dielectric liquid as the radiator. To construct a cost-effective and nearly transparent liquid Dielectric Resonator Antenna (DRA), materials such as water, ethyl acetate, Ecoflex, a 0.06 mm thickness copper sheet, SMA connector, and copper are utilised.

Ecoflex 0030, showcased in Figure 3.3, is the prime choice for antenna manufacturing due to its transparency, flexibility, chemical inertness, and ability to withstand high temperatures and torsion. Ecoflex has a relative permittivity of 2.02 and a low loss tangent of 0.02 (Low et al., 2020). Although PDMS is more transparent than Ecoflex, the latter is favoured due to its easy purchase accessibility. The ethyl acetate and Ecoflex prices are shown in Figures 3.4 and Figure 3.5.



Figure 3.3: Ecoflex 0030.

HOME → ETHYL ACETATE

Ethyl Acetate

Ethyl acetate (systematically ethyl ethanoate, commonly abbreviated EtOAc, ETAC or EA) is the organic compound with the formula CH₃-COO-CH₂-CH₃, simplified to C₄H₈O₂.

R&M,2402-50, Ethyl Acetate, A.R, 2.5L

* 10 units left

from
MYR89.00

Add to Wishlist BUY NOW or ONLINE QUOTE

Figure 3.4: Price of Ethyl Acetate (KSFE, 2021).

Smooth-On, Inc.

Ecoflex 00-30 – Super-Soft, Addition Cure Silicone Rubber – Pint Unit

Item #: 403325

★★★★★ 4.6 rating Write a review

MYR 245

Order now and get it around Sunday, September 24

Color : Clear

Figure 3.5: Price of Ecoflex (Ubuy.com, n.d.).

3.5 Designing Stage

3.5.1 Designing of the Antenna

The decision to utilise a low-cost liquid Dielectric Resonator Antenna (DRA) for this project stemmed from its affordability and the accessibility of materials, in contrast to other antenna designs. Operating in the HEM₁₁ mode, the resonance frequency of the designed antenna could be calculated using a formula based on antenna size parameters. The resonance frequency equation can be expressed as (Gupta et al., 2009) :

$$f_0 = \frac{3 \times 10^8}{2\pi\sqrt{\epsilon_r}} \sqrt{2\left(\frac{\pi}{a}\right)^2 + \frac{\pi^2}{2h}} \quad (5)$$

where

a = radius of DRA

h = DRA's height

ϵ_r = Relative permittivity of the material

However, this formula became inapplicable due to the design's mesh ground plane structure, which significantly affects the resonant frequency when the ground plane is cut with some slots. As there was no readily available formula for designing this DRA with the mesh slot cutting ground plane, the preliminary design process relied on referencing relevant journal knowledge related to DRAs.

The design process was conducted by applying fundamental principles from these journals and adhering to some basic design requirements. These requirements included designing the antenna to operate at the resonance frequency of 2.4 GHz with a positive far-field gain. The desired radiation pattern for the antenna was unidirectional, meaning that radiation should be concentrated in a specific direction. Before designing the antenna, it was essential to establish the coordinate system's location, serving as the reference point for the antenna's components. While it was possible to change the coordinate system's position for convenience, doing so for different parts could lead to confusion during the tuning process.

Furthermore, the antenna's dimensions and parameters played a vital role in its performance. Consequently, the design process required multiple iterations until the desired requirements were met. To streamline this process, the dimensions of the antenna components were set using specific parameters. All these parameters were consolidated in a parameter list, simplifying the modification of component dimensions. Figure 3.6 shows an example of a parameter setup for reference.

Name	Expression	Value
ground_thickness	= 1	1
ground_long	= 65	65
ground_length	= 65	65
cylinder_d	= 35	35
cylinder_h	= 30	30
water_d	= 33	33
water_offset	= 4	4
pin_L	= 20	20
move_z	= 0.22	0.22
water_h	= 25	25
move_x	= 6.2	6.2
DG_L	= 45	45
DG_WIDTH	= 1	1
DG_DISTANCE	= 2	2
DG_OFFSET	= 5	5
DFG_OUTERr	= 15	15
DFG_INNERr	= 10	10

Figure 3.6: Dimensions Setting.

Numerous iterations are carried out after the design or modification phases during the simulation phase of the antenna design. Two approaches might be used for this iterative simulation procedure. The parametric sweep function of CST is used in the first technique. This method gives results for various dimension settings by specifying precise dimensions of the antenna components within a given range. Although this strategy simplifies the simulation process, the lengthy simulation times make it time-consuming. As an alternative, the second simulation technique uses a trial-and-error process. Each antenna component's unique dimensions are changed until the design requirements are satisfied. Although this approach is more flexible, running simulations and changing the dimensions may need more manual work.

Monitoring key parameters such as S-parameters, far-field gain, E-fields, and H-fields is essential throughout the simulation. The S-parameters, notably S_{11} , measure the antenna's reflection coefficient, revealing how much energy is reflected to the port. A favourable outcome is attained when the reflection coefficient falls below -10 dB. The lowest peak in the S_{11} graph indicates the frequency at which the antenna resonates, implying minimal power reflection. This signifies that the antenna absorbs approximately 90% of its energy, thereby mitigating reflections. The equation for S_{11} is expressed as:

$$S_{11} = 20 \log_{10} \frac{V_{reflected}}{V_{incident}} \quad (6)$$

where

$V_{reflected}$ = Voltage of the reflected wave

$V_{incident}$ = Voltage of the incident wave

After assessing impedance matching using S_{11} , the antenna's input impedance is further evaluated using the Z-matrix (Z-parameters). The consistency between the resistance and impedance findings obtained from S_{11} at the resonance frequency is examined using the Z-parameters. Z_{11} denotes the antenna's impedance, typically set to 50Ω to match the characteristic impedance of the transmission line or cable. This alignment ensures efficient power transfer, minimises signal reflections, and optimises the system's overall performance, facilitating seamless signal transmission between the antenna and the rest of the system components. The far-field simulation outcomes also show the antenna's radiation pattern and gain at a specific frequency. The magnetic field (H-field) may be used to find the locations where the magnetic field is being projected, and the electric field (E-field) assesses the performance and behaviour of an antenna, including impedance matching, radiation pattern, and polarisation.

3.5.2 Conceptual and Actual Design of the Antenna

Based on a design detailed in a specific paper (Xing et al., 2015), the preliminary design was created. It involves a cylindrical structure with 25 mm in diameter and 100 mm in height, as shown in Figure 3.7. A metallic ground plane with a dimension of $200 \text{ mm} \times 200 \text{ mm} \times 2 \text{ mm}$ is also supplied. The metallic ground plane supports the liquid holder, and the probe is fastened between these two elements. Additionally, since the cylinder holder's material is not specified, Ecoflex was employed in this design.

However, this design is optimised for low-frequency applications, while the desired application in this study is at a high frequency of 2.4 GHz. Moreover, the large size of the ground plane increases costs and does not fulfil the transparency requirement. Modifications or a new design may be necessary to address these issues. Alternative antenna designs suitable for high-frequency

applications, such as miniaturised or mesh ground design antennas, should be explored to meet the specific requirements of the study.

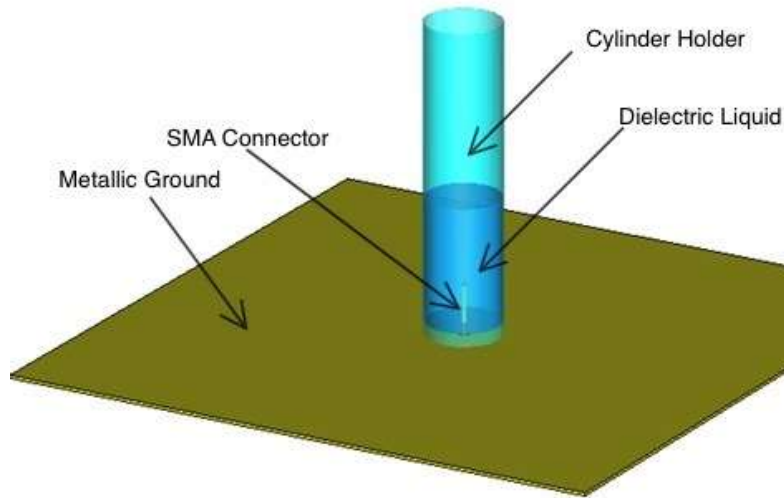


Figure 3.7: Preliminary Design of Liquid DRA.

The secondary antenna design underwent significant modifications, as illustrated in Figure 3.8. Notably, the antenna's size was substantially reduced for both the ethyl acetate and water models. This reduction was a critical step to minimise losses and lower fabrication costs. In Figure 3.9, adjustments were made to the antenna ground plane by introducing slots using a mesh technique, thereby improving visibility and aligning to create a nearly transparent antenna. Additionally, the size of the cylinder holder was fine-tuned until optimal performance was achieved. It is essential to highlight that despite the differences in dimensions and the use of distinct dielectric liquids in the two models, they both resonated at the same frequency, approximately 2.4 GHz.

For the ethyl acetate model, the modified antenna design produced the best results at a frequency of 2.408 GHz, yielding a far-field gain of 2.88 dBi. Similarly, in the case of the water model, the modified antenna design demonstrated optimal performance at a frequency of 2.412 GHz, resulting in a far-field gain of -2.55 dBi.

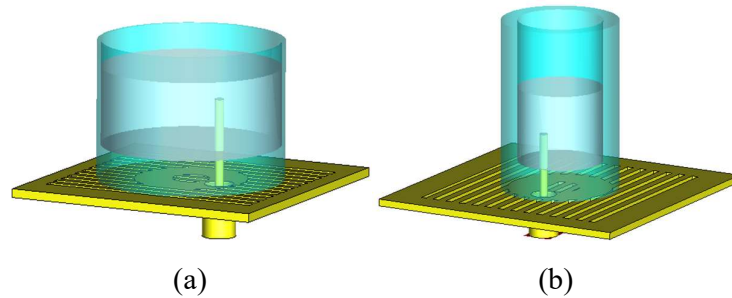


Figure 3.8: Secondary Antenna Design (a) Ethyl Acetate Model and (b) Water Model.

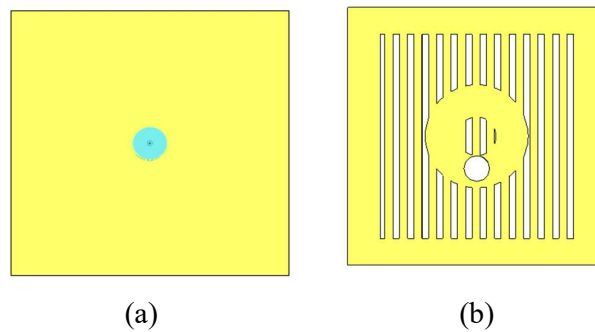


Figure 3.9: Ground Plane Modification (a) Conceptual Design without Mesh and (b) Using Mesh Technique.

The final antenna design underwent significant modifications, as illustrated in Figure 3.10. The amendment is on the metallic ground plane, initially using a 1 mm thickness copper plate and changing to a 0.06 mm copper sheet. This reduction was a critical step to minimise losses and lower fabrication costs. A specific laser cutter is required to perform the mesh ground technique on a 1 mm thick copper plate, which may need to be more cost-friendly. The antenna's far-field gain increased by reducing the ground plane's thickness. Additionally, a cap was added to seal the liquid, providing flexibility in positioning the antenna. Furthermore, the width of the mesh ground slot was increased to enhance transparency, allowing light to pass through more easily. Additionally, the thickness of the cylinder-shaped DRA has been reduced from 5 mm to 3 mm. This reduction lowers fabrication costs due to decreased Ecoflex required and improves overall transparency.

For the ethyl acetate model, the modified antenna design produced the best results at a frequency of 2.408 GHz, yielding a far-field gain of 5.13 dBi.

Similarly, in the case of the water model, the modified antenna design demonstrated optimal performance at a frequency of 2.4 GHz, resulting in a far-field gain of 4.13 dBi.

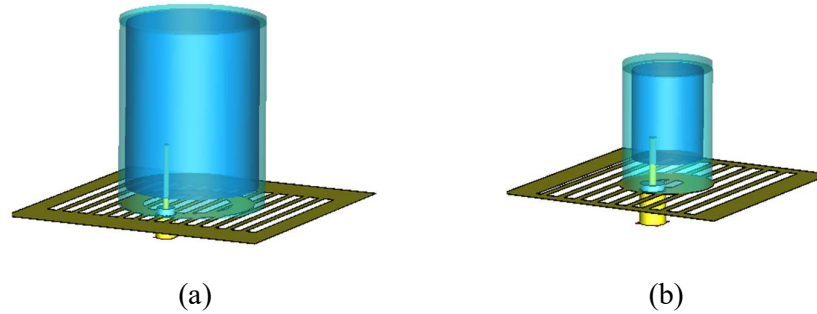


Figure 3.10: Final Antenna Design (a) Ethyl Acetate Model and (b) Water.

3.6 Fabrication and Assembly of Antenna

3.6.1 Molding, Curing and Demolding Process

Following the design, simulation, and modification phases, moulds for the antenna are generated using Solidworks. The dimensions of these moulds are extracted from CST software. Polylactic acid (PLA) filaments are employed with the assistance of a 3D printer to create these moulds. Two sets of moulds are crafted: one for the water-based antenna and another for the ethyl acetate-based antenna, as shown in Figure 3.11 and Figure 3.12.

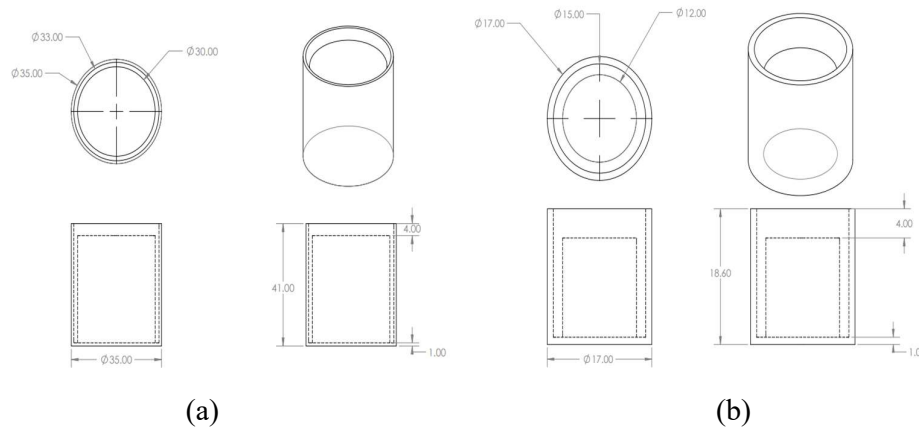


Figure 3.11: DRA Mould Design of (a) Ethyl Acetate Model and (b) Water Model.

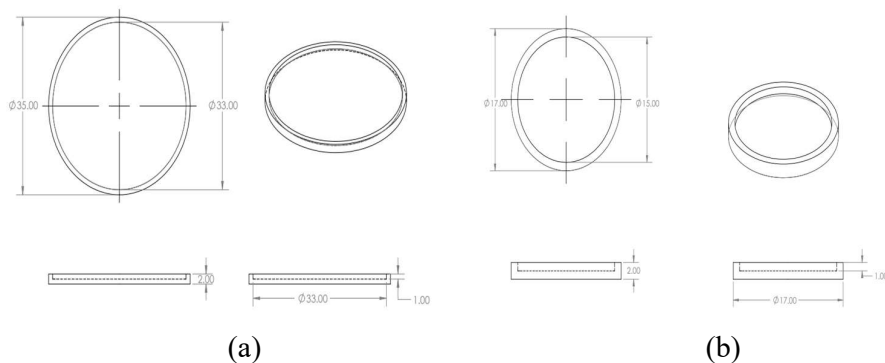


Figure 3.12: Cap Mould Design of (a) Ethyl Acetate Model and (b) Water Model.

The Ecoflex mixture preparation, as depicted in Figure 3.13, adheres to the instructions specified in the datasheet, which involve mixing solutions A and B in a 1:1 ratio. Three containers are employed: solution A is poured into Container A, solution B into Container B, and Container C is allocated for mixing purposes. The mixing procedure necessitates the use of a precision weighing scale. Subsequently, once the Ecoflex mixture is prepared, it is poured into the 3D-printed mould, as illustrated in Figure 3.14.



Figure 3.13: Preparation of Ecoflex.

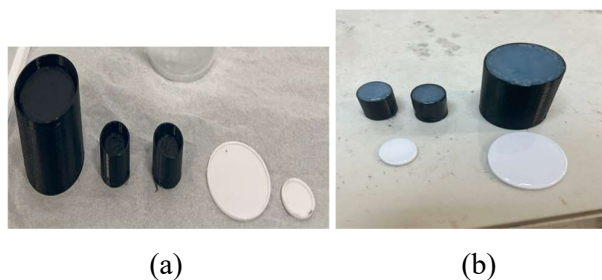


Figure 3.14: 3D Printing Mould (a) Before Ecoflex Filling and (b) After Ecoflex Filling.

To ensure the quality of the moulding process using Ecoflex, a vacuum pump with a chamber is employed to eliminate air bubbles, as shown in Figure 3.15. Once the Ecoflex is poured into the 3D-printed mould, it must be promptly placed into the vacuum chamber. Ecoflex cures rapidly, and any delay in vacuuming may result in trapped air bubbles within the material. Therefore, immediate vacuuming is essential to achieve a bubble-free mould and ensure the integrity of the final product.



Figure 3.15: Vacuum Pump with Chamber.

Once the Ecoflex has cured and solidified, it can be removed from the mould, as depicted in Figure 3.16. The DRA and cap are combined into a single rigid body using a small amount of Ecoflex. The process may need to be repeated if the final product fails to meet quality standards due to air bubbles or defects. These precautions are taken to guarantee the production of a high-quality and defect-free Ecoflex antenna.

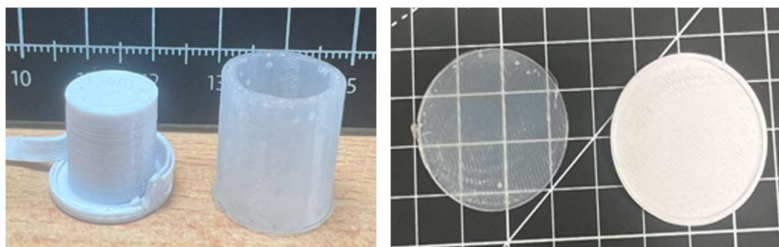


Figure 3.16: The DRA and Cap Extracted from The Mold.

3.6.2 Mesh Ground Plane Fabrication

Once the antenna design is completed, the 2D ground plane can be exported from the CST Simulation software to Silhouette Studio in DXF format. These designs are then utilised to cut the copper sheet using a Silhouette Portrait

machine, as depicted in Figure 3.17. The decision to employ the Silhouette Portrait cutter is based on its superior cutting precision compared to manual cutting techniques involving blades and scissors. Figure 3.18 showcases the slot design for both the ethyl acetate and water DRA.

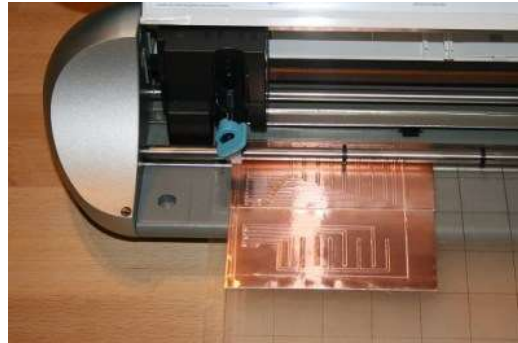


Figure 3.17: Silhouette Portrait Cutter.

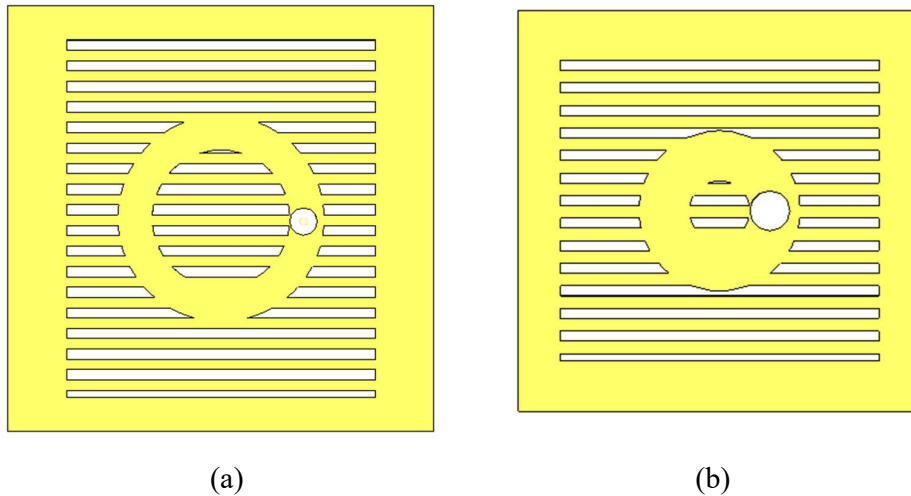


Figure 3.18: Slot Design of Ground in (a) Ethyl Acetate Model and (b) Water Model.

To minimise the wastage of the copper sheet, the recycled paper was utilised for testing purposes to determine the cutter blade reference point, as shown in Figure 3.19. Specific precautions must be taken when cutting the copper sheet with the Silhouette Portrait. To prevent unintended movement during the cutting process, it is essential to securely affix the copper sheet to the cutting board. This can be achieved using adhesive tape or clamps to hold the sheet firmly. Furthermore, careful attention should be given to verifying the

alignment of the slot designs within the Silhouette Studio software to ensure their precise correspondence with the intended locations on the copper sheet. Figure 3.20 depicts the surface of the copper sheet before and after the cutting process. Despite the cutting attempt, the sheet remains incompletely cut through, necessitating manual tearing to remove the cut rectangle slot. The final product is depicted in Figure 3.21.



Figure 3.19: Trial Cutting Process.

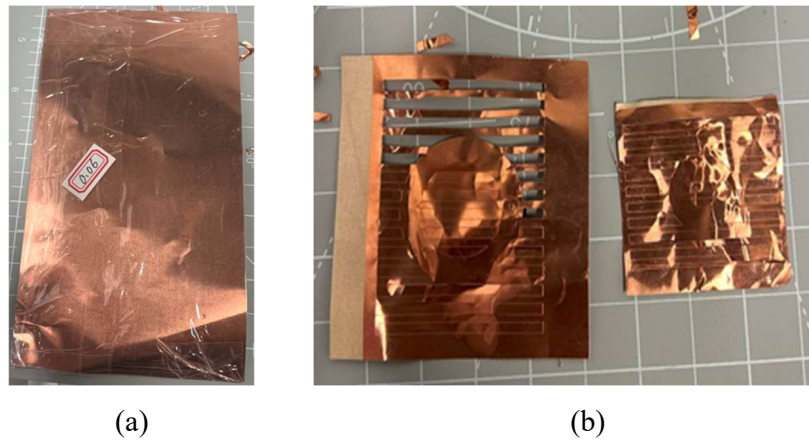


Figure 3.20: Copper Sheet (a) Before and (b) After Cut.

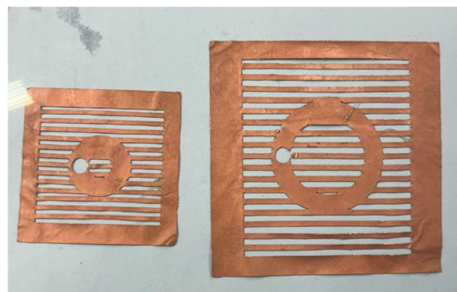


Figure 3.21: Final Product.

To address the risk of the thinner copper sheet warping and potentially impacting antenna performance, a transparent plastic sheet was cut and carefully taped to the copper, as shown in Figure 3.22. This method ensures that the copper remains flat and securely adhered to the plastic without compromising the performance and transparency of the antenna.

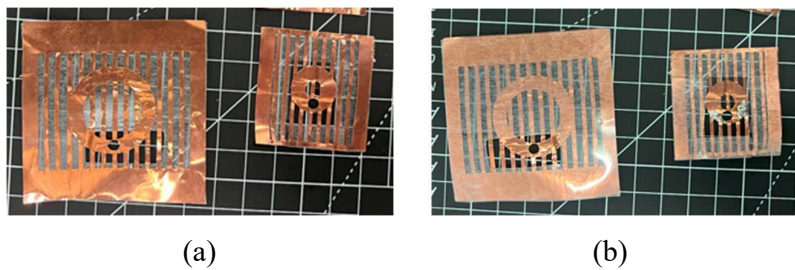


Figure 3.22: Copper Sheet with Transparent Plastic (a) Top View and (b) Bottom View.

3.6.3 SMA Connector Fabrication

SMA stands for “SubMiniature version A”, a coaxial RF connector widely used for connecting antennas to radio frequency (RF) equipment, such as routers, radios, and other communication devices. SMA connectors are popular due to their compact size, robustness, and suitability for high-frequency applications. They come in various sizes, including SMA male and SMA female connectors, and are commonly used in wireless communication systems. An SMA connector with a centre conductor and external copper is shown in Figure 3.23.

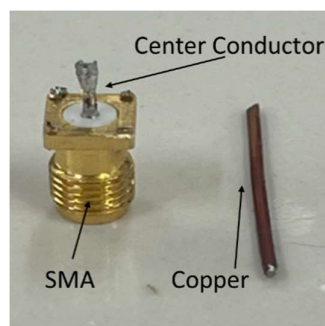


Figure 3.23: SMA with Copper.

A longer centre conductor is essential to fulfil the antenna’s performance criteria: 6 mm for the distilled water set and 15.25 mm for the ethyl

acetate set. Consequently, an external copper needs soldering onto the SMA connector to extend the centre conductor. The length of the copper is precisely measured using vernier callipers to ensure the desired performance can be achieved, as shown in Figure 3.24. For the soldering procedure, preparations include the soldering iron and solder, as depicted in Figure 3.25. The end product is illustrated in Figure 3.26. This soldering process establishes a conductive connection that facilitates the flow of electricity and the transfer of electromagnetic waves. Conductive materials like copper are crucial for conducting electricity and enabling the generation and transmission of signals within the antenna.



Figure 3.24: Measurement of Copper.



Figure 3.25: Soldering Station.



Figure 3.26: SMA with External Copper.

3.6.4 Assembly of Antenna Parts

The soldering process for attaching the SMA connector to the mesh ground plane is similar to the previous step, as depicted in Figure 3.27.

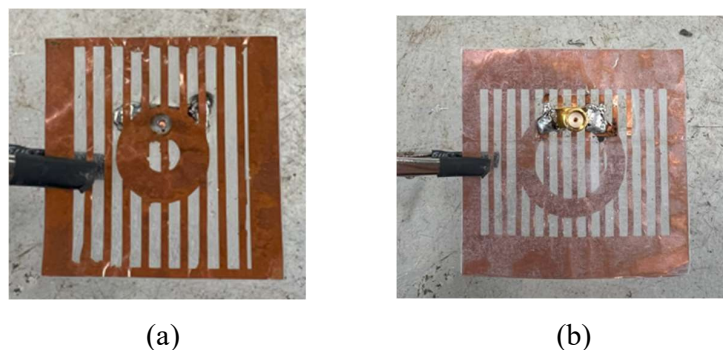


Figure 3.27: Distilled Water DRA Ground Plane with SMA (a) Top View and (b) Bottom View.

To ensure a stable connection between the Ecoflex container, cap, and the SMA connector on the ground plane, a small amount of Ecoflex is applied. This guarantees a secure and reliable attachment among the components. Figure 3.28 illustrates the combination of the Ecoflex container, cap, and ground plane before and after this process.

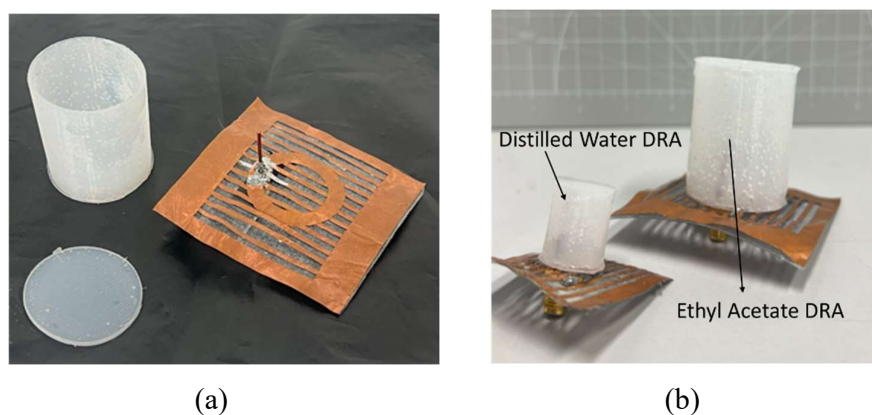


Figure 3.28: Assembly of Prototypes (a) Before Assembly and (b) After Assembly.

Following the completion of this assembly, the liquid will be introduced into the cylinder holder using a syringe during the characterisation process.

3.7 Characterization

3.7.1 Reflection coefficient, S_{11}

The performance of an antenna can be thoroughly assessed using a Vector Network Analyser (VNA), as shown in Figure 3.29. A Vector Network Analyzer (VNA) is instrumental in determining the behaviour of electronic components or circuits, known as the Device Under Test (DUT). Before measurements, calibration is imperative to eliminate systematic errors, ensuring precision by accounting for setup intricacies, cable characteristics, connector quality, and inherent VNA imperfections.



Figure 3.29: Vector Network Analyser (VNA).

The calibration setup, depicted in Figure 3.30, involves securing the cable so the reflection coefficient measurements are referenced to the probe aperture plane throughout the experiment. The VNA starts by generating a high-frequency signal, either continuous or swept, known as the incident signal. This signal travels through a transmission line like a coaxial cable or waveguide into the DUT. Some of this signal is reflected from the DUT due to impedance differences or other factors. The VNA's receiver circuitry measures both the incident and reflected signals.



Figure 3.30: Calibration Setup.

Central to its functionality is measuring the S_{11} parameter, which signifies the ratio of reflected power from the DUT to the incident power upon it. Then, the connector cable will connect to port 1 of the VNA, and another end will connect to the DUT, as shown in Figure 3.31. The configuration depicted in Figure 3.32 illustrates the setup. The connector cable is secured in place by a retort stand, and an additional syringe is employed to administer the liquid into the liquid antenna.

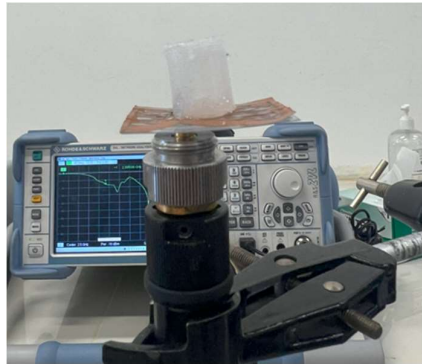


Figure 3.31: Connector Cable with Device Under Test (DUT).

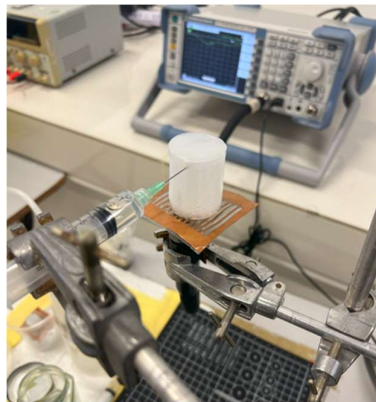


Figure 3.32: Setup of S_{11} Measurement.

Calculating the S_{11} parameter is essential for understanding the impedance matching and reflection properties of the Device Under Test (DUT). Since only port one is used, the calculation, expressed as in equation 6, delineates the reflected signal power from the incident signal power. The VNA conducts this measurement process across a spectrum of frequencies, ultimately producing a frequency response plot of S_{11} versus frequency.

Engineers use the S_{11} parameter to optimise RF and microwave circuits and systems. This includes analysing impedance matching, identifying resonance frequencies, assessing bandwidth, and other essential characteristics. Typically, the VNA represents the S_{11} parameter as a complex quantity, including both magnitude (reflection coefficient) and phase information, providing a comprehensive understanding of the reflection's characteristics induced by the DUT (Zhang et al., 2015).

In addition to assessing antenna performance, the Vector Network Analyzer (VNA) will also be employed to measure ethyl acetate's dielectric constant and loss tangent using an open-ended coaxial probe. The process begins with calibration, similar to the previous step. Following calibration, a standard step is performed, which involves using a short, an open, and a referenced liquid at the end of the probe, as shown in Figure 3.33. The probe is immersed in ethyl acetate for the referenced liquid, data is recorded, the liquid is removed, and data is collected again with the probe in the open air. Lastly, data is collected using a known liquid such as water. This process yields three data sets, which are then post-processed to obtain the dielectric parameters using a MATLAB program. In the post-processing phase, open-air measurements are utilised to compensate for the received data. The known result of water serves as a reference point to calculate the percentage error between theoretical and measured values. This error is then applied to the data collected for ethyl acetate, aiding in determining its dielectric properties.



Figure 3.33: Setup of Liquid Dielectric Properties Measurement.

Precautionary steps include ensuring no air gaps between the probe and the liquid and wiping the probe dry before measuring another result.

3.7.2 Far-field Measurement

A specific combination of equipment is typically employed to conduct measurements of the far-field region, which encompasses radiation patterns and far-field gain. This includes a signal generator connected to the Device Under Test (DUT) and a horn antenna linked to the spectrum analyser.

The signal generator, depicted in Figure 3.34 (a), produces electronic signals with precise characteristics like frequency, amplitude, phase, and modulation. In antenna testing, it generates signals spanning various frequencies, amplitudes, or modulation schemes, allowing evaluation of the antenna's responsiveness to different signal parameters.

Conversely, the spectrum analyser, depicted in Figure 3.34 (b), plays a crucial role in analysing and characterising signals received from the antenna. It measures signal amplitudes across a broad frequency spectrum. Spectrum analysers, which can be analogue or digital, aid in identifying and quantifying signal aspects such as noise presence, harmonics, spurious signals, noise levels, and interference (ELPROCUS, 2021).



(a)



(b)

Figure 3.34: Equipment (a) Signal Generator and (b) Spectrum Analyser.

The experimental setup, illustrated in Figure 3.35, involves calculating the distance between the DUT and the horn antenna using the far-field region equation:

$$R > \frac{2D^2}{\lambda} \quad (7)$$

where

R = Minimum distance between the far-field measurement

D = Maximum linear dimension of DUT

λ = Wavelength

These conditions must be fulfilled for the fields in the far-field region to behave like plane waves.



Figure 3.35: Setup of Far-field Measurement.

Before measurements, it is essential to calculate the cable losses of the two cables used, space loss, and the gain of the horn antenna, as they will be compensated during post-processing. To measure cable loss, a signal generator is connected to one end of the cable, and a spectrum analyser is connected to the other, as shown in Figure 3.36. Calibrate the spectrum analyser and generate a known signal. Measure its level at the input as the reference, transmit it through the cable and measure the output. For space loss and horn antenna gain, a setup utilising two horn antennas can be utilised, as shown in Figure 3.37. The distance between the antennas remains consistent with previous calculations. Cable A connects the signal generator to horn antenna A, while cable B links the spectrum analyser to horn antenna B. This setup enables direct measurement and compensation of space loss and horn antenna gain effects within the experimental configuration.

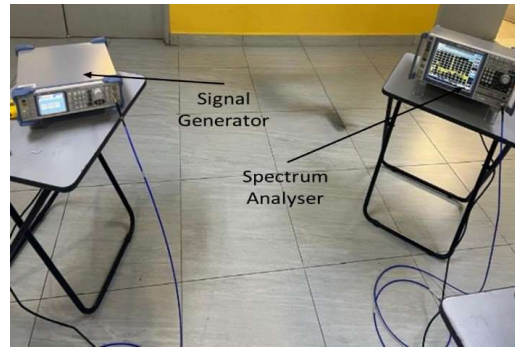


Figure 3.36: Setup of Cable Loss Measurement.

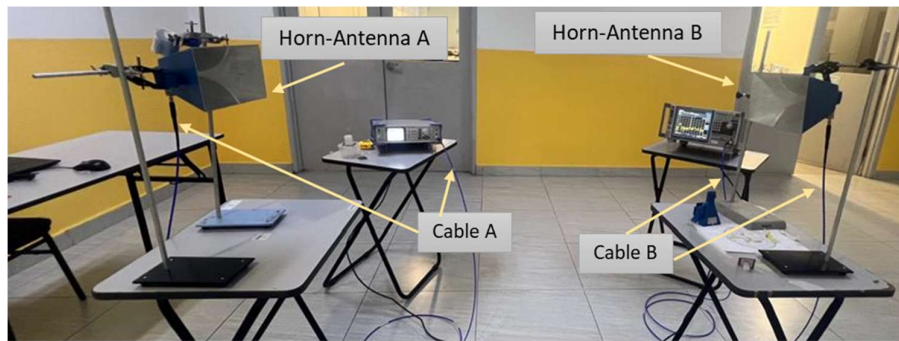


Figure 3.37: Setup of Space Loss and Antenna Gain Measurement.

For far-field measurement, the antennas are specifically engineered to optimise transmission or reception in a single polarisation orientation, known as co-polarization, which is pivotal for assessing antenna performance. Conversely, cross-polarization signals are generally deemed undesirable, representing energy transmitted or received in unintended orientations. Therefore, the emphasis is on co-polarization in far-field measurements. To conduct these measurements, a 360° marking beneath the DUT enables rotation in 10° intervals, as shown in Figure 3.38. For subsequent analysis, received power in dBm is logged at each 10° rotation. Co-polarization is assessed for the YZ plane ($\Phi 90^\circ$) and XZ plane orientation ($\Phi 0^\circ$), as shown in Figure 3.39. During post-processing, the received power in dBm will be adjusted to account for total cable loss, space loss, and the gain of the horn antenna. This compensation ensures that the measured values accurately reflect the performance of the antenna system. Subsequently, the compensated values will be compared with simulation results to validate the measurement's accuracy and assess the antenna design's effectiveness.

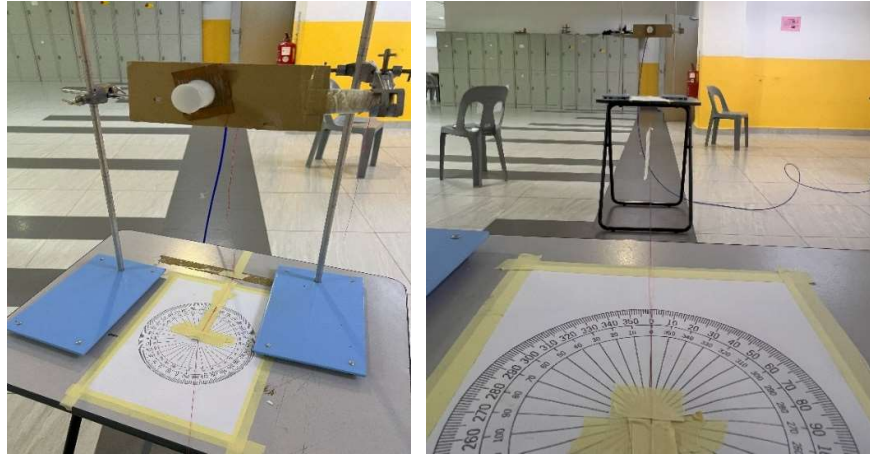


Figure 3.38: 360° Marking.



Figure 3.39: Orientation of Antenna at $\Phi = 90$.

3.7.3 Transparency Evaluation

The transparency evaluation aims to validate that the antenna achieves the objective of being nearly transparent. This assessment is conducted using an ambient light sensor built into the smartphone. The Phyphox software is utilised to record the data, as depicted in Figure 3.40.



Figure 3.40: Phyphox Application Logo.

The ambient light sensor (ALS) in a phone works based on the principle of photodetection. It measures the intensity of ambient light falling on

the sensor and adjusts the brightness of the phone's display accordingly to optimise visibility and conserve battery life. It utilises a photodetector, like a photodiode or phototransistor, which generates a current proportional to incident light. An amplifier circuit converts This current into a voltage signal, with the output voltage directly proportional to the light intensity. The equation representing ALS operation can be expressed as:

$$V_{\text{out}} = I_{\text{photo}} \times R_{\text{feedback}} \quad (8)$$

where

V_{out} = Output voltage

I_{photo} = Photocurrent

R_{feedback} = Feedback resistance

In practice, the output voltage V_{out} is directly proportional to the intensity of ambient light falling on the sensor, allowing the phone's software to adjust the display brightness accordingly.

When attaching the fabricated antenna to the light bulb, the aim is to assess the extent to which the antenna's transparency allows light to pass through, aiming for near-transparency. Instead of measuring light intensity directly from the bulb's centre, measurements are taken from the side. This approach serves two purposes: firstly, it prevents the sensor from being overwhelmed by the intense direct light emitted from the bulb's centre, thus avoiding inaccurate readings. Secondly, measuring from the side enables the capture of ambient light diffused and scattered by the surroundings, thereby providing a more accurate representation of overall lighting conditions.

Three prototypes will be utilised to conduct illumination measurements, as depicted in Figure 3.41. These prototypes include the water antenna (A), the ethyl acetate antenna (B) fabricated in the previous section, and an existing liquid antenna prototype (C), which shares similar dimensions with the ethyl acetate antenna. The setup, outlined in Figure 3.42, aims to determine whether the antenna size influences illumination levels and assess the effectiveness of the defective ground plane design.

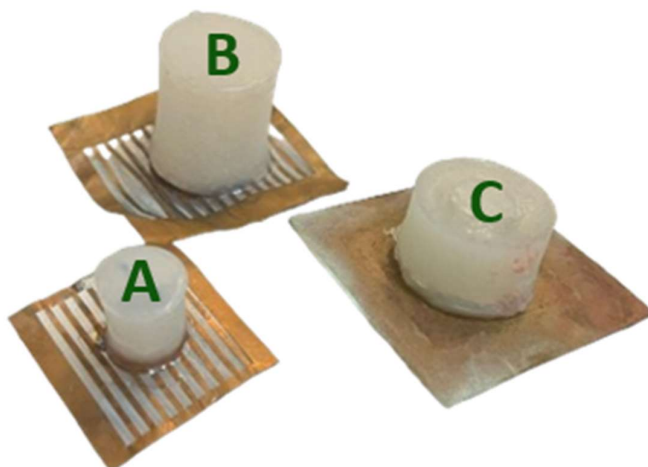


Figure 3.41: Three Different Designs of Antennas.

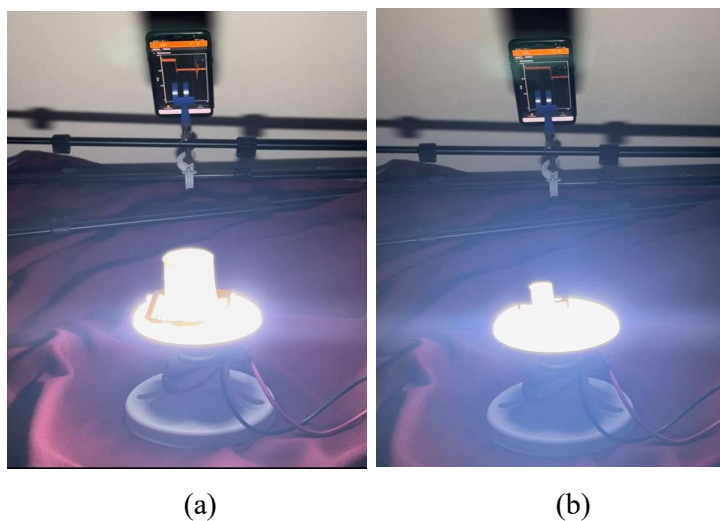


Figure 3.42: Setup of Illumination Measurement for (a) Ethyl Acetate DRA and (b) Distilled Water DRA.

3.7.4 Antenna Signal Strength Assessment using ESP-32 Cam

The ESP32-CAM is a versatile and compact module designed for camera applications, integrating the powerful ESP32 microcontroller with a camera module. Developed by Espressif Systems, the ESP32-CAM module offers a convenient platform for projects requiring image or video capture capabilities. ESP32 is a versatile microcontroller that has Wi-Fi and Bluetooth capabilities. This allows ESP32 to communicate wirelessly with multiple devices with Wi-

Fi and Bluetooth connectivity. So, ESP32 is popular in the Internet of Things (IoT) application.

The ESP32 chip supports various applications, including data processing, web servers, and networking. Additionally, the ESP32 can function as a processor due to its integrated processing capabilities, making it ideal for operating IoT devices in IoT applications. The ESP32-CAM's ability to use an external antenna goes beyond just boosting signal strength. In this case, the aim is to evaluate the performance of the fabricated antennas. Removing the onboard antenna resistor and attaching an external antenna allows for an assessment of the performance of the antennas in real-world scenarios. Figure 3.43 illustrates the selection between internal and external antennas, and the choice of antenna can be made by connecting the pins accordingly. The desoldering outcome of the onboard antenna is illustrated in Figure 3.44, while Figure 3.45 depicts the soldering location necessary for connecting an external antenna. This method can evaluate signal strength and overall wireless performance, offering valuable insights into the design and optimisation of the constructed antennas.

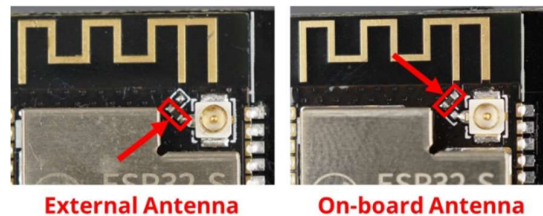


Figure 3.43: Selections of External or On-board Antenna.

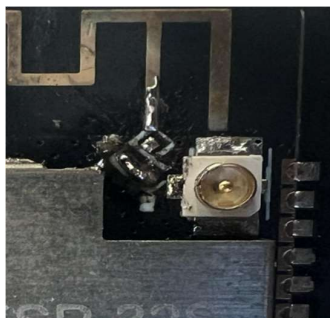


Figure 3.44: Desoldering Product indicates that the External Antenna has been Selected.



Figure 3.45: Soldering Station.

The RSSI value serves as a crucial indicator for evaluating antenna signal strength. By measuring the power level of signals received from nearby Wi-Fi access points or routers via the external antenna, the ESP32 chip derives this value. A high RSSI value typically signifies robust signal strength, suggesting adequate Wi-Fi signal reception by the antenna. This often correlates with reliable data transmission and good connectivity. The experimental setup, outlined in Figure 3.46, involves programming the ESP32-CAM to establish a connection with a web server. This setup enables the antenna to assess the smoothness or potential lag in the produced image. Initially, the antenna is attached to the ESP32-CAM using an IPEX-SMA connector, and the focus is on the ESP32 controller's calculation of the RSSI value. Subsequently, the antenna is removed to observe the difference in signal reception with and without the antenna. Finally, the antenna is reconnected to evaluate the impact. The program integrates the RSSI value as supplementary evidence to validate the findings. Figure 3.47 showcases the web server interface, presenting the web server on the left, the first-person view on the right, and the serial monitor displaying the current RSSI value. Additionally, Figure 3.48 illustrates the connection of the ESP32-CAM to the laptop. Accessing the web server is simple, one needs to insert the provided code into the Arduino IDE. The code for this section is shown in Appendix A.



Figure 3.46: Setup of Signal Strength Measurement.

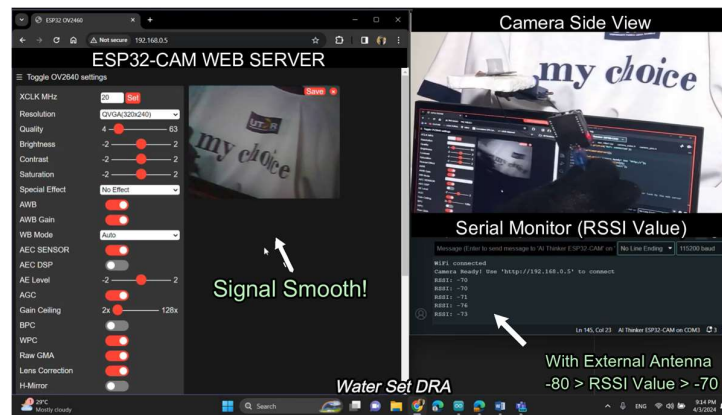


Figure 3.47: Result Presentation of Signal Strength Measurement.

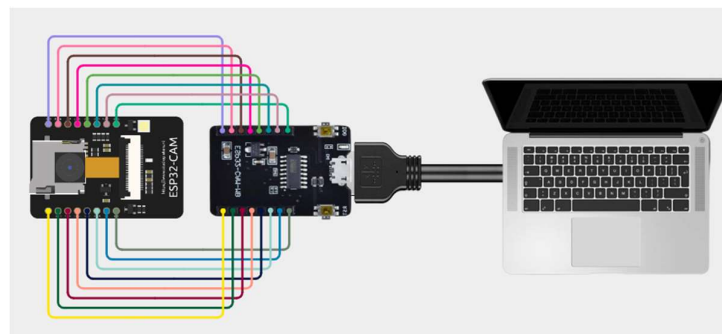


Figure 3.48: Electrical Circuit Diagram of ESP32-Cam with Laptop.

3.7.5 Web-connected Smart Lighting (IoT Application)

This section utilised the ESP32-cam with an external antenna from the previous section. Integrating the ESP32-CAM with an external antenna into a lamp marks the inception of a wireless-connected smart lighting IoT application. It is crucial

to emphasise that while the antenna is pivotal for wireless data transfer, its efficacy hinges on its application. In this context, the antenna and the IoT system hold equal importance, as one complements the other in enabling seamless wireless communication. To elaborate, picture an automated robot without an antenna. It is practically useless because it cannot catch wireless signals. On the other hand, imagine an antenna without a purpose. It is also meaningless because there is no way to demonstrate what it can do. Thus, the presence of an antenna is indispensable for facilitating communication and enabling the intelligent features of IoT devices like lamps, robots, and various other smart systems.

This IoT application facilitates the control of lamp functions, allowing users to toggle its state remotely via a smartphone or any Wi-Fi-connected device. Numerous essential steps involve how an ESP32 receives signals from a web server. First, the ESP32 connects to a Wi-Fi network using its integrated Wi-Fi module. Once connected, it uses Wi-Fi to communicate with the web server over the typical HTTP or HTTPS protocols. It indicates the intended action or data it requires in HTTP requests it sends to the server. The web server receives these requests, processes them, and returns with HTTP headers that either include the requested information or a confirmation of the action taken. The necessary information, including commands or data that has to be acted upon, is then extracted by the ESP32 from these responses. Based on this information, the ESP32 takes particular actions, such as updating sensor readings, actuating devices, or sending data back to the server. The whole procedure takes place inside the confines of the local network or, if necessary, to a remote server via the internet.

While this research primarily focuses on the implementation of the antenna framework in the context of smart lighting applications, it is worth noting that the framework has the potential to extend to a variety of other IoT implementations, including smart curtains, smart windows, and more. The program for this IoT application is provided in the appendix. There is one part where the web server can show the current state's signal status. As shown in Figure 3.49, The program is to be when the RSSI value falls below -75, it indicates a LOW signal; when the RSSI is between -60 to -75, it will indicate a HIGH signal. The code of this application can be found in Appendix B.


```
// Add the signal status information
String SignalStatus;
if (rssiValue < -60 && rssiValue >= -75) {
  SignalStatus = "HIGH";
} else {
  SignalStatus = "LOW";
}

HTML += "<p>Signal Status: " + SignalStatus + "</p>";
```

Figure 3.49: RSSI Measurement Program Code.

The electrical circuitry for this application, as depicted in Figure 3.50, is simple, reflecting its conceptual integration of the antenna into a smart lighting system. Here, the smart lighting system connects to a relay, controlled by the ESP32-CAM microcontroller via a trigger signal received on the web server, activating pin 12. This pin sends a signal to the relay, turning the lamp on or off and connecting to a power supply. This wireless control over the web server allows seamless operation. The primary focus remains on developing a cost-effective and minimally intrusive antenna. Thus, this application serves as crucial evidence, affirming the functionality and contribution of the designed antenna to the IoT application. As illustrated in Figure 3.51, the equipment setup will initially involve testing the smart lighting system with the antenna to control the smart light bulb through the web interface wirelessly. This will enable assessing the signal strength displayed on the web server interface. Subsequently, experimentation will involve removing the antenna to observe signal strength and behaviour changes.

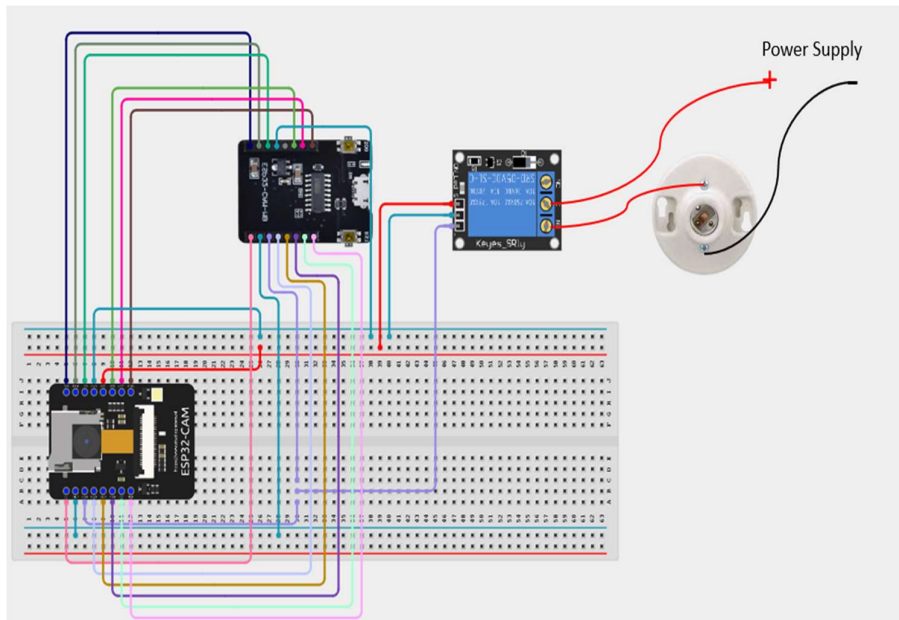


Figure 3.50: Electrical Circuit Diagram of the Smart Lighting Application.

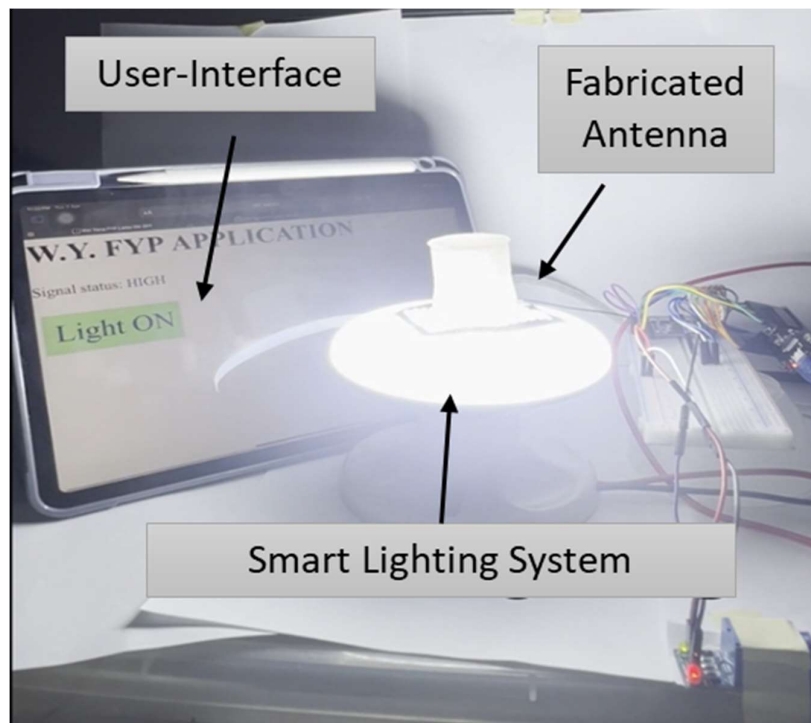


Figure 3.51: Setup of IoT Application Experiment.

CHAPTER 4

RESULTS AND DISCUSSION

4.1 Introduction

This project began with creating a nearly transparent liquid dielectric resonator antenna (DRA) featuring a mesh ground plane. Two distinct models were formulated, and the antenna geometry is discussed in this section. Each employs different dielectric liquids, namely water and ethyl acetate. The forthcoming chapter will thoroughly examine the simulation results of these fabricated antennas. Various analyses and evaluations of the antenna have been performed, and it has been integrated into an IoT application to showcase its functionality.

4.2 Antenna Geometry

Constructing the antenna involves using water, ethyl acetate, and Ecoflex as the primary materials. The essential components of the antenna include a ground plane, a cylinder-shaped liquid container, an SMA connector, and copper. It is worth noting that ethyl acetate is utilised in the first model, while water is employed exclusively in the second model. Figure 4.1 provides a clear view of the designed antenna with labelled parts. The design is similar for both models, so only one labelled antenna is shown for simplicity.

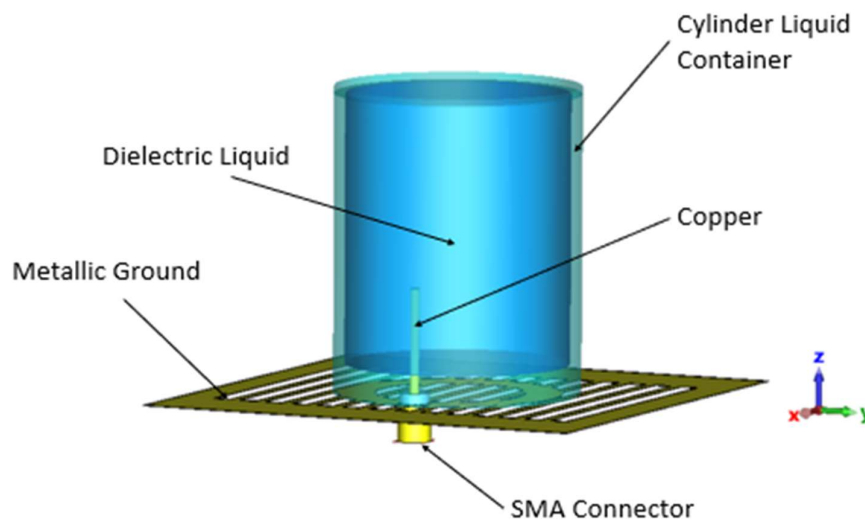


Figure 4.1: Antenna Components.

The cylinder-shaped liquid holders in both models are crafted from Ecoflex material. These containers house the respective dielectric liquids, ethyl acetate for the first model and water for the second model. Moreover, a 50 Ω copper is connected through the centre conductor and linked to the SMA connector, which functions as the antenna feed. The SMA connector is designed to traverse the antenna's ground plane and enter the cylinder-shaped liquid container.

4.3 Antenna Dimensions

Two near-transparent antenna are proposed for comparison purposes, it will be discussed in the following sections.

For both fabricated antennas, the cylinder liquid holder has a thickness of 3 mm, ensuring transparency. An inner diameter offset distance of 4 mm from the metallic ground is maintained to prevent direct contact between the dielectric liquid and the ground plane. Additionally, a circular feature is integrated into the centre of the ground plane to house the SMA connector securely.

The parameters specified for the design and configuration of the cylindrical liquid antenna system are crucial for its optimal performance and functionality. The cylinder holder diameter, denoted as `cylinder_d`, establishes the size of the holder, while `cylinder_h` determines its height. The liquid diameter (`water_d`) and height (`water_h`) define the dimensions of the liquid container, with `water_offset` indicating its distance from the ground plane. The water probe length (`pin_L`) and offset from the x-axis (`move_z`) contribute to precise positioning and functionality. Ground-related parameters include `ground_length`, `DG_OFFSET` for the ground without cuts, `DG_WIDTH` for mesh ground cutting slot width, `DG_DISTANCE` for slot spacing, `DFG_OUTERr`, and `DFG_INNERr` for the circular ground radii, and `ground_thickness` for copper thickness. `DG_L` defines mesh ground-cutting slot characteristics. Additionally, `DRA_offset_x` and `DRA_offset_y` specify the distance of the cylinder centre from the x and y axes, respectively. These parameters collectively ensure the effective operation of the liquid antenna system in wireless communication applications. Detailed part labels and dimensions are provided in Tables 4.1 to 4.4 for easy reference.

Table 4.1: Parts Label of Ethyl Acetate Antenna Model.

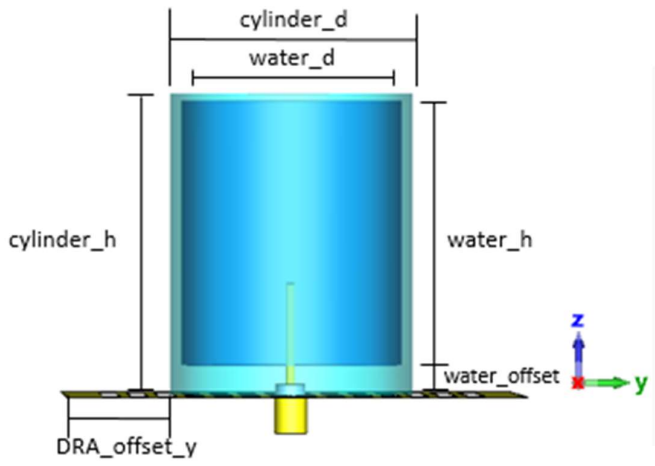
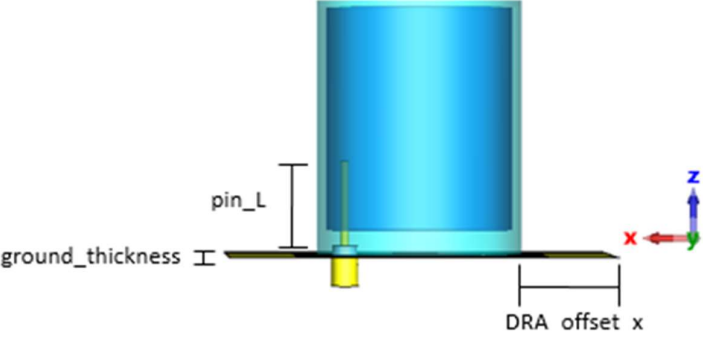
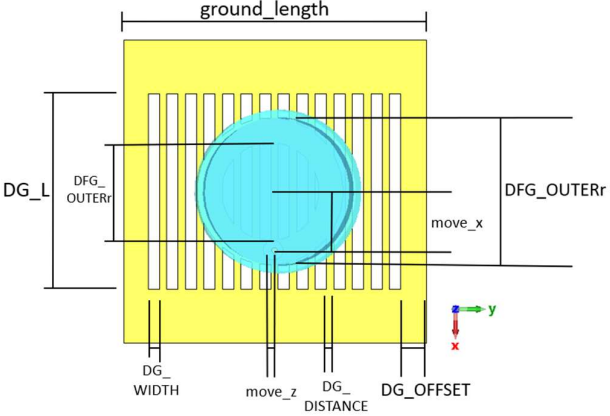
View	Model
Front View	 <p>Diagram illustrating the front view of the antenna model. The model consists of a blue cylindrical structure (antenna) mounted on a yellow ground plane. Key dimensions and parameters are labeled:</p> <ul style="list-style-type: none"> cylinder_d: Diameter of the cylinder. water_d: Diameter of the water layer inside the cylinder. cylinder_h: Height of the cylinder. water_h: Height of the water layer. water_offset: Offset of the water layer from the bottom of the cylinder. DRA_offset_y: Offset of the antenna from the center of the ground plane. <p>A coordinate system is shown with the z axis pointing up (blue), the y axis pointing right (green), and the x axis pointing out of the page (red).</p>
Side View	 <p>Diagram illustrating the side view of the antenna model. The model shows the cylinder and the ground plane. Key dimensions and parameters are labeled:</p> <ul style="list-style-type: none"> pin_L: Length of the antenna pin. ground_thickness: Thickness of the ground plane. DRA offset x: Offset of the antenna from the center of the ground plane. <p>A coordinate system is shown with the z axis pointing up (blue), the x axis pointing left (red), and the y axis pointing out of the page (green).</p>
Top View	 <p>Diagram illustrating the top view of the antenna model. The model shows the ground plane with a grid of vertical lines and a central blue circle. Key dimensions and parameters are labeled:</p> <ul style="list-style-type: none"> ground_length: Length of the ground plane. DG_L: Length of the ground plane. DFG_OUTERr: Radius of the outer dielectric ground plane. move_x: Offset of the antenna from the center of the ground plane. DG_WIDTH: Width of the ground plane. move_z: Offset of the antenna from the center of the ground plane. DG_DISTANCE: Distance between the ground plane and the antenna. DG_OFFSET: Offset of the antenna from the center of the ground plane. <p>A coordinate system is shown with the y axis pointing right (green), the x axis pointing down (red), and the z axis pointing up (blue).</p>

Table 4.2: Dimensions of Antenna of Ethyl Acetate Model.

Parameter	Dimension (mm)	Parameter	Dimension (mm)
cylinder_d	33	DG_OFFSET	5
cylinder_h	40	DG_WIDTH	2.3
water_d	30	DG_DISTANCE	1.5
water_h	36	DFG_OUTERr	15
water_offset	4	DFG_INNERr	10
pin_L	15.25	ground_thickness	0.06
move_z	0.22	DG_L	40
move_x	6	DRA_offset_x	14.5
ground_length	61.99	DRA_offset_y	14.5

Table 4.3: Parts Label of Distilled Water Antenna Model.

View	Model
Front View	<p>The front view diagram shows a cylindrical antenna structure. The outer cylinder has a diameter labeled 'cylinder_d' and a height labeled 'cylinder_h'. Inside it, a smaller cylinder has a diameter labeled 'water_d' and a height labeled 'water_h'. The water cylinder is offset from the bottom of the outer cylinder by a distance labeled 'water_offset'. The antenna is mounted on a ground plane, with the offset from the center of the antenna to the edge of the ground plane labeled 'DRA_offset_y'. A coordinate system is shown with the z-axis pointing up and the y-axis pointing right.</p>
Side View	<p>The side view diagram shows the antenna from the side. The length of the antenna is labeled 'pin_L'. The thickness of the ground plane is labeled 'ground_thickness'. The offset from the center of the antenna to the edge of the ground plane in the x-direction is labeled 'DRA_offset_x'. A coordinate system is shown with the z-axis pointing up and the x-axis pointing left.</p>

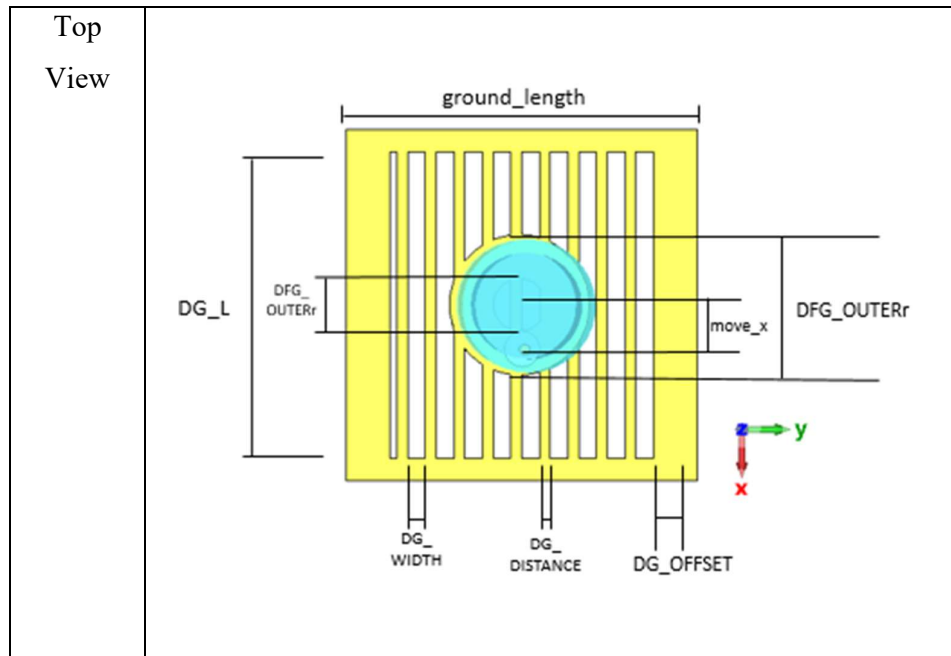


Table 4.4: Dimensions of Antenna of Distilled Water Model.

Parameter	Dimension (mm)	Parameter	Dimension (mm)
cylinder_d	15	DG_WIDTH	2
cylinder_h	17.6	DG_DISTANCE	1.25
water_d	12	DFG_OUTERr	8
water_h	13.5	DFG_INNERr	3
water_offset	4	ground_thickness	0.06
pin_L	8	DG_L	35
move_x	2.5	DRA_offset_x	12.5
ground_length	40.01	DRA_offset_y	12.5
DG_OFFSET	5		

4.4 Parametric Sweep Analysis

Parametric analysis is performed to simultaneously examine changes in the antenna's S_{11} parameters and present the results in a consolidated graph for easier comparison. This study analyses specific parameters, including water_d, water_h, DG_WIDTH, DG_OFFSET, and ground_length. It is important to note that this analysis is based on the ethyl acetate model, as the effects are consistent between the two models.

4.4.1 Liquid Diameter

When the liquid diameter in the cylindrical liquid container is increased from 25 mm to 35 mm, the resonant frequency shifts backwards from 2.39 GHz to 2.43 GHz. Additionally, the reflection coefficient increases from -17 dB to -23 dB. Figure 4.2 illustrates a parametric sweep of liquid diameter in the cylindrical liquid holder. In summary, an increase in liquid diameter causes a backward shift in the resonant frequency and an increase in the reflection coefficient. For the design, the optimal liquid diameter settings for the ethyl acetate and distilled water models are 30 mm and 12 mm, respectively, as they offer the best performance. When the diameter increases, the current distribution of the liquid increases. Also, it will make the bandwidth wideband, improving radiation efficiency.

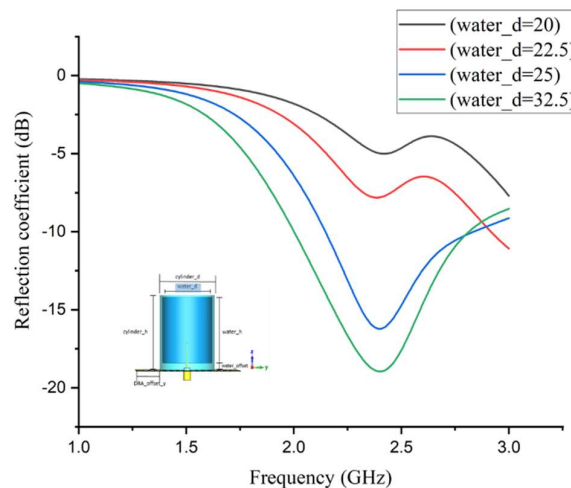


Figure 4.2: Results of Simulated Parametric Sweep of Liquid Diameter in Container.

4.4.2 Liquid Height

When the liquid height in the cylindrical liquid container is increased from 32 mm to 44 mm, the resonant frequency shifts to the left from 2.43 GHz to 2.35 GHz; additionally, the reflection coefficient decreases from -21.85 dB to -17.54 dB. Figure 4.3 illustrates a parametric sweep of liquid height in the cylindrical liquid holder. In summary, an increase in liquid height causes a forward shift in the resonant frequency and a decrease in the reflection coefficient. For the

design, the optimal liquid height settings for the ethyl acetate and distilled water models are 36 mm and 13.5 mm, respectively, as they offer the best performance. When the liquid height is increased, the liquid allows more EM waves to pass through, increasing the dielectric loss. It will decrease the radiation efficiency.

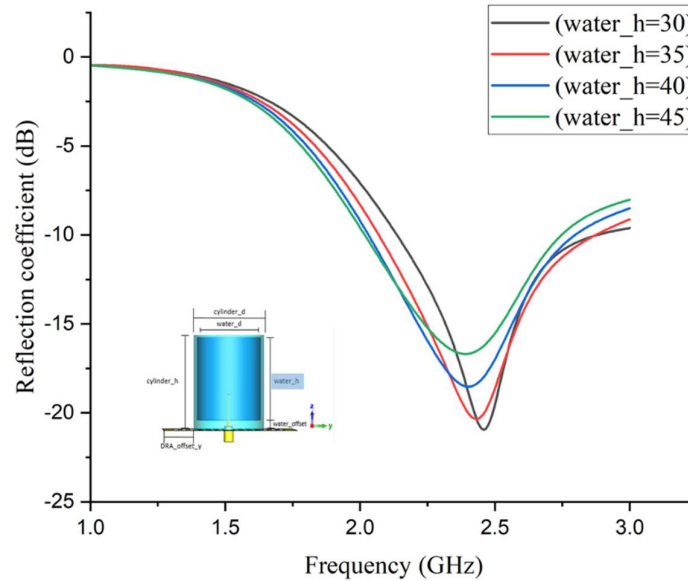


Figure 4.3: Results of Simulated Parametric Sweep of Liquid Height in Container.

4.4.3 Mesh Ground Width

When the mesh ground cutting slot width is increased from 0.5 mm to 2 mm, the resonant frequency shifts to the left from 2.5 GHz to 2.33 GHz; additionally, the reflection coefficient increases from -16.5 dB to -23.4 dB. Figure 4.4 illustrates the parametric sweep of mesh ground plane slot cutting. In summary, an increase in the cutting slot causes a forward shift in the resonant frequency and an increase in the reflection coefficient. Increasing the slot width might affect the antenna's impedance in a way that brings it closer to the desired match, thus reducing the reflection coefficient. For the design, the optimal mesh ground cutting slot width settings for the ethyl acetate and distilled water models are 2.3 mm and 2 mm, respectively, as they offer the best performance. The less the metal content in the ground plane, the metallic loss will be reduced, which will increase the radiation efficiency.

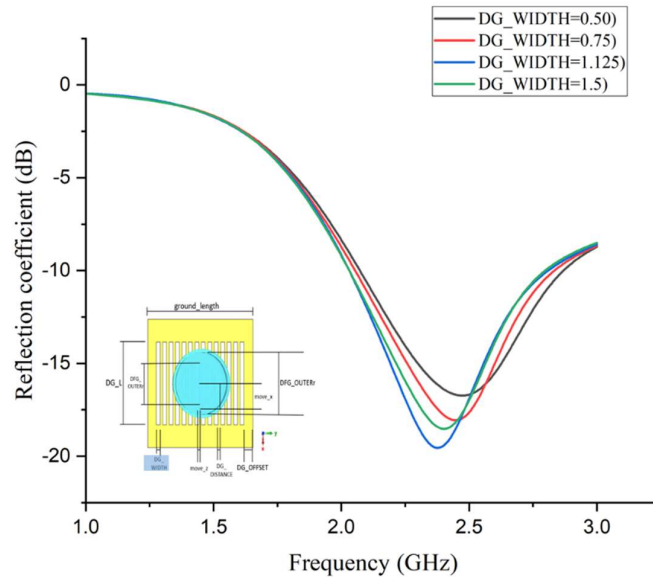


Figure 4.4: Results of Simulated Parametric Sweep Results of Mesh Ground Cutting Slot Width.

4.4.4 Mesh Ground Length

When the mesh ground cutting slot length is increased from 45 mm to 60 mm, the resonant frequency shifts to the left from 2.35 GHz to 1.81 GHz; additionally, the reflection coefficient increases from -20.6 dB to -26.3 dB. Figure 4.5 illustrates the parametric sweep of mesh ground plane slot length. In summary, an increase in cutting slot length causes a forward shift in the resonant frequency and an increase in the reflection coefficient. Increasing the ground slot cutting size may be beneficial up to a certain point, but beyond that, it can lead to diminishing returns or even degraded performance. For the design, the optimal mesh ground cutting slot length settings for the ethyl acetate and distilled water models are 40 mm and 35 mm, respectively, as they offer the best performance. When the length is cut, it indicates that the metallic loss will be reduced due to some of the metal being removed away from the ground plane.

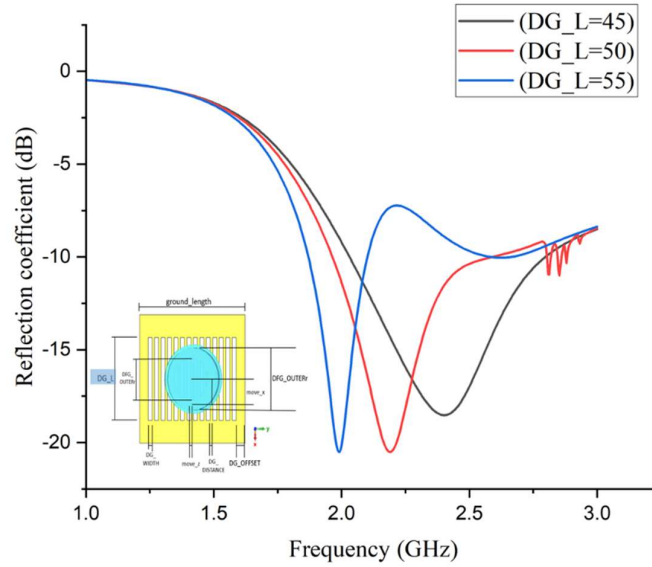


Figure 4.5: Results of Simulated Parametric Sweep Results of Mesh Ground Cutting Slot Length.

4.4.5 Ground Plane Size

When the ground plane area is increased from 50 mm^2 to 70 mm^2 , the resonant frequency shifts to the left from 2.5 GHz to 2.21 GHz; additionally, the reflection coefficient decreases from -37.8 dB to -19.9 dB. Figure 4.6 illustrates a parametric sweep of ground plane size. In summary, an increase in ground plane size causes a forward shift in the resonant frequency and a decrease in the reflection coefficient. When the ground plane is significantly larger than the wavelength, it can cause changes in the electromagnetic field distribution around the antenna. These changes can result in impedance mismatches. For the design, the optimal ground plane size settings for the ethyl acetate and distilled water models are 61.99 mm and 40.01 mm, respectively, as they offer the best performance. This is likely due to increasing the metal, which will further induce the metallic loss, significantly affecting the radiating efficiency.

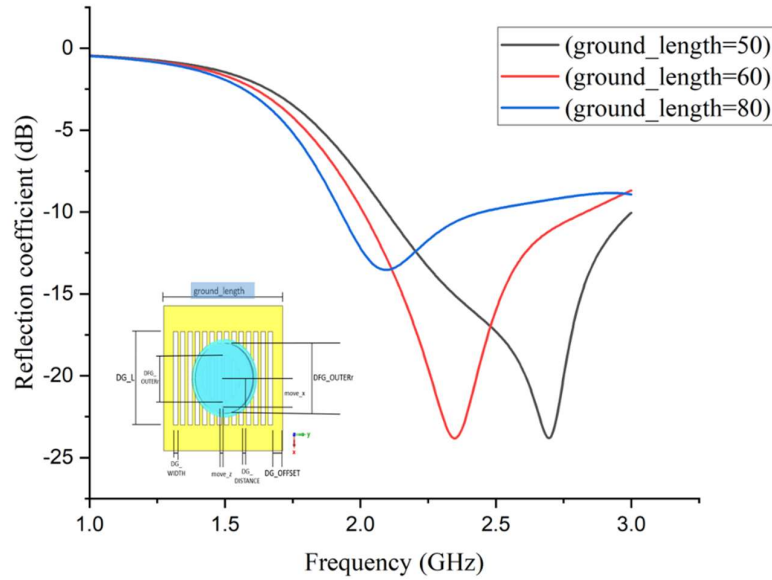


Figure 4.6: Results of Simulated Parametric Sweep Results of Ground Plane Size.

4.4.6 SMA Probe Length

When the SMA probe length is increased from 15 mm to 70 mm, the resonant frequency shifts to the right from 2.37 GHz to 2.46 GHz; additionally, the reflection coefficient increases from -5.8 dB to -22.5 dB. Figure 4.7 illustrates the parametric sweep of the SMA probe length. In summary, an increase in SMA probe length causes a backward shift in the resonant frequency and an increase in the reflection coefficient. For the design, the optimal SMA probe settings for the ethyl acetate and distilled water models are 15.25 mm and 8 mm, respectively, as they offer the best performance. Note that the probe length cannot exceed half of the liquid height; otherwise, it may function as a different type of antenna, such as a monopole antenna, as the metallic probe would begin to conduct rather than the liquid radiating.

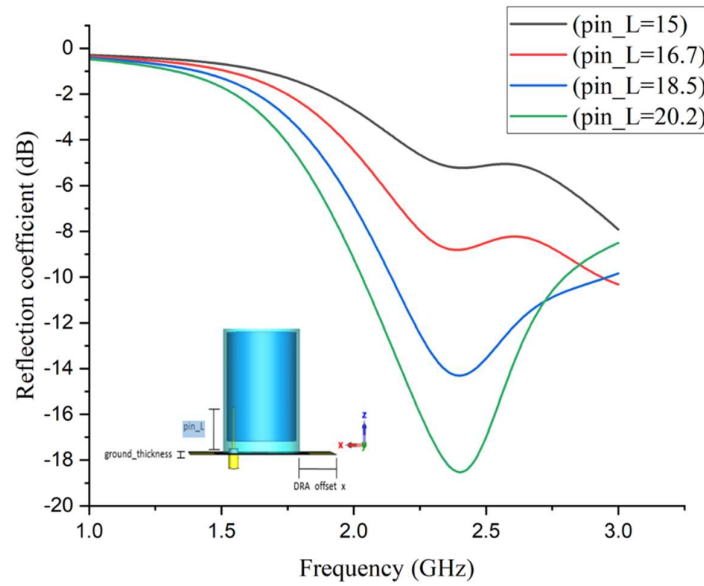


Figure 4.7: Results of Simulated Parametric Sweep Results of SMA Pin Length.

4.5 Analysis of Result

4.5.1 S-parameter, S_{11}

The S-parameter, specifically S_{11} , provides insights into the reflection coefficient or return loss, represented in decibels (dB), concerning the frequency in gigahertz (GHz). Simulated S_{11} data was obtained using CST software for the ethyl acetate and distilled water antennas. The simulation outcomes revealed that the ethyl acetate antenna exhibited a resonant frequency of 2.408 GHz and a reflection coefficient of -14.88 dB. In contrast, the distilled water antenna displayed a resonant frequency of 2.4 GHz and a reflection coefficient of -14.76 dB. The reflection coefficient needs to be below -10 dB to signify the antenna's effective performance in signal transmission, indicating that a minimal amount of power is reflected to the source from the antenna. The simulation results have successfully met this requirement, operating near the resonant frequency of 2.4 GHz with a reflection coefficient exceeding -10 dB. Figure 4.8 illustrates the simulated S_{11} results for the ethyl acetate model, while Figure 4.9 depicts the simulated S_{11} results for the distilled water model. Regarding impedance matching, the ethyl acetate antenna demonstrated superior performance to the distilled water antenna. This suggests that the ethyl acetate model is more effective in transmitting and receiving signals, likely due to its lower loss tangent when compared to distilled water. Despite initially exhibiting weaker

performance, the distilled water antenna configuration was optimised, achieving nearly identical performance to ethyl acetate.

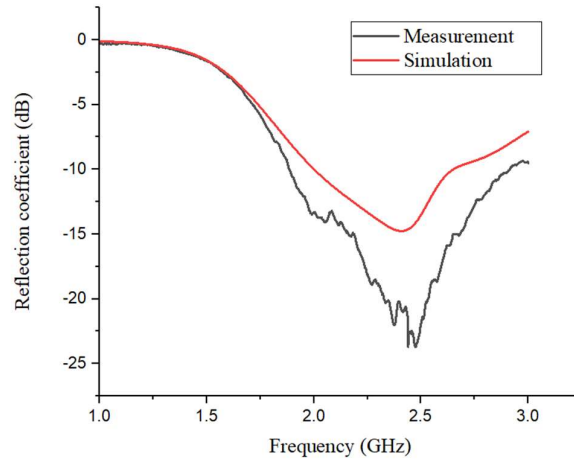


Figure 4.8: Measured and Simulated Reflection Coefficient of Ethyl Acetate Model.

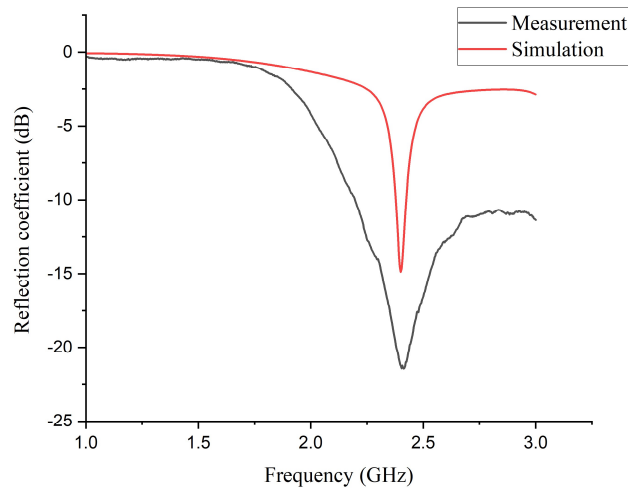


Figure 4.9: Measured and Simulated Reflection Coefficient of Distilled Water Model.

4.5.2 Input Impedance, Z_{11}

An antenna's input impedance, represented by the symbol Z_{11} , is crucial in determining how responsive the antenna is at different frequencies. It plays a vital part in antenna engineering by directly affecting how well the antenna transmits and receives signals. Inducing electric and magnetic fields as

electromagnetic waves interact with the antenna results in the creation of voltage and current. The input impedance fundamentally controls how effectively the antenna can manage power or messages by altering the voltage and current distribution.

Various factors closely integrated into the design process determine an antenna's impedance characteristics. These elements include the antenna's actual size, the materials used, and its general design. The main goal is to minimise signal loss and maximise power transmission by closely matching the antenna's impedance to that of the source or receiver. The input impedance is a complex parameter that consists of two parts: reactance, which is hypothetical, and actual resistance. Reactance denotes power storage within the antenna, whereas resistance represents power dissipation, including radiation and absorption. The S_{11} parameter, which quantifies the reflection coefficient or return loss, is also related to impedance. When the impedance of an antenna is well-matched to the source (usually 50Ω), S_{11} will be close to 0 dB, indicating that very little power is reflected by the source. However, more power is reflected when there is an impedance mismatch, resulting in a higher S_{11} value in decibels (dB).

By preserving impedance balance, one can reduce signal reflections and improve power transmission by ensuring the antenna, source, and receiver all have suitable impedance values. Impedance variations can cause signal reflections and deteriorated performance. Simultaneously, simulations were conducted using CST software to evaluate the input impedance. The ethyl acetate model, with a resonant frequency of 2.408 GHz, displayed simulated resistance and reactance values of 49.22Ω and 9.01Ω , as shown in Figure 4.10, respectively, in the evaluation of input impedance performed using CST software simulations. The resistance and reactance measurements for the 2.4 GHz distilled water antenna were 39.87Ω and -13.17Ω , respectively, as shown in Figure 4.11. From the result, it can be concluded that distilled water initially exhibited under-performance, which indicates it does not match well with the source or receiver. However, it still has an acceptable performance, as the S_{11} is still below -10 dB. The ethyl acetate model antenna offers a better impedance match, indicating potentially superior performance in signal transmission and reception.

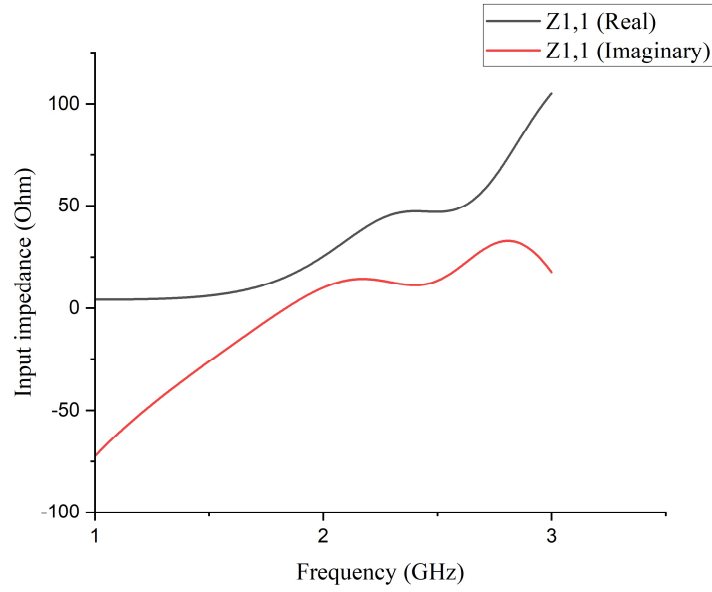


Figure 4.10: Simulated Z-parameter of the Ethyl Acetate Model.

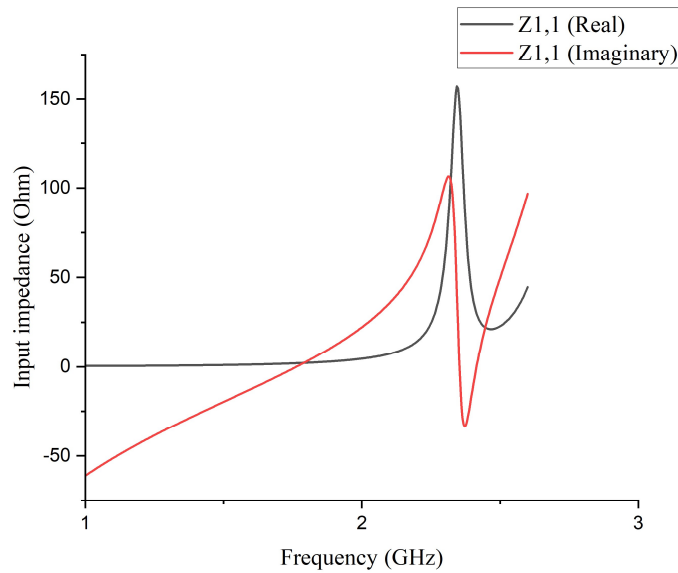


Figure 4.11: Simulated Z-parameter of the Distilled Water Model.

4.5.3 Far-field Radiation Gain

The antenna's radiation pattern provides insights into the directions in which it can effectively radiate energy or signals. This pattern and far-field gain data are obtained through simulations conducted in CST software. Figure 4.12 illustrates the three distinct planes where the radiation pattern is generally depicted in polar graphs: the XY, XZ, and YZ planes. These planes are defined by two angles:

theta (θ) and phi (ϕ). Theta represents the angle between the X and Y axes, defining the XY plane, while phi represents the angle between the Z axis and either the X or Y axis.

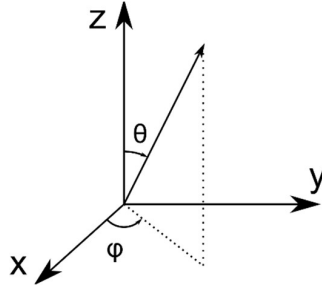


Figure 4.12: Spherical Coordinate System.

At a phi angle of 90° , the far-field analysis reveals essential details about the antenna's radiation pattern. The antenna exhibits a primary lobe with a magnitude of 5.18 dBi, centred at -12° , as shown in Figure 4.13. This indicates that the antenna's strongest radiation or reception occurs at this specific angle within the YZ plane. Furthermore, the radiation pattern of this antenna is notably directional; The central lobe is situated above the ground, indicating that the antenna's primary radiation is directed upwards. The main lobe's width of 111.1° indicates its coverage area. However, the side lobe level of -7.0 dB is attributed to radiation interactions with the metallic ground, a common phenomenon in antenna design that can result in the formation of secondary lobes or reflections.

At a phi angle of 0° , the antenna's radiation pattern exhibits a main lobe with a magnitude of 5.17 dBi, tightly focused at -10° within the XZ plane, as shown in Figure 4.14. In this scenario, a single lobe dominates, concentrating its radiation in the upper right direction, specifically at -10° . This suggests that the antenna's primary radiation occurs in this particular direction within the XZ. Furthermore, the radiation strength is almost identical in the XZ and YZ directions. This similarity is also reflected in the gain values, with a gain of 5.18 dBi recorded in the YZ plane and 5.17 dBi in the XZ plane. This distinctive pattern suits applications requiring directional transmission or reception in the upper region, showcasing intense upward radiation.

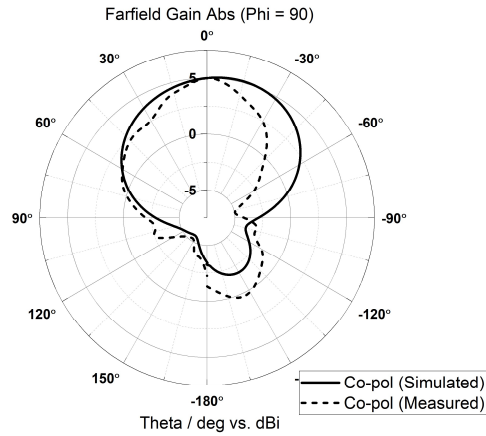


Figure 4.13: Far-field Gain at $\Phi = 90$ of Ethyl Acetate Model.

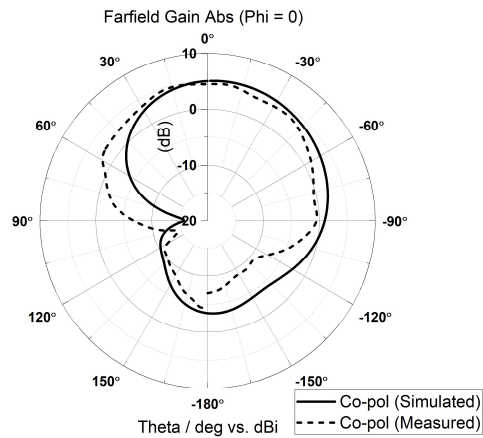


Figure 4.14: Far-field Gain at $\Phi = 0$ of Ethyl Acetate Model.

For the distilled water antenna, at a phi angle of 90° and a frequency of 2.4 GHz, the radiation pattern exhibits a primary lobe focused on the upper region of the antenna, with a central lobe magnitude of 4.13 dBi at 0° as shown in Figure 4.15. The broad angular width of 273.2° suggests the antenna's primary focus is upward, which can be advantageous for elevated signal transmission or reception. There is also a secondary lobe at the lower lobe under the metallic ground; the presence of the side lobe can be attributed to radiation interactions with the metallic ground.

At a phi angle of 0° , the antenna's radiation pattern shifts towards the left side, corresponding to the location of the SMA probe. The main lobe, measuring 4.53 dBi in magnitude, is directed at a 20° angle within the XZ plane, as illustrated in Figure 4.16. This asymmetrical pattern concentrates radiation in

the upper-left region while experiencing a decrease in the lower-left portion, suggesting some radiation is directed downwards. Furthermore, a side lobe with a level of -5.3 dB occurs below the ground plane, indicating a loss at the ground level. This unique pattern is well-suited for applications requiring directional transmission or reception in the upper-left region, demonstrating intense radiation directed upwards. Additionally, the antenna's radiation extends towards both the upper and lower regions of the ground plane in the YZ plane and towards both the upper-left and bottom regions of the ground plane in the XZ plane, making it suitable for applications needing radiation above and below the ground.

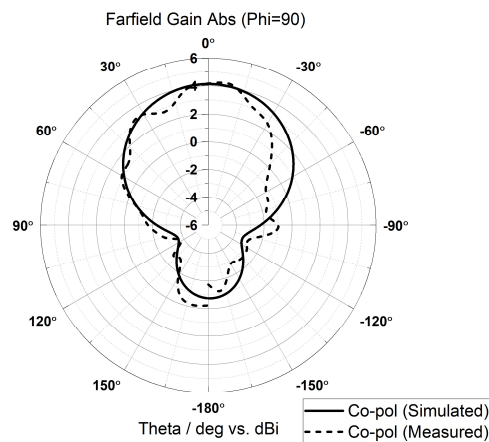


Figure 4.15: Far-field Gain at $\Phi = 90$ of Distilled Water Model.

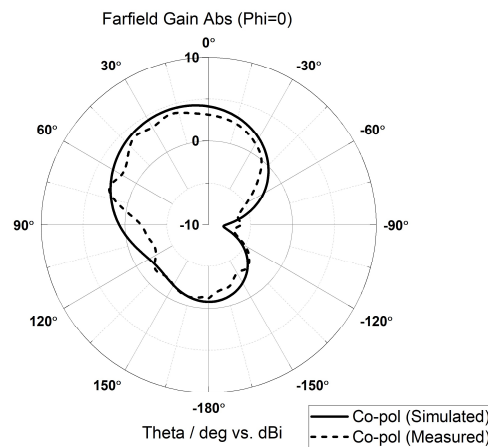


Figure 4.16: Far-field Gain at $\Phi = 0$ of Distilled Water Model.

The ethyl acetate antenna consistently outperforms the distilled water antenna when comparing radiation gain. It demonstrates higher positive gain values, indicating superior signal amplification, while the distilled water antenna exhibits less positive gain. The ethyl acetate antenna delivers stronger radiation in the YZ plane (at a phi angle of 90°) and the XZ plane (at a phi angle of 0°). Moreover, the ethyl acetate antenna offers greater flexibility in directionality, radiating predominantly in the upper region, thereby covering a wider area. In contrast, the distilled water antenna is optimised for applications above reflective surfaces.

4.5.4 E-field and H-field

The E-field, or electric field, is a crucial aspect of antenna behaviour. It is generated when there is a flow of current in the antenna. In antennas where radiation predominantly occurs from the top, as in both antennas, the E-field is most vital in the direction of radiation, which is in the Z-direction. To visualise the E-field of the antenna, observation is made from the XZ plane, as illustrated in Figure 4.17 for the ethyl acetate model and Figure 4.18 for the distilled water antenna model.

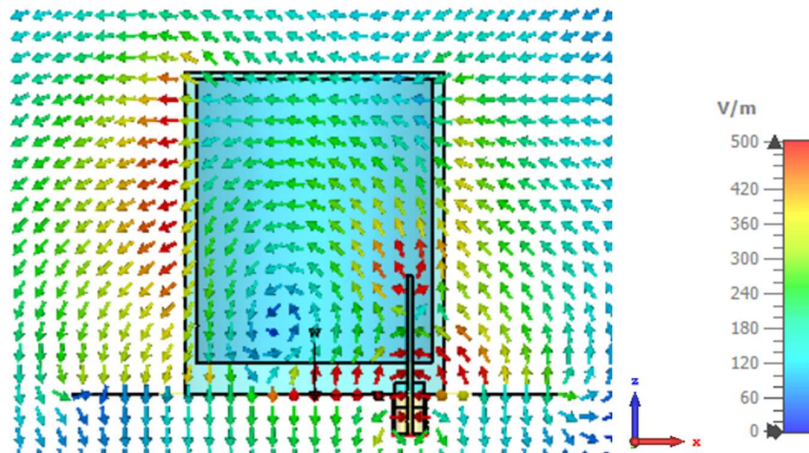


Figure 4.17: Simulated E-field of Ethyl Acetate Model.

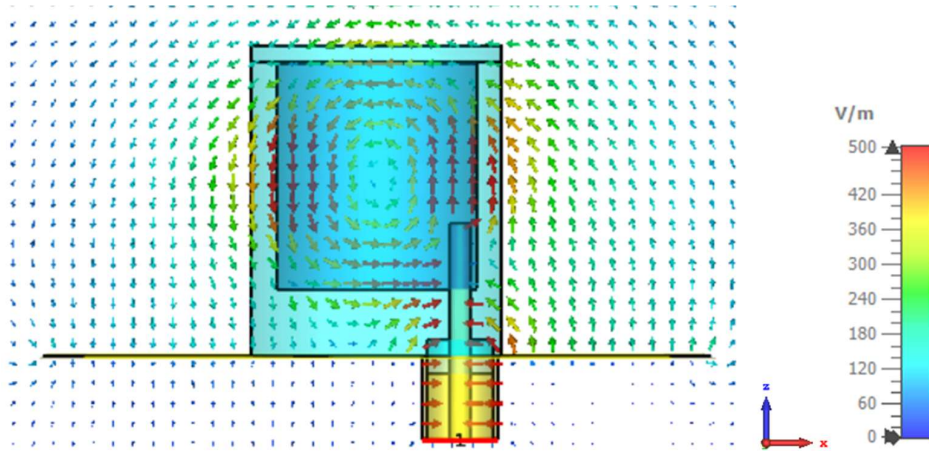


Figure 4.18: Simulated E-field of Distilled Water Model.

The H-field, or magnetic field, is another essential component of antenna behaviour. It is generated when the antenna has an E-field (electric field) and current flow. Typically, the direction of the magnetic field is perpendicular to the direction of the E-field. While these two fields are independent of each other, their combination is what forms and propagates electromagnetic waves. To visualise the H-field of the antenna, observation is made from the XY plane, which is perpendicular to the XZ plane, as depicted in Figure 4.19 and Figure 4.20. It is worth noting that the proposed LDRA (Liquid Dielectric Resonator Antenna) is excited in its fundamental HEM_{11} mode (Low et al., 2020).

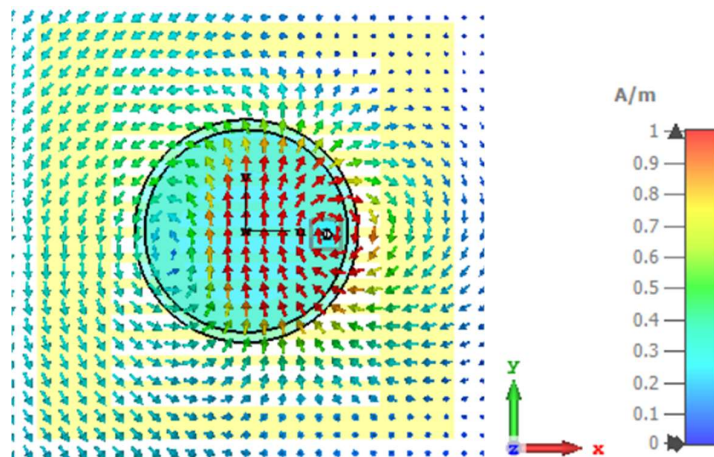


Figure 4.19: Simulated H-field of Ethyl Acetate Model.

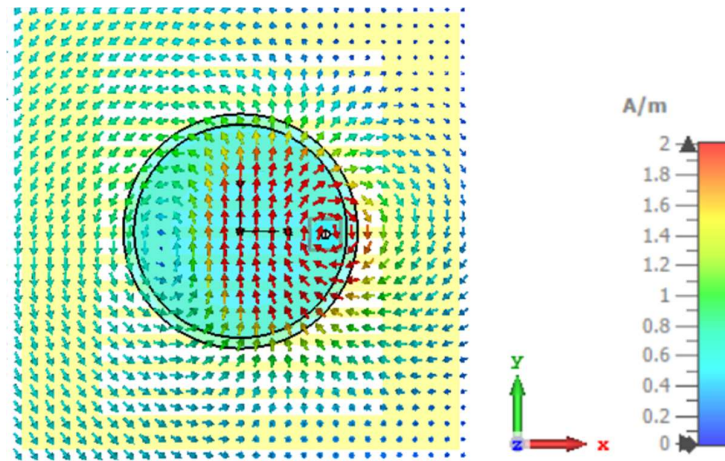


Figure 4.20: Simulated H-field of Distilled Water Model.

As the DRA uses distilled water and ethyl acetate as the dielectric materials, the simulation of surface current is irrelevant and will not be presented in this study. This is because dielectric materials are non-conductive, and current only flows through conductive materials like the metallic ground in the antenna.

4.6 Antenna's Signal Strength Assessment using ESP-32 Cam

The experimental process was recorded and converted into a video format to enhance the visualisation and representation of the Received Signal Strength Indication (RSSI) values. The video features the webserver display on the left and the corresponding RSSI values on the right. The RSSI values, calculated by the ESP32, and the web server's signal response are depicted in Figures 4.21 to Figure 4.25. As lower RSSI values indicate poorer connectivity in signal reception, the RSSI results are crucial for assessing signal strength.

In Figures 4.21 and 4.22, the RSSI values corresponding to the web server response indicate strong acceptable signal conditions. RSSI values range between -60 and -70 for the ethyl acetate antenna, while for the distilled water set, they fall between -70 and -80. Despite visually smooth results on the web server display in both experiments, the RSSI values reveal differences.

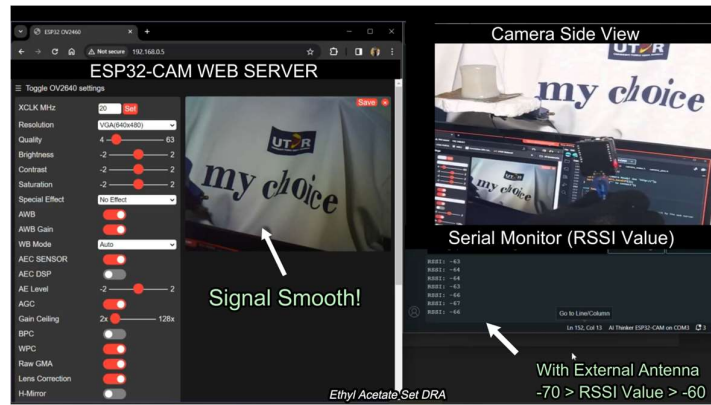


Figure 4.21: RSSI of Ethyl Acetate DRA.

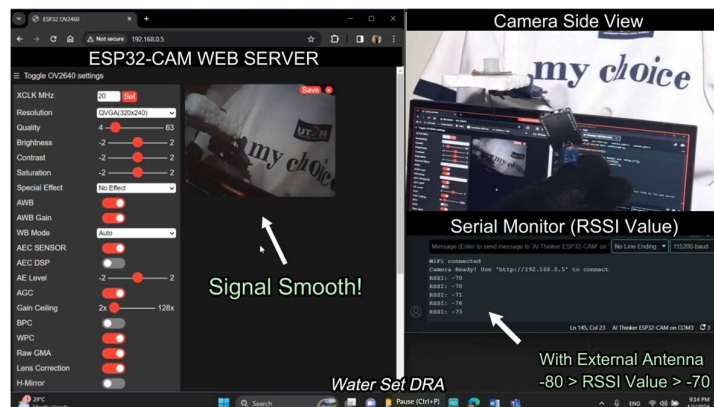


Figure 4.22: RSSI of Distilled Water DRA.

Subsequently, in Figure 4.23, the antenna was removed to test whether the RSSI values would decrease further. As depicted in Figures 4.24 and 4.25, the RSSI values dropped close to -80, and eventually, the web server stopped responding due to signal loss.

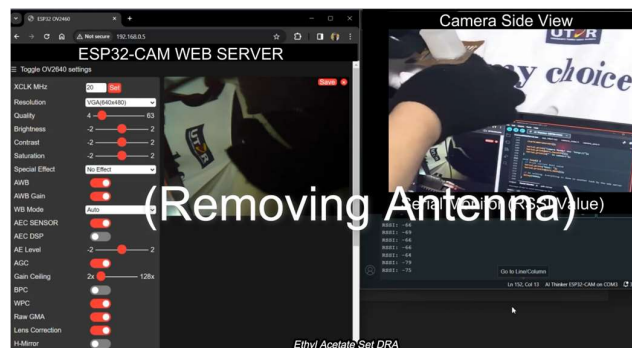


Figure 4.23: Removal of DRAs.

in antenna material. In the final test, the conventional Dielectric Resonator Antenna (DRA) was used to assess the illumination reduction. As shown in Figure 4.27 (b), the illuminance dropped significantly to about 80 lx, representing a substantial 70% reduction in illumination.

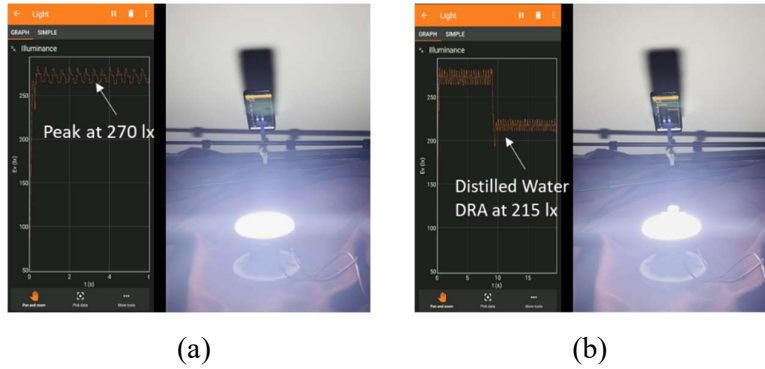


Figure 4.26: Light Illuminance (a) Without Antenna and (b) With Distilled Water DRA.

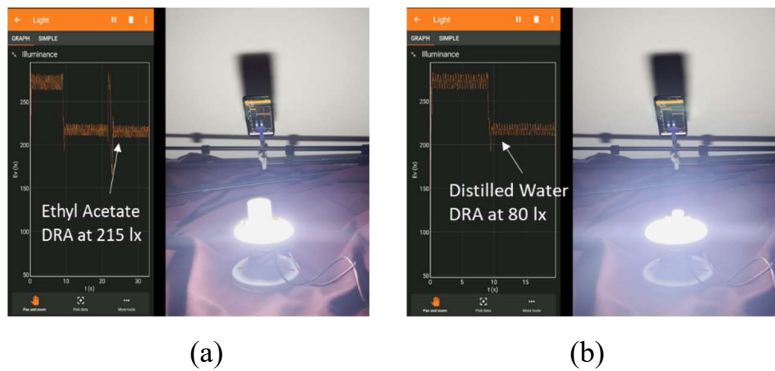


Figure 4.27: Light Illuminance with (a) Ethyl Acetate DRA and (b) Conventional DRA.

As shown in Figure 4.28, the results confirm the successful realisation of a semi-transparent antenna that aligns with the objectives. Despite the material selection being constrained by cost considerations, achieving complete transparency could have been attainable. Nonetheless, both designed antennas demonstrated commendable transparency compared to conventional liquid antennas. Furthermore, the effectiveness of the mesh ground structure in enhancing antenna transparency was verified through these results.

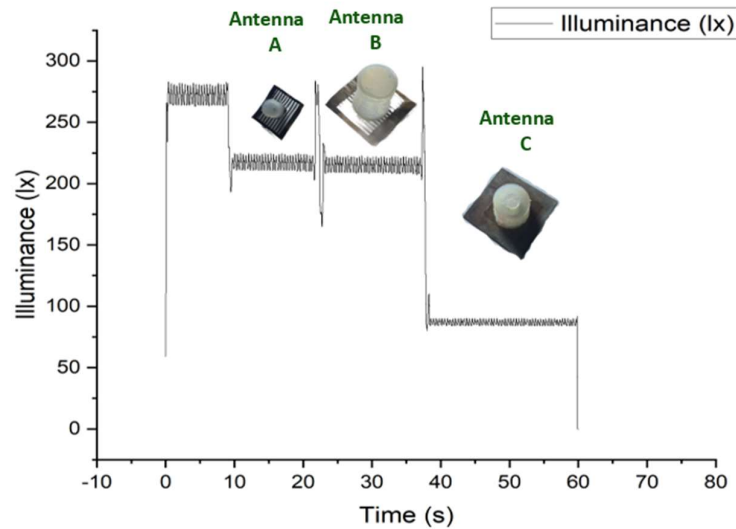


Figure 4.28: Illuminance Test with Three Different DRAs.

4.8 Web-Connected Smart Lighting (IoT Application)

In the IoT application, accessing the user interface is possible by typing the URL into the web server. Upon accessing the user interface, users can interact with red or green buttons to toggle the light on or off, with the text inside the box updating to reflect the current status, such as “Light OFF” or “Light ON”.

In Figure 4.29 (a), the application with the antenna is depicted in the Light OFF status, with the signal status indicating HIGH. Clicking the red button triggers the lamp to turn on, as shown in Figure 4.29 (b), while the signal status remains HIGH, and the Light ON indication appears in the green box. Subsequently, clicking the green button turns off the lamp, causing the button to revert to red with “Light OFF” text inside, as shown in Figure 4.30.



Figure 4.29: Light is (a) OFF and (b) Turned On with Ethyl Acetate DRA.

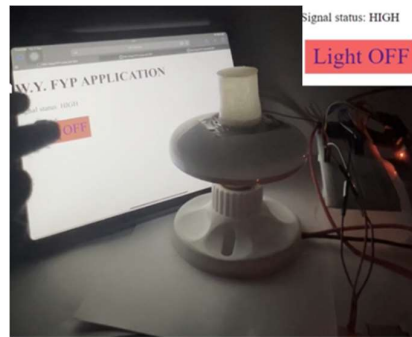


Figure 4.30: Light is Turn Off Again with Ethyl Acetate DRA.

Figure 4.31 depicts the antenna's removal, while Figure 4.32 illustrates the testing of the smart lighting system without using an antenna. Upon refreshing the web server, the signal status changes to LOW. Clicking the red button yields no response, eventually leading to the web server becoming unresponsive due to poor signal, as shown in Figures 4.33 and Figure 4.34. To restore functionality, the antenna is reconnected to the smart lighting, as shown in Figure 4.35, enabling the lamp to turn on again, with the signal status returning to HIGH, as shown in Figures 4.36 and 4.37.



Figure 4.31: Removal of DRA.

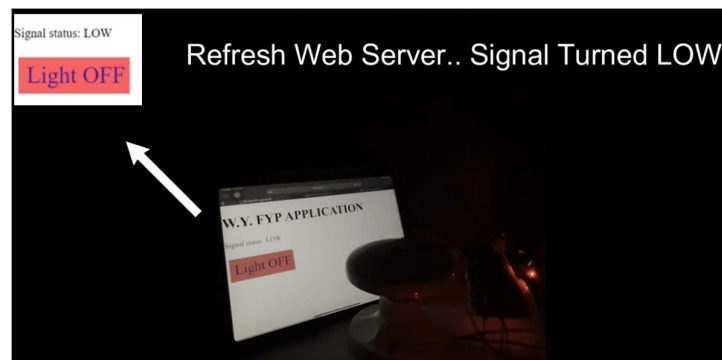


Figure 4.32: Light is Turn Off Without DRA.



Figure 4.33: Light is Unable to Turn On Without DRA.

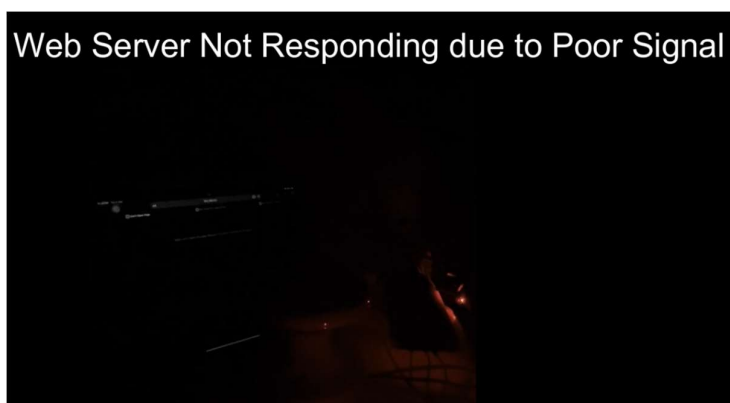


Figure 4.34: Web Server Not Responding With Ethyl Acetate DRA.

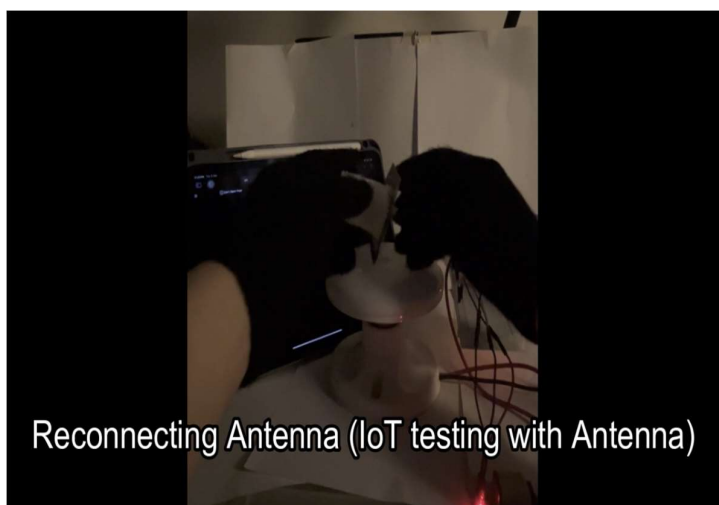


Figure 4.35: Reconnect Ethyl Acetate DRA with ESP32 Microcontroller.

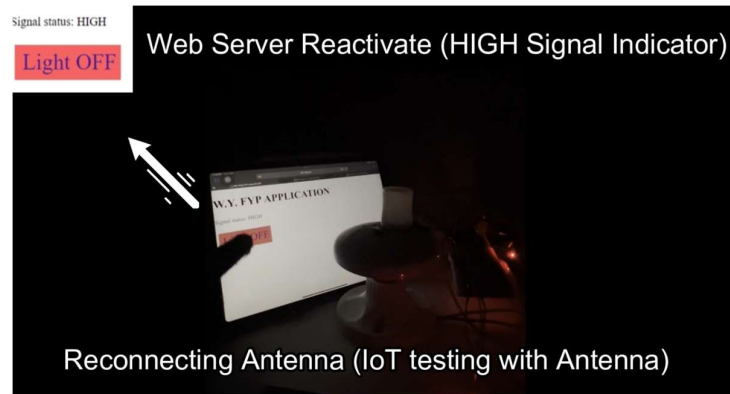


Figure 4.36: Web Server Reactivated with Ethyl Acetate DRA.

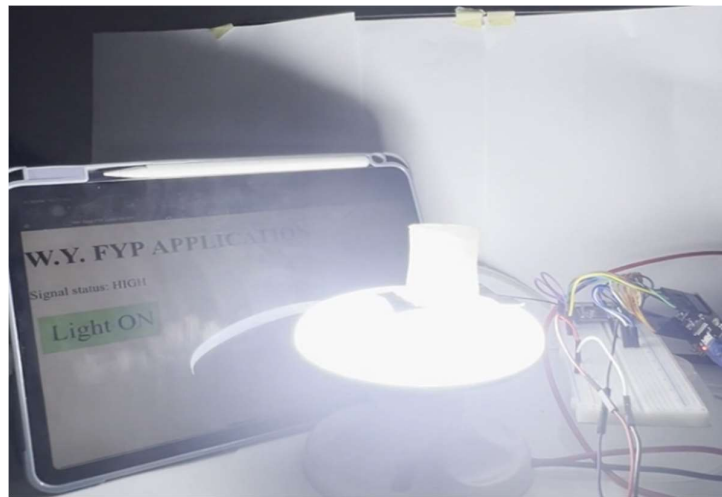


Figure 4.37: Light is Turned On Again With Ethyl Acetate DRA.

4.9 Summary

In this project, two nearly transparent Liquid Dielectric Resonator Antennas (LDRA) were designed, one utilising ethyl acetate and the other distilled water as dielectric materials. Through parametric sweep analysis, optimal design parameters for both models were identified. Both antennas met the requirement of a reflection coefficient below -10 dB for effective signal transmission. Notably, the ethyl acetate antenna exhibited superior impedance matching to the distilled water antenna, suggesting enhanced signal transmission and reception performance. The ethyl acetate antenna also displayed a more directional radiation pattern with higher gain values. Analysis of the E-field and H-field indicated operation in HEM_{11} mode. Signal strength evaluation revealed a stronger reception with the ethyl acetate antenna than with the distilled water

antenna. Transparency evaluation showed that both prototypes exhibited around a 20% reduction in illumination, indicating greater transparency than traditional DRA designs. The IoT application successfully demonstrated antenna functionality, emphasising the antenna's near-transparency and enhancing the application's visual appeal, particularly in web-connected smart lighting scenarios. Overall, this chapter provided a comprehensive discussion of the parametric analyses, characterisation, and evaluation of the antennas, emphasising performance differences and transparency.

CHAPTER 5

CONCLUSIONS AND RECOMMENDATIONS

5.1 Conclusions

In the project, a low-cost and near-transparent liquid antenna was successfully fabricated. Initially, simulations were conducted to design an antenna resonating at 2.4 GHz frequency and with an S_{11} below -10 dB. Low-cost materials such as distilled water and ethyl acetate were utilised for fabrication, while Ecoflex and mesh ground structures were introduced for transparency enhancement.

The final ethyl acetate antenna was designed in a rectangular copper ground shape measuring 61.99 mm \times 61.99 mm \times 0.06 mm, with a cylindrical DRA standing at 40 mm in height and 33 mm in diameter. Conversely, the distilled water antenna was designed with a rectangular copper ground of 40.01 mm \times 40.01 mm \times 0.06 mm and a cylindrical DRA measuring 17.6 mm in height and 15 mm in diameter.

Characterisation of the liquid antennas demonstrated their ability to resonate at 2.4 GHz and achieve reflection coefficients (S_{11}) below -10 dB. The ethyl acetate DRA outperforms the distilled water DRA in terms of gain, showcasing higher positive gain values and indicating superior signal amplification capabilities. Notably, the ethyl acetate DRA exhibits stronger radiation, particularly in the YZ plane (at a phi angle of 90°) and the XZ plane (at a phi angle of 0°). However, it is important to note that both antennas exhibit acceptable performance levels, with the distilled water DRA optimised for applications above reflective surfaces. While the ethyl acetate DRA demonstrates higher gain and more directional radiation, both antennas possess suitable performance characteristics for their intended applications. Additionally, both antennas were found to operate in HEM_{11} mode.

Furthermore, both antennas produced smooth images on the web server, and transparency evaluations revealed significant improvements compared to traditional liquid DRAs, with the new designs reducing illumination by only 20% compared to the conventional 70%. Most importantly, the fabricated antennas seamlessly integrated into lighting systems, transforming them into smart lighting solutions as expected, thereby serving as practical IoT

applications. Moreover, this Final Year Project (FYP) title has been shortlisted in the FYP poster competition and honoured with a silver award. Supporting evidence can be found in Appendix C and Appendix D.

5.2 Recommendations for Future Work

In this antenna design, the ethyl acetate is easily evaporated and lead to frequently recalibrated to achieve the desired performance. To address the need for frequent tuning caused by the high volatility of ethyl acetate and its impact on antenna performance due to evaporation, replacing it with a material characterised by low vapour pressure and high chemical stability is recommended (libretexts, 2020). Suitable alternatives such as mineral oil or silicone can mitigate the effects of evaporation. Introducing the liquid in powder form presents an intriguing alternative. Concerns regarding liquid evaporation are mitigated by transforming transparent materials like glass, alumina, or Teflon into powder form. This approach offers the advantage of maintaining transparency while addressing the issue of liquid evaporation.

Additionally, consideration is given to more transparent materials like glass or plastics instead of Ecoflex for improved transparency, which may not achieve complete transparency and could contain air bubbles during curing. Furthermore, replacing copper sheets with copper tape can reduce costs without compromising performance. Copper tape is generally used for smaller-scale applications where a thinner material is sufficient, which suits the antenna design.

To improve antenna orientation flexibility, transitioning from probe feed to side feed is suggested. This shift relocates the SMA connector from the bottom to the side of the antenna, simplifying placement on flat surfaces and offering greater orientation flexibility. Additionally, minimising the antenna size is proposed because the ethyl acetate antenna size is relatively larger compared to the distilled water set. This can be achieved by replacing the low dielectric constant ethyl acetate with a material possessing a higher dielectric constant. A smaller size antenna operating at the same frequency can be obtained. These recommendations aim to enhance antenna stability, transparency, flexibility, and cost-effectiveness in future iterations, reducing the need for frequent tuning.

REFERENCE

- A.H.Systems. 2023. *Practical Overview of Antenna Parameters* [online]. Available at: <https://www.ahsystems.com/articles/Practical-overview-of-antenna-parameters.php> [Accessed 20 August 2023].
- Antenna_Theory. 2015. *S-Parameters* [online]. Available at: <https://www.antennatheory.com/definitions/sparameters.php#:~:text=In%20practice%2C%20the%20most%20commonly,antenna%20and%20nothing%20is%20radiated.> [Accessed 20 August 2023].
- Balanis, C.A. 1992. Antenna theory: A review. *Proceedings of the IEEE* 80(1) 7-23.
- Baytöre, C., Zoral, E.Y., Göçen, C., and Palandöken, M., 2018. Coplanar flexible antenna design using conductive silver nano ink on paper substrate for wearable antenna applications. 2018 28th International Conference Radioelektronika (RADIOELEKTRONIKA), IEEE.
- Bennett, E.L., Song, C., Huang, Y. and Xiao, J., 2019. Measured relative complex permittivities for multiple series of ionic liquids. *Journal of Molecular Liquids* 294 111571.
- Bo, G., Ren, L., Xu, X. and Yi, D., 2018. Recent progress on liquid metals and their applications. *Advances in Physics: X* 3(1) 1446359.
- Boley, J.W., White, E.L., Chiu, G.T.C. and Kramer, R.K., 2014. Direct writing of gallium - indium alloy for stretchable electronics. *Advanced Functional Materials* 24(23) 3501-3507.
- Chen, Z. and Wong, H., 2017. Wideband glass and liquid cylindrical dielectric resonator antenna for pattern reconfigurable design. *IEEE Transactions on Antennas and Propagation* 65(5) 2157-2164.
- Chen, Z., Wong, H., Yuan, T. and Hu, X., 2022. A Water-loaded Frequency-Reconfigurable Antenna. TENCON 2022-2022 IEEE Region 10 Conference (TENCON), IEEE.
- Clasen, G. and Langley, R., 2004. Meshed patch antennas. *IEEE Transactions on Antennas and Propagation* 52(6) 1412-1416.
- Colombel, F., Castel, X., Himdi, M. and Legeay, G., 2009. Ultrathin metal layer, ITO film and ITO/Cu/ITO multilayer towards transparent antenna. *IET science, measurement & technology* 3(3) 229-234.
- Dey, A., Guldiken, R. and Mumcu, G., 2016. Microfluidically reconfigured wideband frequency-tunable liquid-metal monopole antenna. *IEEE Transactions on Antennas and Propagation* 64(6) 2572-2576.

ELPROCUS., 2021. *What is a Spectrum Analyzer : Working & Its Applications* [online]. Available at: <https://www.elprocus.com/what-is-a-spectrum-analyzer-working-its-applications/>.

everythingRF., 2018. *What are Near Field and Far Field Regions of an Antenna?* [online]. Available at: <https://www.everythingrf.com/community/what-are-near-field-and-far-field-regions-of-an-antenna> [Accessed 20 August 2023].

Fayad, H. and Record, P., 2006. Broadband liquid antenna. *Electronics Letters* 42(3) 133-134.

Frenzel, L.E. 2021. *4.3: Antenna Components and Definitions* [online]. Available at: [https://eng.libretexts.org/Bookshelves/Electrical_Engineering/ElectroOptics/Direct_Energy_\(Mitofsky\)/04%3A_Antennas/4.03%3A_Antenna_Components_and_Definitions](https://eng.libretexts.org/Bookshelves/Electrical_Engineering/ElectroOptics/Direct_Energy_(Mitofsky)/04%3A_Antennas/4.03%3A_Antenna_Components_and_Definitions) [Accessed 20 August 2023]

Goliya, Y., Rivadeneyra, A., Albrecht, A. and Mock, J., 2019. Next Generation Antennas Based on Screen - Printed and Transparent Silver Nanowire Films. *Advanced Optical Materials* 7(21) 1900995.

Gupta, N., Rout, S. and Sivaji, K., 2009. Characteristics of Cylindrical Dielectric Resonator Antenna. *Microwave Review* 29-32.

Hayes, G.J., So, J., Qusba, A. and Lazzi, G., 2012. Flexible liquid metal alloy (EGaIn) microstrip patch antenna. *IEEE Transactions on Antennas and Propagation* 60(5) 2151-2156.

Helena, D., Ramos, A., Varum, T. and Matos, J.N., 2020. Antenna design using modern additive manufacturing technology: A review. *IEEE Access* 8 177064-177083.

Hua, C., Shen, Z. and Lu, J., 2014. High-efficiency sea-water monopole antenna for maritime wireless communications. *IEEE Transactions on Antennas and Propagation* 62(12) 5968-5973.

Huang, Y., Xing, L., Song, S. and Wang, S., 2021. Liquid antennas: Past, present and future. *IEEE Open Journal of Antennas and Propagation* 2 473-487.

inhand. 2022. *What is Antenna Gain? Is Higher Antenna Gain Better?* [online]. Available at: <https://www.inhandnetworks.com/article/277.html#:~:text=If%20you%20want%20to%20focus,desired%20location%2C%20as%20illustrated%20below.>[Accessed 20 August 2023].

Ito, K. and Wu, M., 1991. See-through microstrip antennas constructed on a transparent substrate. 1991 Seventh International Conference on Antennas and Propagation, ICAP 91 (IEE), IET.

Jang, T., Zhang, C., Youn, H. and Zhou, J., 2016. Semitransparent and flexible mechanically reconfigurable electrically small antennas based on tortuous

metallic micromesh. *IEEE Transactions on Antennas and Propagation* 65(1) 150-158.

Jobs, M., Hjort, K., Rydberg, A. and Wu, Z., 2013. A tunable spherical cap microfluidic electrically small antenna. *Small* 9(19) 3230-3234.

Kingsley, S. and O'Keefe, S., 1999. Beam steering and monopulse processing of probe-fed dielectric resonator antennas. *IEE Proceedings-Radar, Sonar and Navigation* 146(3) 121-125.

Konca, M. and Warr, P.A., 2015. A frequency-reconfigurable antenna architecture using dielectric fluids. *IEEE Transactions on Antennas and Propagation* 63(12) 5280-5286.

KSFE 2021. Kumpulan Saintifik KSFE I Malaysia's Scientific Laboratory Supplier.

Leung, K.W., Lim, E.H. and Fang, X.S., 2012. Dielectric resonator antennas: From the basic to the aesthetic. *Proceedings of the IEEE* 100(7) 2181-2193.

Li, W., Yarali, E., Bakytbekov, A. and Anthopoulos, T.D., 2020. Highly transparent and conductive electrodes enabled by scalable printing-and-sintering of silver nanowires. *Nanotechnology* 31(39) 395201.

Li, Y. and Luk, K.-M. 2015. A water dense dielectric patch antenna. *IEEE Access* 3 274-280.

Libretexts. 2023 Vapor pressure, Chemistry LibreTexts. Available at: [https://chem.libretexts.org/Bookshelves/Physical_and_Theoretical_Chemistry_Textbook_Maps/Supplemental_Modules_\(Physical_and_Theoretical_Chemistry\)/Physical_Properties_of_Matter/States_of_Matter/Properties_of_Liquids/Vapor_Pressure](https://chem.libretexts.org/Bookshelves/Physical_and_Theoretical_Chemistry_Textbook_Maps/Supplemental_Modules_(Physical_and_Theoretical_Chemistry)/Physical_Properties_of_Matter/States_of_Matter/Properties_of_Liquids/Vapor_Pressure) (Accessed: 28 April 2024).

Low, J.-H., Chee, P.-S. and Lim, E.-H., 2019. Deformable liquid metal patch antenna for air pressure detection. *IEEE Sensors Journal* 20(8) 3963-3970.

Low, J.-H., Chee, P.-S., Lim, E.-H. and Lee, K.-Y., 2020. Compact organic liquid dielectric resonator antenna for air pressure sensing using soft material. *Scientific reports* 10(1) 14907.

Martínez, J.O., Rodríguez, J.R., Shen, Y. and Tong, K., 2022. Toward liquid reconfigurable antenna arrays for wireless communications. *IEEE Communications Magazine* 60(12) 145-151.

MobileSystems., 2017a. *HOW DO ANTENNAS WORK* [online]. Available at: https://www.mobilesystems.co.nz/news_and_publications/id/167/How%20do%20antennas%20work [Accessed 17 August 2023].

MobileSystems., 2017b. *How do antennas work: Mobile Systems - Tait Mobile Radio (BOP), Tauranga* [online]. Available at: https://www.mobilesystems.co.nz/news_and_publications/id/167/How%20do%20antennas%20work [Accessed 14 August 2023].

Moharram, M.A. and Kishk, A.A., 2016. Optically transparent reflectarray antenna design integrated with solar cells. *IEEE Transactions on Antennas and Propagation* 64(5) 1700-1712.

Morishita, A., Kitamura, C., Ohta, A. and Shiroma, W., 2014. Two - octave tunable liquid - metal monopole antenna. *Electronics Letters* 50(1) 19-20.

Motovilova, E. and Huang, S.Y., 2020. A review on reconfigurable liquid dielectric antennas. *Materials* 13(8) 1863.

Paracha, K.N., Butt, A.D., Alghamdi, A.S. and Babale, S.A., 2019. Liquid metal antennas: Materials, fabrication and applications. *Sensors* 20(1) 177.

Park, Y.-G., An, H.S., Kim, J.-Y. and Park, J.-U., 2019. High-resolution, reconfigurable printing of liquid metals with three-dimensional structures. *Science advances* 5(6) eaaw2844.

Perez, R., 1998. *Chapter 7 - Satellite Antennas* [online]. Available at: <https://www.sciencedirect.com/topics/engineering/antenna-element> [Accessed 20 August 2023].

Redmond, J., 2023. *Different Antenna Connector Types* [online]. Available at: <https://history-computer.com/different-antenna-connector-types/> [Accessed 20 August 2023].

Ren, J., Zhou, Z., Wei, Z.H. and Ren, H.M., 2020. Radiation pattern and polarization reconfigurable antenna using dielectric liquid. *IEEE Transactions on Antennas and Propagation* 68(12) 8174-8179.

Sa'ad, B.M., Rahim, S.K.A., Peter, T. and Krishnan, C., 2014. Transparent branch-line coupler using micro-metal mesh conductive film. *IEEE Microwave and Wireless Components Letters* 24(12) 857-859.

Sayem, A.S.M., Esselle, K.P., Hashmi, R.M. and Liu, H., 2020. A method to develop flexible robust optically transparent unidirectional antennas utilizing pure water, PDMS, and transparent conductive mesh. *IEEE Transactions on Antennas and Propagation* 68(10) 6943-6952.

Sayem, A.S.M., Esselle, K.P., Thalakituna, D.N. and Lalbakhsh, A., 2021. An electronically-tunable, flexible, and Transparent antenna with unidirectional radiation pattern. *IEEE Access* 9 147042-147053.

seimw.com., 2020. *Why are Antennas Important?* [online]. Available at: <https://www.seimw.com/gps-antenna/why-are-antennas-important/#:~:text=Antennas%20are%20normally%20used%20in,provide%20an%20effective%20wireless%20connection.> [Accessed 16 August 2023].

Simons, R.N. and Lee, R.Q., 1997. Feasibility study of optically transparent microstrip patch antenna. International Symposium and Radio Science Meeting.

Singh, A., Goode, I. and Saavedra, C.E., 2019. A multistate frequency reconfigurable monopole antenna using fluidic channels. *IEEE Antennas and Wireless Propagation Letters* 18(5) 856-860.

Song, C., Bennett, E.L., Xiao, J. and Alieldin, A., 2019. Metasurfaced, broadband, and circularly polarized liquid antennas using a simple structure. *IEEE Transactions on Antennas and Propagation* 67(7) 4907-4913.

Subashini, V., Raja, A., Lathamaju and Kumar, S.A., 2022. Design high efficiency sea-water antenna for maritime wireless communication. AIP Conference Proceedings, AIP Publishing.

Sun, J. and Luk, K.-M., 2017. A wideband low cost and optically transparent water patch antenna with omnidirectional conical beam radiation patterns. *IEEE Transactions on Antennas and Propagation* 65(9) 4478-4485.

Ubuy.com n.d. Ecoflex 00-30 - Super-Soft, Addition Cure Silicone Rubber - Pint Unit.

vlab.amrita.edu. 2011. *Antenna Radiation Pattern (theory) : Wireless Lab : Biotechnology and Biomedical Engineering : Amrita Vishwa vidyapeetham virtual lab* [online]. Available at: <https://vlab.amrita.edu/?sub=3&brch=179&sim=400&cnt=1#:~:text=Antennas%20demonstrate%20a%20property%20known,in%20space%20a%20certain%20way.> [Accessed 14 August 2023].

Vorobyov, A., Henemann, C. and Dallemagne, P., 2016. Liquid metal based antenna for wearable electronic. 2016 10th European Conference on Antennas and Propagation (EuCAP), IEEE.

Wang, M. and Chu, Q.-X., 2019. A wideband polarization-reconfigurable water dielectric resonator antenna. *IEEE Antennas and Wireless Propagation Letters* 18(2) 402-406.

Xing, L. 2015. Investigations of water-based liquid antennas for wireless communications.

Y, R. n.d. *Antenna – Need and Parameters* [online]. Available at: <https://electronicsdesk.com/antenna.html> [Accessed 17 August 2023].

Yasin, T., Baktur, R. and Furse, C. 2011. A study on the efficiency of transparent patch antennas designed from conductive oxide films. 2011 IEEE International Symposium on Antennas and Propagation (APSURSI), IEEE.

Zamudio, M., Busani, T., Tawk, Y. and Costantine, J., 2016. Design of AZO film for optically transparent antennas. 2016 IEEE International Symposium on Antennas and Propagation (APSURSI), IEEE.

Zhang, H., Krooswyk, S. and Ou, J. 2015. *High speed digital design: design of high speed interconnects and signaling*: Elsevier.

Zhong, Z.-P., Liang, J.-J., Huang, G.-L. and Yuan, T. 2018. A 3D-printed hybrid water antenna with tunable frequency and beamwidth. *Electronics* 7(10) 230.

Zou, M., Shen, Z. and Pan, J. 2016. Liquid antennas. 2016 IEEE MTT-S International Microwave Workshop Series on Advanced Materials and Processes for RF and THz Applications (IMWS-AMP), IEEE.

APPENDICES

Appendix A: Supporting Attachment for Antenna Signal Strength Assessment

```
#include <WiFi.h>
#include <WebServer.h>
#include "esp_camera.h"

WebServer server(80);

const char* ssid = "Khouse3_2.4ghz@unifi";
const char* password = "YOUR_PASSWORD";

// Camera configuration
#define CAMERA_MODEL_AI_THINKER // Modify this based on your
camera model
#include "camera_pins.h"

unsigned long lastUpdateTime = 0; // Variable to keep track of
the last update time

void setup() {
  Serial.begin(115200);

  // Connect to Wi-Fi
  WiFi.begin(ssid, password);
  while (WiFi.status() != WL_CONNECTED) {
    delay(1000);
    Serial.println("Connecting to WiFi...");
  }
  Serial.println("WiFi connected!");

  // Initialize camera
  camera_config_t config;
  config.ledc_channel = LEDC_CHANNEL_0;
  config.ledc_timer = LEDC_TIMER_0;
  config.pin_d0 = Y2_GPIO_NUM;
  config.pin_d1 = Y3_GPIO_NUM;
  config.pin_d2 = Y4_GPIO_NUM;
  config.pin_d3 = Y5_GPIO_NUM;
  config.pin_d4 = Y6_GPIO_NUM;
  config.pin_d5 = Y7_GPIO_NUM;
  config.pin_d6 = Y8_GPIO_NUM;
  config.pin_d7 = Y9_GPIO_NUM;
```



```

config.pin_xclk = XCLK_GPIO_NUM;
config.pin_pclk = PCLK_GPIO_NUM;
config.pin_vsync = VSYNC_GPIO_NUM;
config.pin_href = HREF_GPIO_NUM;
config.pin_sscb_sda = SIOD_GPIO_NUM;
config.pin_sscb_scl = SIOC_GPIO_NUM;
config.pin_pwdn = PWDN_GPIO_NUM;
config.pin_reset = RESET_GPIO_NUM;
config.xclk_freq_hz = 20000000;
config.pixel_format = PIXFORMAT_JPEG;

if(psramFound()){
    config.frame_size = FRAMESIZE_UXGA;
    config.jpeg_quality = 10;
    config.fb_count = 2;
} else {
    config.frame_size = FRAMESIZE_SVGA;
    config.jpeg_quality = 12;
    config.fb_count = 1;
}

// Initialize camera
esp_err_t err = esp_camera_init(&config);
if (err != ESP_OK) {
    Serial.printf("Camera init failed with error 0x%x", err);
    return;
}

// Start the web server
server.on("/", handleRoot);
server.begin();
Serial.println("Web server started!");
}

void loop() {
    server.handleClient();

    // Update RSSI every 5 seconds
    if (millis() - lastUpdateTime >= 5000) {
        Serial.print("RSSI: ");
        Serial.println(WiFi.RSSI());
        lastUpdateTime = millis(); // Update last update time
    }
}

void handleRoot() {
    // Capture a photo
    camera_fb_t *fb = NULL;

```

```

fb = esp_camera_fb_get();
if (!fb) {
    Serial.println("Camera capture failed");
    server.send(500, "text/plain", "Camera capture failed");
    return;
}

// Generate HTML page with photo and RSSI value
String page = "<html><body>";
page += "<h1>ESP32-CAM Web Server</h1>";
page += "<p>Current RSSI: " + String(WiFi.RSSI()) + " dBm</p>";
page += "<img src='data:image/jpeg;base64," +
base64Encode(fb->buf, fb->len) + "'/>";
page += "</body></html>";

// Send HTML page to client
server.send(200, "text/html", page);

// Cleanup
esp_camera_fb_return(fb);
}

// Function to encode image data as base64
String base64Encode(const uint8_t *data, size_t len) {
    const char b64_alphabet[] =
"ABCDEFGHIJKLMNOPQRSTUVWXYZabcdefghijklmnopqrstuvwxyz0123456789+/
";
    String encoded = "";
    size_t i = 0;
    uint8_t a, b, c;
    while (i < len) {
        a = data[i++];
        b = (i < len) ? data[i++] : 0;
        c = (i < len) ? data[i++] : 0;
        uint32_t triple = (a << 16) | (b << 8) | c;
        encoded += b64_alphabet[(triple >> 18) & 0x3F];
        encoded += b64_alphabet[(triple >> 12) & 0x3F];
        encoded += (i < len + 2) ? b64_alphabet[(triple >> 6) &
0x3F] : '=';
        encoded += (i < len + 1) ? b64_alphabet[triple & 0x3F] : '=';
    }
    return encoded;
}

```

Appendix B: Supporting Attachment for Web-connected Smart Lighting Application

```

#include <WiFi.h>
#include <WiFiClient.h>
#include <WebServer.h>
#include <ESPmDNS.h>

const char *ssid = "Khouse3_2.4ghz@unifi";
const char *password = "khouse2049";

WebServer server(80);
const int led = 13;
int relayPin = 12; // define a pin for relay
String buttonTitle1 = "Light ON";
String buttonTitle2 = "Light OFF";
int relayStat = 0; // initial state: OFF

void handleRoot() {
    digitalWrite(led, 1);
    String HTML = "<!DOCTYPE html>\n
    <html>\n
    <head>\n
    \t\n<title>Wei Yang FYP Lamp ON OFF</title>\n
    \t\n<meta name=\"viewport\" contenWt=\"width=device-width,\n
initial-scale=1\">\n
    \n<style>\n
    \nhtml,body{\t\nwidth:100%;\nheight:100%;\nmargin:0}\n*{box-
sizing:border-box}kkk\n.colorAll{\n\tbackground-
color:#90ee90}\n.colorBtn{\n\tbackground-
color:#add8e6}\n.anglButtdon,a{\n\tfont-size:30px;\nborder:1px
solid #ccc;\ndisplay:table-caption;\npadding:7px 10px;\ntext-
decoration:none;\ncursor:pointer;\npadding:5px 6px 7px
10px}a{\n\tdisplay:block}\n.btn{\n\tmargin:5px;\nborder:none;\n
display:inline-block;\nvertical-align:middle;\ntext-
align:center;\nwhite-space:nowrap}\n";

    HTML += "</style>\n\n</head>\n\n<body>\n<h1>W.Y. FYP
APPLICATION </h1>\n";

    // Get RSSI value
    int rssiValue = WiFi.RSSI();

    // Add the signal status information
    String SignalStatus;
    if (rssiValue < -60 && rssiValue >= -75) {
        SignalStatus = "HIGH";
    }

```

```

    } else {
        SignalStatus = "LOW";
    }

    HTML += "<p>Signal Status: " + SignalStatus + "</p>";

    if (relayStat) {
        HTML += "\t<div class=\"btn\">\n\t\t<a class=\"angleButton\"
style=\"background-color:#90ee90\" href=\"/relay?do=off\">";
        HTML += buttonTitle1; // Light ON title
    } else {
        HTML += "\t<div class=\"btn\">\n\t\t<a class=\"angleButton \"
style=\"background-color:#f56464\" href=\"/relay?do=on\">";
        HTML += buttonTitle2; // Light OFF title
    }
    HTML += "</a>\t\n\t</div>\n";

    HTML += "</body>\n</html>\n";
    server.send(200, "text/html", HTML);
    digitalWrite(led, 0);
}

void handleNotFound() {
    digitalWrite(led, 1);
    String message = "File Not Found\n\n";
    message += "URI: ";
    message += server.uri();
    message += "\nMethod: ";
    message += (server.method() == HTTP_GET) ? "GET" : "POST";
    message += "\nArguments: ";
    message += server.args();
    message += "\n";

    for (uint8_t i = 0; i < server.args(); i++) {
        message += " " + server.argName(i) + ": " + server.arg(i) +
"\n";
    }

    server.send(404, "text/plain", message);
    digitalWrite(led, 0);
}

void setup(void) {
    pinMode(led, OUTPUT);
    digitalWrite(led, 0);
    pinMode(relayPin, OUTPUT); // define a pin as output for relay
    digitalWrite(relayPin, relayStat); // initial state: OFF
    Serial.begin(115200);
}

```

```
Serial.println("Wei Yang FYP");

WiFi.mode(WIFI_STA);
WiFi.begin(ssid, password);
Serial.println("");

while (WiFi.status() != WL_CONNECTED) {
    delay(500);
    Serial.print(".");
}

Serial.println("");
Serial.print("Connected to ");
Serial.println(ssid);
Serial.print("IP address: ");
Serial.println(WiFi.localIP());

if (MDNS.begin("weiyangfyp")) {
    Serial.println("MDNS responder started");
}

server.on("/", handleRoot);
server.on("/relay", HTTP_GET, relayControl);
server.onNotFound(handleNotFound);
server.begin();
Serial.println("HTTP server started");
}

void loop(void) {
    server.handleClient();
}

void relayControl() {
    if (server.arg("do") == "on") {
        relayStat = 1;
    } else {
        relayStat = 0;
    }
}

digitalWrite(relayPin, relayStat); // Set relay pin according
to relayStat
handleRoot(); // Update web page
}
```

Appendix C: Supporting Attachment of Being Shortlisted for The FYP Poster Competition

UTAR UNIVERSITI TUNKU ABDUL RAHMAN Lee Kong Chian Faculty of Engineering and Science LKC

DEVELOPMENT OF A LOW-COST AND NEAR-TRANSPARENT LIQUID ANTENNA

Prepared by Tan Wei Yong under supervision of Dr. Low Joo Min

ABSTRACT
This study investigates the development of nearly-transparent liquid antennas, which offer a seamless integration into various environments while maintaining excellent signal coupling at 2.4 GHz. These antennas aim to be cost-effective and accessible by utilizing affordable materials such as ethyl acetate, water, and coffee, we have designed and analyzed near-transparent antenna models. Additionally, we have incorporated a defected ground structure to enhance transparency. In conclusion, this research contributes to advancing antenna design by prioritizing functionality, affordability, and visual appeal, offering promising solutions for contemporary communication demands.

OBJECTIVES

- Develop a transparent and low-cost liquid antenna using substitutes and defected ground.
- Design a transparent liquid antenna that can operate at the resonant frequency of 2.4 GHz.

METHODOLOGY

- Simulation CST simulation software
- Defected Ground Structure
- Selection of Copper Sheet
- Create Mold
- Cut Copper Sheet
- Preparation of Ethyl Acetate
- Outcome
- Fabrication of Prototype
- Soldering of SMA Connector
- Solder Copper Rod
- Combine with Ground
- Cut Copper Rod and Solder into Copper Ground
- Performance Validation
- Signal Strength Assessment
- Transparency Evaluation
- Application

RESULTS

Performance Validation

Figure 1: Graph of Measured and Simulated Resonance Frequency of Ethyl Acetate Die. Figure 2: Graph of Measured and Simulated Resonance Frequency of Water Die.

Figure 3: Graph of Measured and Simulated Return Loss of Ethyl Acetate Die. Figure 4: Graph of Measured and Simulated Return Loss of Water Die.

Signal Strength Assessment

Figure 5: Signal and RSSI levels for Ethyl Acetate Resonant Antenna (Left) and Water Resonant Antenna (Right) (Prototype and Simulation).

Transparency Evaluation

Figure 6: Graph of Light Intensity with Antenna A (center) with Right Copper Ground, Antenna B and C (Left) (Prototype and Simulation).

Remote Application

Figure 7: An ESP-8266 Chip with External Resonant Antenna Connected to Run On the Lamp (Intensity is High) (Left) and ESP-8266 Chip with External Resonant Antenna Connected to Turn Off the Lamp (Intensity is High) (Right). Figure 8: ESP-8266 Chip with External Resonant Antenna Connected to Turn Off the Lamp (Intensity is High) (Left) and ESP-8266 Chip with External Resonant Antenna Connected to Turn On the Lamp (Intensity is High) (Right).

CONCLUSION
This project achieved the design and analysis of low-cost and near-transparent liquid antennas. Simulation software CST simulated at 2.4 GHz. Both antennas met the requirements for effective signal transmission with reflection coefficients below -10 dB. The ethyl acetate antenna outperformed the water antenna in impedance matching and exhibited a more directional radiation pattern with higher gain.

UTAR LKC FES Page
18 April at 10:20

DMBE \ T3-05 : Development of a Low-cost and Near-transparent Liquid Antenna -- Like this poster? Vote for it at <https://forms.gle/uaBvxf1voVsrwYHG9>

You, Keh Yifan, Wei Kong Tan and 13 others

Like Comment Share

Write a comment...

Appendix D: Supporting Documentation of Silver Award in FYP Competition

